An Abstract of the Thesis of

Jefferson Vincent Fahey for the degree of **Master of Science** in **Chemistry** presented on **April 27, 1989.** Title: **Electrochemistry at a Reticulated Vitreous Carbon Flow Electrode**

Redacted for Privacy

Abstract approved: _____

John C. Westall

The electrochemistry of cadmium at a Reticulated Vitreous Carbon (RVC) electrode has been studied to determine the suitability of RVC as a working electrode for the electrochemical preconcentration of cadmium in the corrosive environment of zirconium dissolved in hydrofluoric acid.

The electrochemistry in this investigation deals with deposition of solid reduction products on the working electrode. The theory of cyclic voltammetry (CV) when solid products are deposited differs from the theory when soluble products are produced because diffusion of the solid reduction product does not occur. Schiffrin (1986) has developed the theory of cyclic voltammetry for the case of solid product formation under the assumptions of instantaneous nucleation and no overpotential effects. Cadmium, however, has a significant nucleation overpotential at RVC. This nucleation overpotential causes 1) an apparent dependence between the CV scan speed and the observed reduction potential and 2) cyclic voltammograms which cross themselves after

scan reversal.

Flow cells of several different styles were built and evaluated before it became obvious that a theoretical evaluation of the sources of potential drop within the cell was essential to the design of a flow cell. The theoretical evaluation revealed that the most critical problem in flow cell operation was the iR drop in the electrolyte within the pores of the porous working electrode. Simple computer programs demonstrated that cells with cylindrical symmetry could reduce the electrolyte iR drop to a minimum. Flow cells with cylindrical symmetry were constructed, and they were found to be stable and capable of 100% conversion efficiency. The sensitivities of these flow cells compare favorably to literature reports of flow cells. These cells also perform according to the theoretical predictions of variation of current and conversion efficiency with flow rate.

The suitability of RVC as a working electrode for electrochemical preconcentration of cadmium in zirconium solutions is not verified by this work because the poor reliability of the cells constructed in this study. This work suggests that automation of cell manufacture may improve consistency between cells so that the factors affecting reliability may be investigated. This work also suggest that automation of flow cell control would reduce the number of operator caused cell failures.

ELECTROCHEMISTRY AT A RETICULATED VITREOUS CARBON FLOW ELECTRODE

by

Jefferson Vincent Fahey

A THESIS

submitted to

Oregon State University

in partial fulfillment of
the requirements for the
degree of

Master of Science

Completed April 27, 1989

Commencement June 1989

APPROVED:

Redacted for Privacy

Professor of Chemistry in charge of major

Redacted for Privacy

Chairman of Department of Chemistry

Redacted for Privacy

Dean of Graduate School

Date thesis is presented April 27, 1989

Typed by the researcher for Jefferson V. Fahey

ACKNOWLEDGEMENT

I wish to acknowledge the advice and help received during my graduate career from my major professor, Dr. John C. Westall. In addition, I acknowledge the advice and guidance received from the faculty and staff of the Department of Chemistry. Fellow graduate student Jeff Louch was always available for commiseration, and he had some excellent abrasive papers too!

The understanding and support of J. H. Schlewitz, G. L. Beck and K. C. Ash of the Analytical Laboratories of Teledyne Wah Chang Albany is greatly appreciated. L. W. Latimer of the laboratory staff made many critical suggestions, all of which were extremely helpful. G. L. Hanson contributed definitive photographs from the Scanning Electron Microscope. M. E. Hancock and E. T. Drake of the Wah Chang library made the job of literature searching and retrieval a pleasurable experience.

The patience and understanding of the many people I work with has not been taken for granted, even though their names are taken for granted because they are not listed here. Special thanks go to D. L. Babcock, O. T. Farmer, J. Blickenstaff, D. Morris and B. Kelly for their patience.

DEDICATION

To Quinn and Ian, that their health and welfare may benefit and, some day, that they may understand the costs and benefits of this thesis. To Margaret and Linda, for demonstrating that there is a purpose for all the paths we travel in our lives. To Debbie, with the acknowledgement of her original inspiration, and with the thought that behind every man stands a woman; the question of how far remains as an exercise for the student.

TABLE OF CONTENTS

LIST OF FIGURES

LIST OF TABLES

ELECTROCHEMISTRY AT A RETICULATED VITREOUS CARBON FLOW ELECTRODE

PART 1: INVESTIGATIONS WITH A MICROELECTRODE

1.1. INTRODUCTION

This investigation is a feasibility study in the electrochemical preconcentration of cadmium. The target electrolyte for this study is zirconium which has been dissolved in hydrofluoric acid. The working electrode material investigated here is reticulated vitreous carbon (RVC), which is a porous, carbonaceous material with a high specific surface area and high resistance to attack by hydrofluoric acid.

The need for the preconcentration of cadmium arises from the need to determine trace concentrations of cadmium in zirconium. Zirconium is routinely dissolved in hydrofluoric acid so that it may be analyzed by inductively coupled plasma optical emission spectrometry (ICP–OES). The detection limit of cadmium in zirconium by ICP–OES is inadequate without some means of increasing the signal to noise ratio for the cadmium measurement.

1.1.1. Anticipated Problems. The major problems we expected in this study are complications from the reduction of hydrogen ion rather than cadmium ion. In the zirconium–hydrofluoric acid matrix, the concentration of cadmium is low and the acid concentration is relatively high. We know that the reduction of cadmium occurs at more

negative potentials as the concentration of cadmium decreases, so trace cadmium concentrations imply very negative cadmium reduction potentials. The conflict we are faced with is that as the acid concentration in the electrolyte increases, the reduction of hydrogen ion occurs at more *positive* potentials. Both of these dependencies are predicted by the Nernst equation, and we have made experimental confirmations of these predictions. These two conflicting phenomena determine the lowest concentration at which the reduction of cadmium in an acid medium can be detected.

1.1.2. State of the Art. The literature reports some examples of how hydrogen ions complicate the reduction of cadmium ion. Ogaram and Snook (1984) studied the suitability of RVC as a flow electrode. They arbitrarily defined the negative potential limit of their RVC electrode as the potential at which the Faradaic current from the reduction of hydrogen ion exceeded 1 microampere. This negative potential limit is pH dependent: for a pH of 6 they found the negative potential limit for RVC to be −750 mV vs SCE. This potential would reduce cadmium ions at a concentration greater than 280 μM or 32 mg/L, according to calculations made with the Nernst equation for reduction at a cadmium electrode. This concentration is higher than trace levels, so it appears that RVC would be unsuitable for preconcentration of trace cadmium because of hydrogen ion interference.

One technique which overcomes hydrogen ion interference at carbonaceous electrodes is to coat the electrode with mercury. The properties of a *mercury coated* RVC flow electrode were reported by Blaedel and Wang (1979). Their electrode was successfully plated with

cadmium at a potential of −950 mV vs SCE, and subsequent stripping revealed cadmium peaks at −700 mV. The electrolyte was 50 nM cadmium in 0.08 M acetate buffered to pH 4.8.

Mercury coating the RVC electrode has obviously made a substantial improvement in the capability of the RVC electrode. First we see that the mercury coated electrode is able to reduce 50 nM cadmium, compared to the 280 μM prediction made from the Nernst equation for a cadmium metal electrode. Second, we see that the mercury coated electrode can be operated at a lower pH value *and* more negative potentials than those recommended by Ogaram and Snook (1984). It appears that a mercury coated RVC working electrode may be suitable for preconcentration of trace level cadmium.

The reasons for the benefit of mercury plating the working electrode are thought to be 1) the cadmium–amalgam reduction potential is less negative than the reduction potentials for cadmium–cadmium or cadmium–RVC, 2) the concentration dependence of the reduction potential (ie 59/2 mV per decade) is eliminated by the mercury coating, and 3) the overpotential for reduction of hydrogen at mercury is high.

1.1.3. Description of the Analyte and Electrolyte. We have discussed the conflict between trace cadmium and high acid content of the electrolyte. In this section, we describe the electrolyte more thoroughly, estimate the hydrogen ion concentration of the electrolyte and calculate the concentration of cadmium which needs to be preconcentrated.

1.1.3.1. Hydrogen Ion Concentration. It is difficult to determine the pH

of hydrofluoric acid solutions since they attack the commonly used glass electrodes. We will make some assumptions about the pH of a HF solution in which zirconium has been dissolved. The solutions in which we are interested are those used in spectroscopic analysis. Typically, 1 gram of Zr is dissolved with 2 mL of 48% HF, then diluted to a final volume of 100 mL. In terms of molar concentrations, 0.58 moles of HF are used to dissolve 0.11 moles of Zr. The solution is then diluted to one liter. If we assume hydrogen is reduced and zirconium is oxidized, then the ***stoichiometry*** of the dissolution reaction is

$$4\ Zr(s) + 21\ HF(aq) = 4\ ZrF_{5.25}^{1.25-}(aq) + 5\ H^{+} + 8\ H_2(g) \qquad (1)$$

The species $ZrF_{5.25}^{1.25-}(aq)$ is a representation for what is really the six zirconium fluoride complexes ZrF^{3+} through ZrF_6^{2-}. The logarithms of the stepwise formation constants of these six complexes are 8.80, 7.32, 5.82, 4.85, 4.65 and 3.98 respectively at 25^{o} C, (Goldstein, 1964), whereas for the weak acid HF, we have pK_a = 3.2. Connick et al. (1949) reported the original data for the zirconium–fluoride species and discusses the aqueous chemistry of zirconium.

According to the stoichiometry in Equation 1, dissolution of 0.11 moles of zirconium will reduce 0.44 moles of hydrogen ion. Since we started with 0.58 moles of HF, 0.14 moles of the hydrogen ion from the HF will remain per liter of acid–zirconium solution. We maintain that the vast majority of the hydrogen ion remaining after zirconium dissolution will be free hydrogen ion which is dissociated from the fluoride ion. We expect the hydrogen ion concentration to be 0.14 M or

pH 0.85, which is the indication we get from "pH paper". When the pH of this solution is raised to about pH=3, polymers of oxide/hydroxide/fluoride/water species of zirconium begin to precipitate.

1.1.3.2. **Cadmium Concentration.** To be a practical benefit, the precon-centration of cadmium must occur at a concentration of 0.2 micrograms of cadmium per gram of zirconium. For a 1% Zr solution, the cadmium concentration is 2×10^{-6} g/l or 1.78×10^{-8} M. This concentration is about three times higher than the concentrations reported by Blaedel and Wang (1979). It appears that the absolute concentration limit is attainable in some electrolytes. We want to work at these concentrations in an electrolyte of zirconium dissolved in hydrofluoric acid.

1.1.4. Compendium. This work deals with solid-product cyclic voltammetry (CV), which is uncommon in the literature. We will see that solid-product CV is significantly different than soluble-product CV because the solid products do not diffuse from and to the electrode surface. The absence of diffusion produces a distinctively sharp oxida-tion or stripping peak in the reverse sweep of solid-product CVs.

We will see that *nucleation overpotential* for the formation of solid products and the *time-dependent formation of nuclei* are two important factors affecting the location and shape of a solid-product CV. First, the nucleation overpotential affects the minimum potential for solid product deposition and the degree to which solid-product CVs cross themselves. (CVs with reversible couples forming soluble products are never expected to cross themselves). Second, the time-

dependence of nuclei formation affects the shape of the CV near both the nucleation potential and in the area of the potential scan where the direction changes from reducing to oxidizing. Since nuclei formation is time–dependent, the affect of this phenomenon on the shape of the CV is dependent of the rate of change of the potential, i.e. the scan rate.

The reduction of hydrogen at the working electrode is found to be a serious complication to cadmium reduction. Once the reduction of hydrogen begins, the electrode is effectively *depolarized* and, if there is any reduction of cadmium occurring, the amount of cadmium reduced is difficult to determine because of the mixture of hydrogen and cadmium reduction currents. To further complicate matters, the generation of hydrogen gas bubbles on the electrode surface insulates the working electrode from the electrolyte, thus reducing the effective surface area of the electrode as gas generation proceeds. The electrode can ultimately be covered with hydrogen gas bubbles and become effectively inactive. The generation of hydrogen gas is a severe limitation in the utility of an electrode and is to be avoided.

In closing this section, we list some of the topics which are discussed in more detail here in Part 1 of this report. We will see that the reduction of nitrate and peroxide in the electrolyte depolarizes the electrode and precludes cadmium reduction. Therefore, when zirconium alloys are dissolved, only the minimum amount of nitric acid or hydrogen peroxide should be used. A pH buffered mixture of sodium chloride and sodium acetate is a very good supporting electrolyte for cadmium reduction. The electrolyte formed by dissolving zirconium in hydrofluoric acid does not interfere with cadmium reduction except for

the obvious pH limitations, provided a minimum of hydrogen peroxide is used to aid dissolution.

1.1.5. Microelectrode Investigations. Part 1 is devoted to microelectrode investigations because they avoid the complications which come from flowing systems and larger electrodes. A *very small fraction* of the test solution is probed with a microelectrode. The purpose of a microelectrode investigation is to obtain information about the chemical environment without significantly changing that environment. The *micro* prefix refers only to the size of the *electroactive* area of the electrode, not necessarily the gross size of the electrode assembly. For example, a small diameter wire could be difficult to handle if it were not enclosed in a package that is easy to handle.

In contrast to the *micro*electrode is the *macro*electrode. Part 2 of this work deals with applying the information gained in the microelectrode investigations to the construction of a macroelectrode to quantitatively reduce the cadmium ions in a flowing electrolyte.

1.2. MICROELECTRODE THEORY

This section discusses a few of the more important aspects of microelectrode theory. The reader is referred to Bard and Faulkner (1980) for a general discussion of electrochemistry and a background for the theory discussed below.

1.2.1. Cyclic Voltammetry. Cyclic voltammetry (CV) is an electrochemical technique which can return a large amount of informa-

tion about an electrochemical system. A sawtooth wave, usually centered about the $E^{o'}$s of interest, is applied to the system. Species which are produced at the electrode surface during the forward sweep (which can be towards either positive or negative potentials) are consumed during the reverse sweep. A *cyclic voltammogram* is a representation of the current–potential or current–time relationship of an electrochemical system.

1.2.1.1. Cyclic Voltammetry with a Soluble Product. For purposes of illustration, let us consider a system with only oxidized species in solution. Point (a) in Figure 1 is at an initial, oxidizing potential, and no Faradaic current flows through the cell. As the potential is swept toward $E^{o'}$, a reduction current begins to flow, and the concentration of the oxidized species at the electrode surface decreases (b). As the potential is swept through $E^{o'}$ (c), the concentration of oxidized species at the electrode surface goes to essentially zero, and the current flowing through the cell becomes diffusion limited. Note that in this description we assume the reduced species remains dissolved in solution and diffuses away from the electrode rather than being plated as a solid on the electrode surface. The applied potential is swept at the same rate for a few more moments in the region of diffusion limited current (d), then the direction of the potential sweep is reversed (between d and e).

Even though we are sweeping the potential towards oxidizing potentials, the reduction current continues until the applied potential again approaches $E^{o'}$, where we begin to see the oxidation of the previously reduced species (e–f). Ultimately the potential will be swept

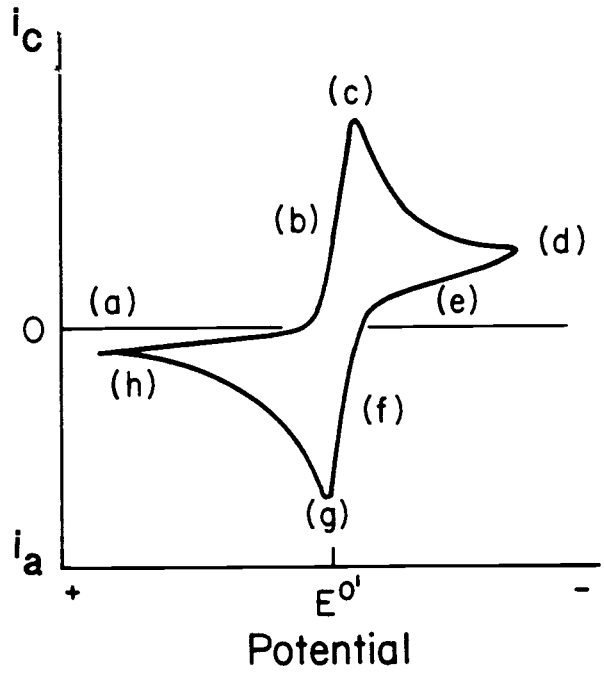

Figure 1. Ideal Soluble Product Cyclic Voltammogram. Both reactants and products are soluble. (After Figure 3.22, Kissinger and Heineman, 1984).

through $E^{o'}$ and all the reduced species remaining at the electrode surface will be immediately oxidized, at which point the current will reach a (negative) maximum (g). As the potential sweep continues in a positive direction, the oxidation current decreases to diffusion limited levels (h).

Quantitative descriptions of CV started in 1948 with solutions to the linear potential sweep voltammetry (LSV) waveform problem (Randles, 1948; Sevcik, 1948). The CV experiment is considered to be two LSV experiments run back–to–back in opposite sweep directions. Nicholson and Shain (1964) provided a full solution to the CV problem with numerical integration techniques because closed form solutions of their integrals could not be obtained. Their equations are for LSV but give insight to the CV experiment.

For the case of linear diffusion, semi–infinite boundary conditions, and a reversible reaction with all species soluble, the peak reduction current at 25^{o} C is (Bard and Faulkner, 1980, Equation 6.2.19)

$$i_p = (2.69 \times 10^5) n^{3/2} A D^{1/2} v^{1/2} C^* \qquad (2)$$

where

i_p	is the peak current of the scan, amperes
n	is the number of electrons involved in the reaction
A	is the electrode area, cm^2
D	is the diffusion coefficient, cm^2/sec
v	is the potential sweep rate, V/sec

C^* is the bulk concentration of the reactive species, mol/cm^3

Equation 2 tells us that in addition to the obvious dependence on area and concentration, the peak current is proportional to the square root of the diffusion coefficient and the square root of the potential sweep rate. The sweep rate is a variable which the experimenter can easily adjust.

The LSV half-peak potential $E_{p/2}$ is defined as the potential at which the current, on the ascending side of the peak, is one half of i_p. The difference in the potential at peak current and $E_{p/2}$ at 25^o is (Bard and Faulkner, 1980, Equation 6.2.22)

$$|E_p - E_{p/2}| = 56.5/n \text{ mV} \quad (3)$$

The peak potential is independent of scan rate for a reversible wave.

For cyclic voltammetry, if both reactants and products are soluble and the electrode reaction is reversible, the separation of peak potentials for the cathodic and anodic scans should be 59/n mV at 25^o. If the potential scan reversal occurs at least 35/n mV past the peak current, the ratio of peak cathodic current to peak anodic current should be 1, independent of scan rate and diffusion coefficients. There is, however, a special technique for determining the baseline from which peak currents are determined.

As stressed by the title of this section, these developments are for reactions in which both reactants and products are soluble.

1.2.1.2. Cyclic Voltammetry with an Insoluble Product. The models developed for CV with soluble reactants and products are not appropriate for the case where the product is a solid deposited on the electrode. First, Equation 2 contains the diffusion coefficient and the concentration of the reactant, but these terms loose their meaning when the reactant is a solid which has been deposited on the surface of the electrode. Second, the complications from nucleation overpotentials and underpotentials, which are common in the deposition of a solid-product, must be considered.

Recent work by Schiffrin (1986) treats the "Theory of Cyclic Voltammetry for Reversible Electrodeposition of Insoluble Products". To simplify his development, Schiffrin ignores nucleation complications and assumes an instantaneous transition from bare electrode, i.e. Pt or carbon, to an electrode of the metal of interest as the first reductive step. He further assumes that the potential at which this transition occurs is the potential predicted by the Nernst equation for the reduction of an ion at the surface of a metal of the same species. Figure 2 is a reproduction of a cyclic voltammogram reported by Schiffrin from that work. The continuous line is an experimentally obtained CV, and the dots represent the response predicted by his theory.

There are two significant differences between the shape of the CV of Figure 1, a soluble-product CV, and Figure 2, an insoluble-product CV. The first difference is stripping peak shape, which is predominately influenced by the fact that the reduced metal does not diffuse to the electrode before oxidation; however the stripping peak

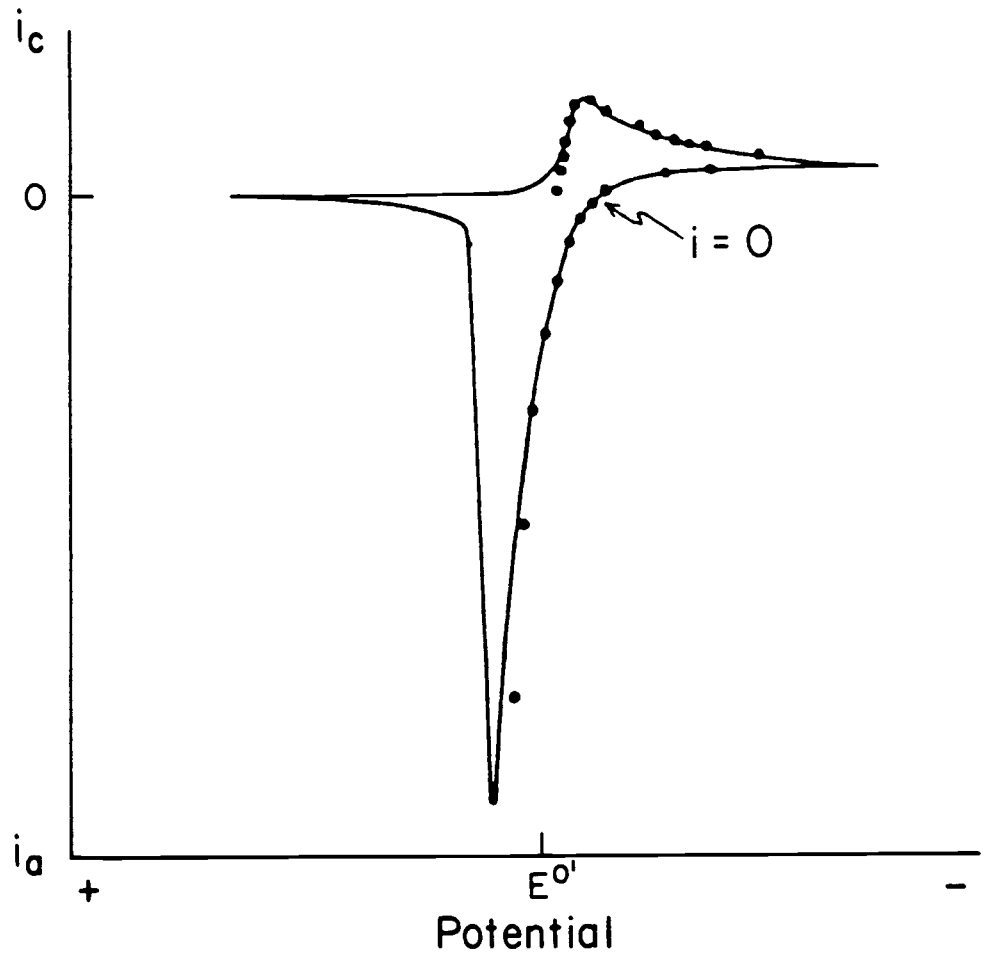

Figure 2. Insoluble Product Cyclic Voltammogram. Oxidized species soluble, reduced species insoluble. The line is an experimentally obtained CV. The dots represent the predictions of Schiffrin's theory. After Figure 1, D. J. Schiffrin, 1986.

shape is influenced by the physical structure or morphology of the deposit. For example, a thin film deposit will be oxidized from the electrode much faster than a large, hemispherical deposit. The second difference between Figures 1 and 2 is the potential and shape of the reduction peak. The potential at the beginning of reduction depends on the formal potential of the species in solution and the nucleation overpotential or underpotential for that species on the electrode. The initial shape of the reduction peak, or more specifically the slope of the reduction peak after the initial nucleation, is dependent on the nucleation rate and the scan rate. Slow nucleation rates will produce a smaller slope than fast rates.

Schiffrin has proposed that "the only potential which is independent of sweep rate ... corresponds to i=0" on the reverse scan, as noted in Figure 2. The cathodic and anodic peak currents and the potentials at which they occur are sweep rate dependent.

1.2.2. Nucleation Overpotential of an Insoluble Product. The term *nucleation overpotential* is an operational definition for the difference between the potential for the reduction of a metal ion at its metal electrode and the potential at which the reduction current of the metal ion at some other electrode material rises significantly above the baseline. When the metal of an electrode is different from the metal ions in solution, the deposition potential is particularly dependent on the condition of the electrode surface, adsorption of the metal ions on the electrode surface, and the tendency for alloy formation. (Bard and Faulkner, 1980, Section 10.2.1.c; Tanaka, 1965, Section III.B).

An inert electrode material like carbon, in contrast to a metal which can *react* with the depositing ions, may require overpotentials of tenths of a volt, as shown by Hills et al, (1974). They found that the "number of available nucleation sites is potential dependent", and implied that the reduction potential for deposition of a solid product is effectively a *range of potentials*. In our study, the nucleation overpotential is invoked to explain two features of the observed cyclic voltammograms: the dependence of scan rate on apparent reduction potential, and the loop (crossed line) in the cyclic voltammogram.

1.2.3. The Formation of Nuclei. Hills et al, (1974) show experimental evidence for the total current at a nucleating electrode *increasing* with time. The time interval for this time dependence is short and occurs before a bare electrode becomes fully nucleated. They observed these phenomena during potential step experiments which started with a bare electrode at an oxidizing potential; the potential was then stepped to a reducing potential. The current increased because the number of nuclei increased with time. The growth in current continued until such time that diffusion zones from adjacent nuclei began to overlap. When the nuclei were large enough that their diffusion zones completely overlapped, the many discrete diffusion zones for each nucleus had merged into a single diffusion layer which took on the shape of the electrode. The current then *decreased* with time, reaching a limit dependent on electrode geometry.

1.2.4. Planar vs Hemispherical Diffusion. Transport to an electrode can be considered in terms of two different modes of diffu-

sion: planar and hemispherical. The major difference between the two is the size of the electrode surface compared to the depth of the diffusion layer.

In the case of planar diffusion, the electrode's dimensions are large compared to the depth of the diffusion layer. A potential step experiment at this electrode will show that the diffusion current is highest immediately after the step and decreases with the square root of time until reaching zero.

Hemispherical diffusion occurs at very small electrodes. A potential step applied to a small electrode will also show that the diffusion current decreases with the square root of time, but the diffusion current reaches a non–zero steady state.

The distinguishing feature of planar diffusion is that the cross sectional area at the outer boundary of the diffusion layer remains constant with time, regardless of the depth of the diffusion layer. In contrast, as the depth of the hemispherical diffusion layer increases, the cross sectional area at the outer boundary of the diffusion layer increases with the square of the diffusion layer thickness.

1.3. EXPERIMENTAL

An RVC and a platinum microelectrode, described in the next section, are fabricated and used to investigate the feasibility of electrochemical concentration of cadmium in zirconium. The dependence of cadmium's reduction potential on concentration, as predicted for reduction of cadmium[II] at a cadmium metal electrode by the Nernst equation, is confirmed. Two methods of RVC electrode pretreatment are compared, and the effects of various electrolytes on RVC are studied. A response

to cadmium at a bare RVC microelectrode in a zirconium – hydrofluoric acid electrolyte is observed, and this response is much larger when the RVC microelectrode is coated with mercury.

1.3.1. Electrodes. An Orion Single Junction Reference Electrode Model 90–01 was used with Catalog No. 90–00–01 filling solution. The potential of this sleeve type Ag/AgCl electrode matched the potential of a conventional SCE.

The auxiliary electrode was a 0.45 mm diameter platinum wire introduced to the cell through a small diameter hose barb in the top of the cell.

The Reticulated Vitreous Carbon (RVC) working electrode was fashioned after Sleszynski and Osteryoung (1984) with several modifications. A cylinder of 100 pores per inch (ppi) RVC 6 mm diameter and 50 mm long was cut from a block of RVC (ERG Inc., Oakland, CA). The RVC cylinder was enclosed in heat shrink Teflon (PTFE) tubing (FIT 400 MS/2, Alpha Wire Corporation, Newark, NJ), Figure 3. One end of this device was placed in a reservoir of epoxy resin (Tra–Bond BB–2129, Tra–Con, Inc., Medford, MA) and the other end connected to a squeeze bulb through a stopcock. The resin was sucked up the tube resulting in air–free epoxy impregnated RVC. The top few millimeters of RVC were left bare to facilitate electrical connection. After hardening, the Teflon sheath was stripped with a razor blade, a 0.45 mm diameter platinum wire was driven through the top unimpregnated end of the RVC and wrapped tightly around the cylinder several times to make electrical contact. This Pt–RVC–resin assembly was centered in 0.5 inch inside diameter Tygon tubing and a similar procedure encapsu–

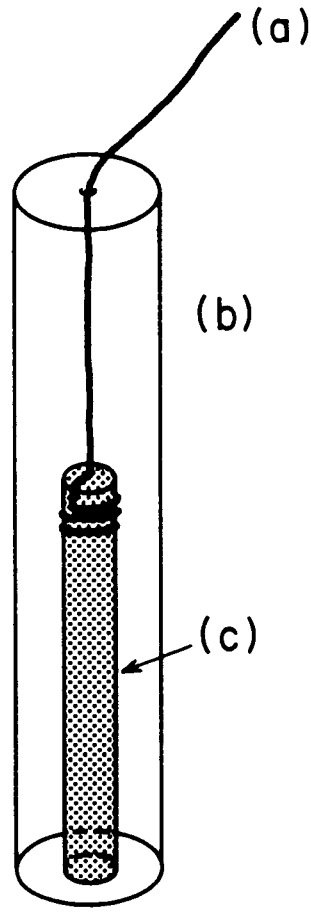

Figure 3. Reticulated Vitreous Carbon (RVC) Microelectrode. (a) 0.45 mm Pt wire, (b) 0.5 in X 6 in epoxy rod, (c) 6 mm X 50 mm epoxy impregnated RVC.

lated the whole assembly inside an epoxy rod. The Tygon was stripped and the working end cut and polished, yielding an epoxy encapsulated RVC microelectrode of about the same gross size as the Orion reference electrode.

The platinum microelectrode was made by encapsulating 0.45 mm diameter platinum wire in 0.5 inch diameter resin using the same techniques described above.

1.3.2. Electrochemical Cell. A sixty milliliter (45 mm dia X 38 mm deep) heavy duty screw top wide mouth teflon jar was used as the electrochemical cell (Savillex, Minneapolis, MN). One jar lid was drilled and tapped to accept two plastic pipe nipples which, when machined with an internal taper, allowed an "O" ring around the electrodes both to seal the cell from the atmosphere and to provide simple vertical adjustment of the electrodes. The lid was also drilled and tapped for three small hose bibs; purge nitrogen, blanket nitrogen, and a platinum wire auxiliary electrode. This lid remained affixed to ring stand equipment with a hose clamp – test solution changes were made by swapping jars, which could be stored with the tight fitting lids. The standard volume of solution used in this cell was 30 milliliters. When necessary, the solutions could be stirred with a magnetic stirrer and a small stir–bar within the cell.

1.3.3. Potentiostat and Recorder. An IBM Instruments Inc. EC/225 Voltammetric Analyzer and Yokogawa Model 3022 XYT Recorder (IBM 7424 MT XYT Recorder) were used.

1.3.4. Na-Cl-Acetate Buffer Electrolyte (SCABE). A

buffered electrolyte that consistently provided good results and did not seem to contribute to electrode passivation was prepared by adding sodium hydroxide to raise the pH of about 700 milliliters of distilled water containing one mole of sodium chloride and one mole of acetic acid to a final pH between 5 and 5.5, followed by diluting to one liter. This electrolyte (SCABE) is one molar in both chloride and total acetate, and is over one molar in sodium. References herein to 33% SCABE mean the solution was 0.33 M chloride, 0.33 M in total acetate, and more than 0.33 M sodium.

1.3.5. Miscellaneous. All acids, bases and salts were ACS grade reagents. No extraordinary precautions were taken to obtain pure water for solution preparation. The source of the water was an in-house designed system with an activated carbon bed, filtration to 0.2 micrometers and ion exchange. The water was delivered to the lab by a nominally all plastic plumbing system. The concentrations of all *stock* solutions were accurate to three significant figures. Expedience, not accuracy, was the objective in preparation of working solutions. Those solutions were often measured with graduate cylinders and their accuracy is estimated to be about 10%.

1.4. RESULTS and DISCUSSION

1.4.1. Platinum - RVC Comparison. Cyclic voltammograms (CVs) of 3.3 mM Cd^{2+} in 33% SCABE were obtained with the platinum and RVC microelectrodes. Representative CVs at different scan rates are shown in Figures 4 and 5. The shapes of the CVs are generally

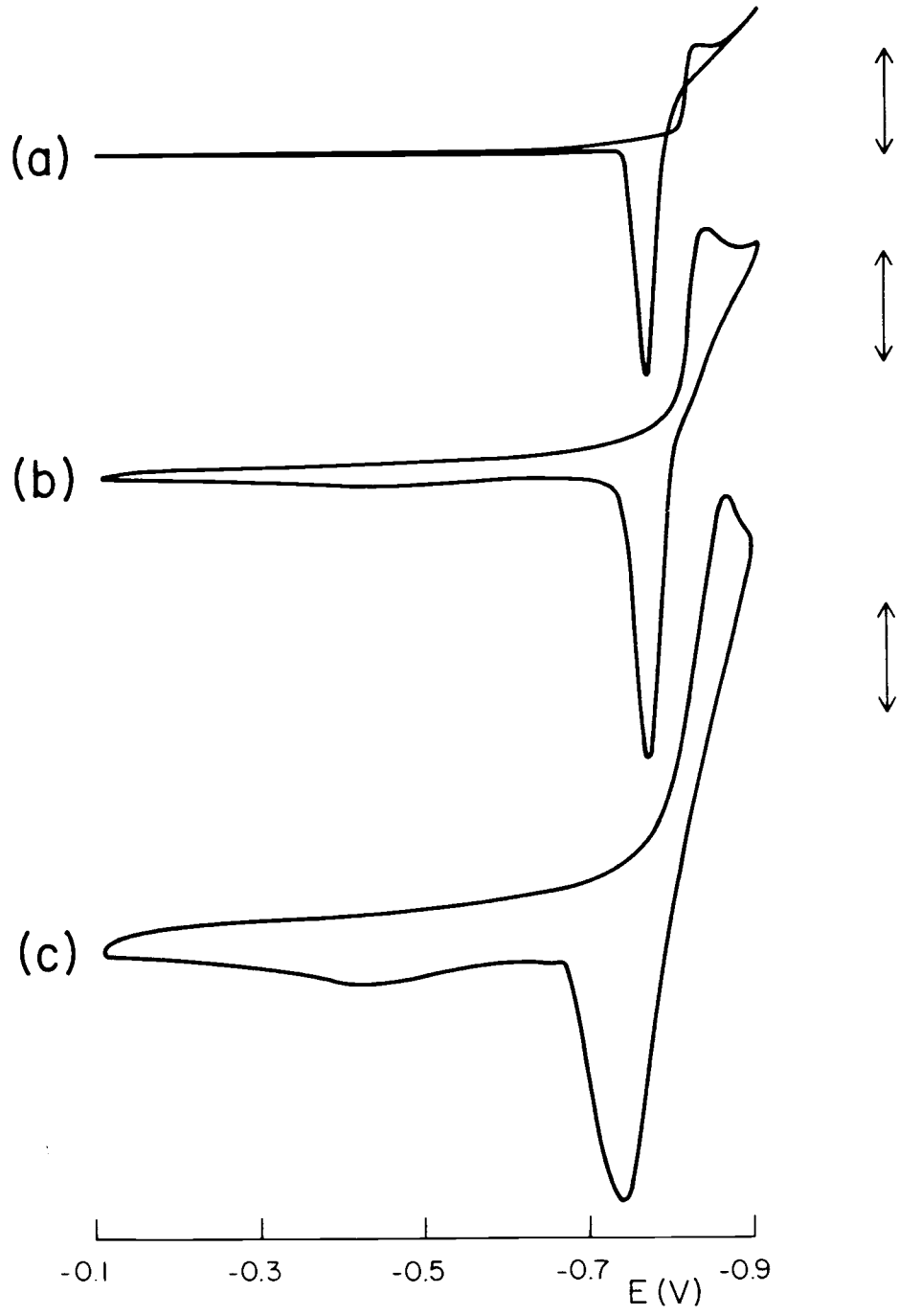

Figure 4. Platinum Microelectrode Cyclic Voltammograms. 33% SCABE, 3.3 mM Cd^{2+}. Scan speeds: (a) 10 mV/s, (b) 100 mV/s, (c) 500 mV/s. The length of the arrows indicate 2.54 microamps.

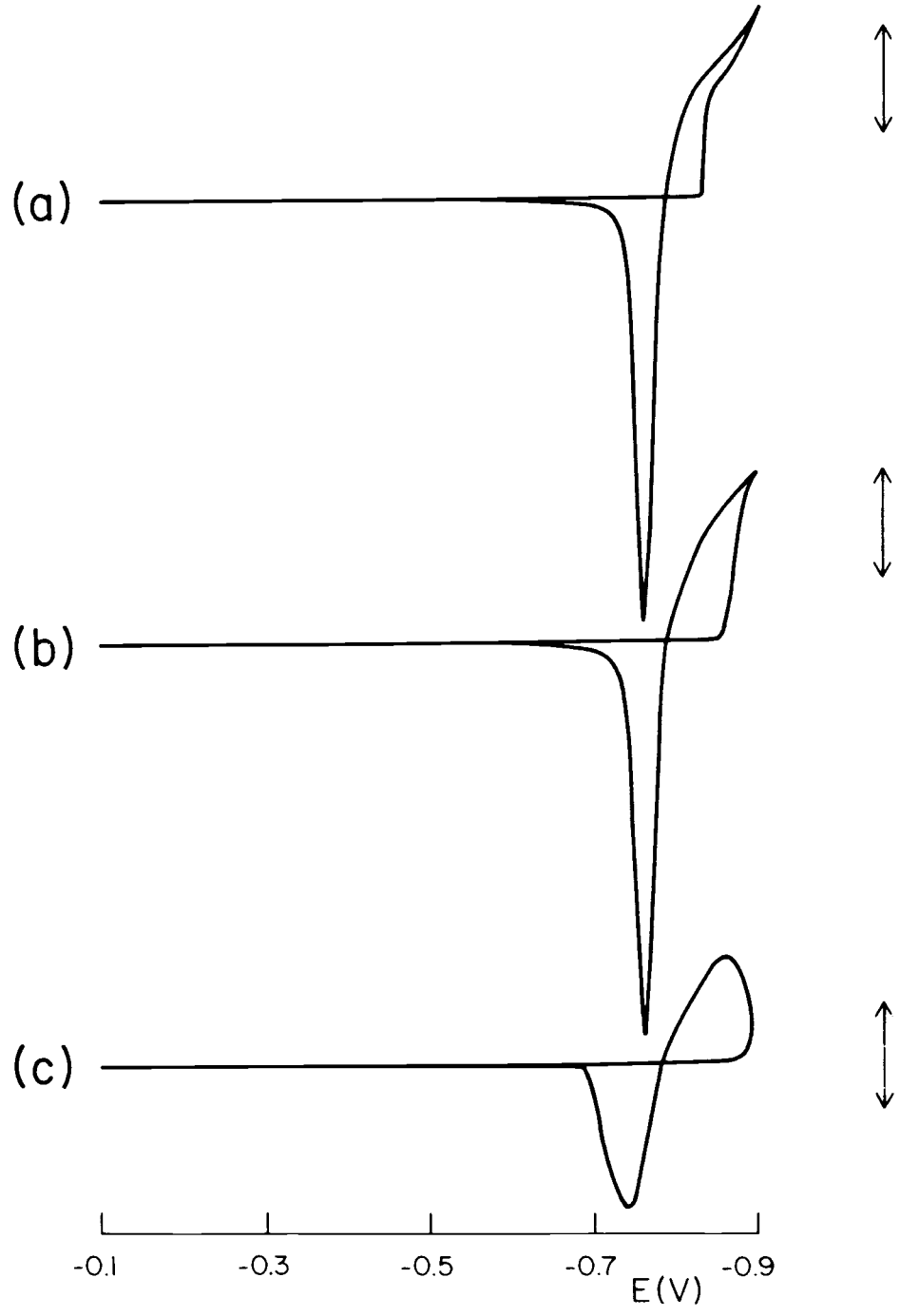

Figure 5. RVC Microelectrode Cyclic Voltammograms. 3.3 mM Cd^{2+} in 33% SCABE. Scan speeds: (a) 10 mV/s, (b) 100 mV/s, (c) 500 mV/s. The length of the arrows indicate 25.4 microamps.

like those of Schiffrin's solid deposit example shown in Figure 2. The crossover observed here in the experimental CVs is caused by nucleation overpotential and will be discussed in the next section.

The features of the CVs in Figures 4 and 5 are summarized in Table 1. In column 1 are the scan rates for the different CVs. The potential at which the current is zero during the oxidative sweeps, as shown in Figure 2 and as listed in the second column of Table 1, is invariant with sweep speed and electrode type. This observation is consistent with oxidation of a solid electrode where mass transport considerations may be ignored. This invariance has been proposed as an indication of reversibility in the deposition of a solid product (Schiffrin, 1986). The potential at the peak stripping current, as shown in the third column of Table 1, is also invariant with sweep speed. This potential, however, is not a reliable one to characterize a system because this potential is dependent on the morphology of the deposit. Invariance is observed here because the comparisons are all made with smooth and regular shaped stripping peaks, as shown in Figures 4 and 5, where morphology does not appear to be a significant factor.

The fourth column of Table 1 shows that the starting potential for the reduction of cadmium at the platinum electrode is not dependent on scan speeds used in this experiment; the value found of −0.800 V vs SCE is in good agreement with that of Tanaka (1963). At the RVC electrode, however, the starting potential for the reduction of cadmium becomes more negative with increasing scan speed. The potential at RVC for the 10 mV/s scan speed is about 30 mV more negative than it is at platinum. This difference increases with increasing scan speed to

--- Platinum Microelectrode ---

scan rate	$E_{i=0}$, V	$E_{p,a}$,V	E_r,V (Cd)	E_r,V (H_2O)
10	−0.786	−0.766	−0.804	−0.859
30	−0.789	−0.766	−0.814	−0.875
50	−0.791	−0.766	−0.804	−0.875
100	−0.794	−0.766	−0.799	−0.900
200	−0.794	−0.763	−0.789	---
500	−0.789	−0.738	−0.789	---
mean	−0.790	−0.761	−0.800	−0.880
RSD,%	0.4	1.5	1.2	2.0

--- RVC Microelectrode ---

scan rate	$E_{i=0}$, V	$E_{p,a}$,V	E_r,V (Cd)	E_r,V (H_2O)
10	−0.789	−0.761	−0.832	−0.870
20	−0.789	−0.758	−0.837	−0.870
50	−0.789	−0.758	−0.844	---
100	−0.791	−0.763	−0.859	---
200	−0.789	−0.758	−0.875	---
500	−0.786	−0.743	−0.885	---
mean	−0.789	−0.757	−0.855	−0.870
RSD,%	0.2	0.9	2.5	

Table 1. Cyclic Voltammogram Characteristics. Platinum and RVC microelectrodes, 3.3 mM Cd^{2+} in 33% SCABE. All potentials vs SCE and scan rates in mV/s. $E_{i=0}$, V is the potential at which the current first becomes zero during the anodic sweep (see Figure 2). $E_{p,a}$,V is the potential at peak anodic (stripping) current. E_r,V (Cd) is potential for start of cadmium reduction. E_r,V (H_2O) is potential for start of water reduction.

an 85 mV disparity at 500 mV/s. It appears that in this electrolyte, the nucleation overpotential for the reduction of cadmium on RVC could be as much as 30 mV more negative than that for the reduction of cadmium on platinum.

1.4.1.1. RVC Scan Speed–Overpotential Dependence. Our first comment in this section is that the reduction potential for cadmium at RVC appears to be more positive for slower scan rates than it is for faster scan rates (Table 1). Second, we note that our definition of reduction potential is "the potential corresponding to a significant increase in cathodic current above the background of the cathodic CV scan". Third, we point out that implicit to our definition of reduction potential is the linear potential sweep of cyclic voltammetry. We believe that the observed relation of reduction potential and scan rate is the result of a slow nucleation rate for the deposition of a solid product on a vitreous carbon electrode.

Hills, et al, (1974) and Astley, et al, (1968) performed *potential step* experiments and observed the initial current *increasing* with time for periods of up to a minute. The length of time the current increased was inversely related to the size of the potential step. In all cases, the current ultimately decreased with time as we expect when nucleation ceases and current is only from the growth of already nucleated sites. Hills, et al, (1974) observed this phenomenon for the reduction of mercury in 1M potassium nitrate at a vitreous carbon electrode.

We maintain that in our experiments at the RVC electrode, the growth in cell current is dominated by the rate of nucleation. In the case of a potential step experiment, the number of nucleated sites on

an electrode surface is related to the product of the nucleation rate and the length of time that the electrode has been at the nucleation potential. In the case of a potential sweep, the dependence of nucleation rate on potential makes our prediction of the number of nucleation sites more complicated. We can, however, compare the relative number of nucleation sites in two experiments which differ only in the rate of the potential sweep (Table 1). The slow-scan experiment will have more nucleated sites (larger current) at any given potential because the electrode will have been at a nucleation potential for a longer time.

1.4.1.2. Nucleation Overpotential and Crossed CVs. The slow rate of nucleation can also explain the loops that are observed at the negative switching potential in some cyclic voltammograms. Hills et al, (1974) reported that "there is a distribution of nucleation sites ... which nucleate at different overpotentials". They give as an example a 100 mV distribution for the nucleation of silver on platinum.

In our CV experiments, the potential is swept through the range of potentials required for nucleation. At the negative limit of the potential sweep, nucleation sites may still remain because of the significant time required to achieve full nucleation. Even though the potential sweep has changed direction, cell current can continue to increase because of continuing nucleation on the electrode. The result of continuing nucleation at the time of change in direction of potential sweep is the loop shown in the cyclic voltammograms of Figure 5.

1.4.2. Nernstian Concentration Dependence. For the purposes of this section, the *potential for the start of reduction* is

defined as the potential at which the trace of the cathodic sweep of the CV (50 mV/sec) is perceived by visual inspection to be above the extrapolation of the trace of the charging current background. Figure 6 is a plot of the potential for the start of cadmium reduction versus the log of the cadmium concentration, and the slope is −57.4/2 mV/decade. Figure 7 is a plot of the potential at which the anodic sweep crosses through zero current and has a slope of −56.0/2 mV/decade. These two slopes are in reasonable agreement with the value of 58/2 mV/decade calculated from the Nernst equation for a system operated at about 20 degrees Celsius. Even though deposition of solid products at the RVC electrode has the complication of nucleation overpotential, the prediction of the Nernst equation appears to be valid. We can assume that the reduction potential for cadmium will change at the nominal rate of 59/2 mV per decade of changing concentration, and the hydrogen reduction potential will change at the rate of 59 mV per decade of hydrogen ion concentration.

1.4.3. Electrode Pretreatment. Electrode pretreatment is the common name for the process polishing, cleaning and activating or deactivating an electrode's surface before its use as an analytical working electrode (Kazee et al, 1985). The purposes for pretreating glassy carbon electrodes, for example, are to remove adsorbed impurities from the surface, improve the reproducibility of measurements and to increase the electron transfer rate of the electrode reaction (Hoogvliet et al, 1986). Typical electrode pretreatment procedures involve mechanical polishing followed by an electrochemical pretreatment of the electrode surface.

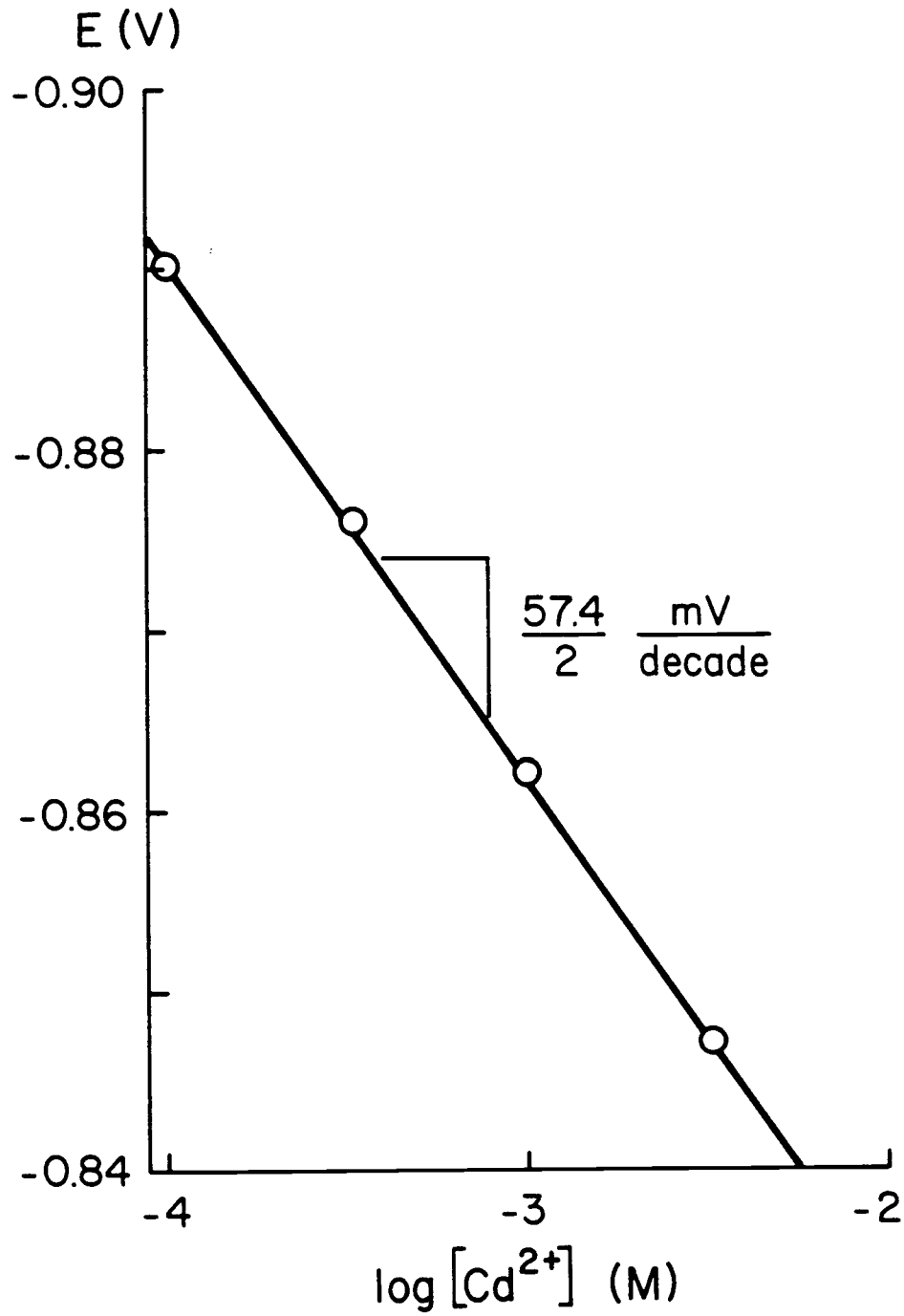

Figure 6. RVC Nernstian Concentration Dependence. Cadmium Reduction Potential vs Cadmium Concentration.

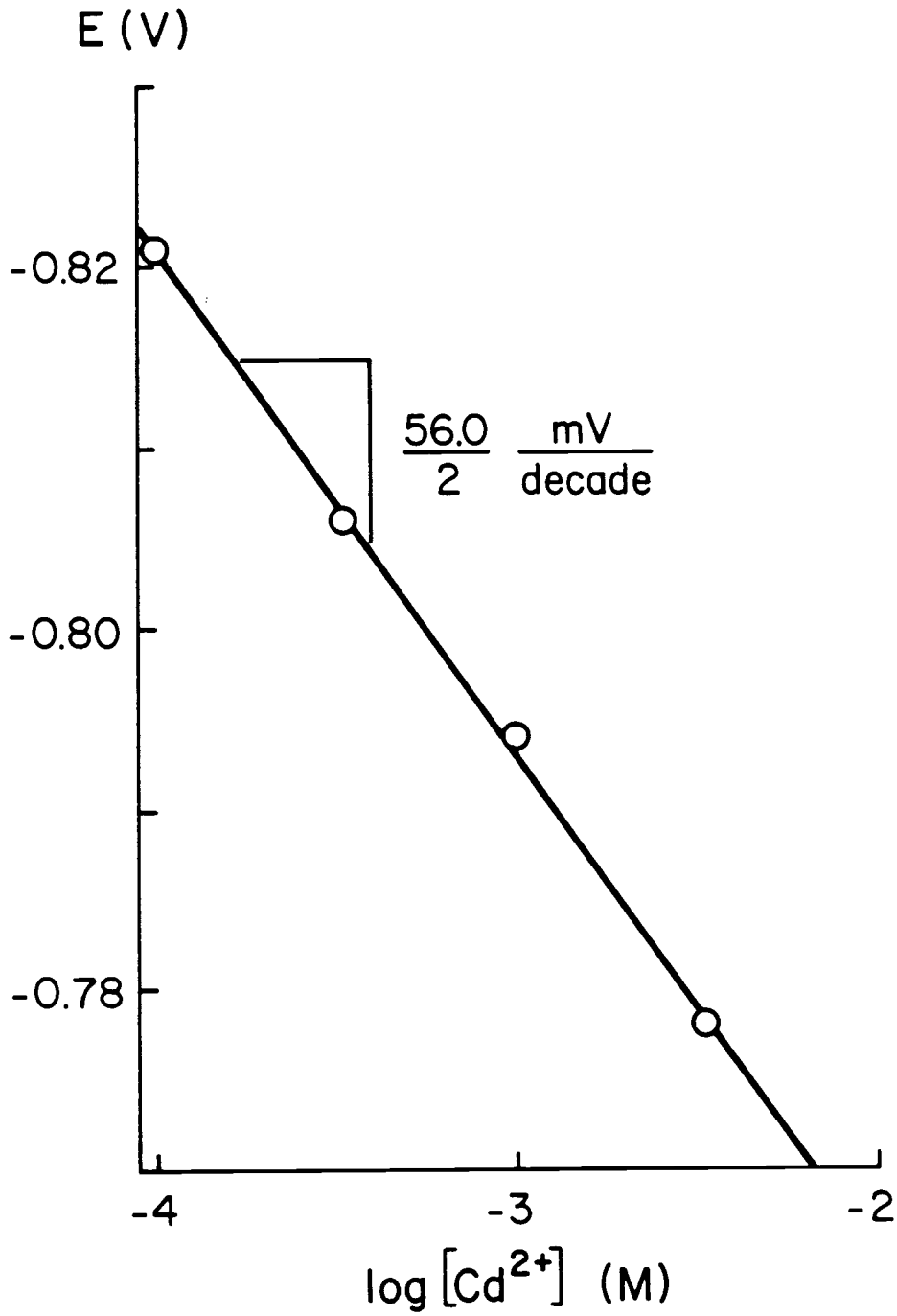

Figure 7. RVC Nernstian Concentration Dependence. Potential where anodic sweep of cyclic voltammogram first reaches zero current vs cadmium concentration.

Sleszynski and Osteryoung (1984) pretreated their RVC electrode by polishing it with decreasing alumina grit sizes, ending with a 0.05 μm size. Then they cycled the electrode between the anodic and cathodic limits of the electrolyte which they had chosen for their application. Their purpose for cycling the electrode was "to reduce background currents to a lower, constant value". Blaedel and Wang (1979–a) used a similar polishing procedure and then cycled the electrode between the anodic and cathodic limits of the electrolyte, holding for ten minutes at each extreme. In another study, Wang and Dewald (1982) expanded the "hold time" to 90 minutes at each extreme for the initial pretreatment, and recommended a daily pretreatment of two minutes at each extreme for three cycles. It appears from the diversity of the methods in these examples that there is no "method of choice".

The following experimental work in electrode conditioning came about during the investigation of the potential limits of the RVC electrode in several different electrolytes. This work resulted in frequent electrode passivation which required subsequent electrode pretreatment.

The first method of electrode pretreatment was to polish the microelectrode with metallurgical polishing equipment and a series of decreasing grit abrasive papers and alumina–water slurries, with a final slurry of 0.05 micrometer alumina. The response of the electrode after this polishing procedure is shown as line ***b*** in Figure 8. The approximate doubling of electrode response per hour of use is very unsatisfactory.

A second method was to polish the electrode manually with

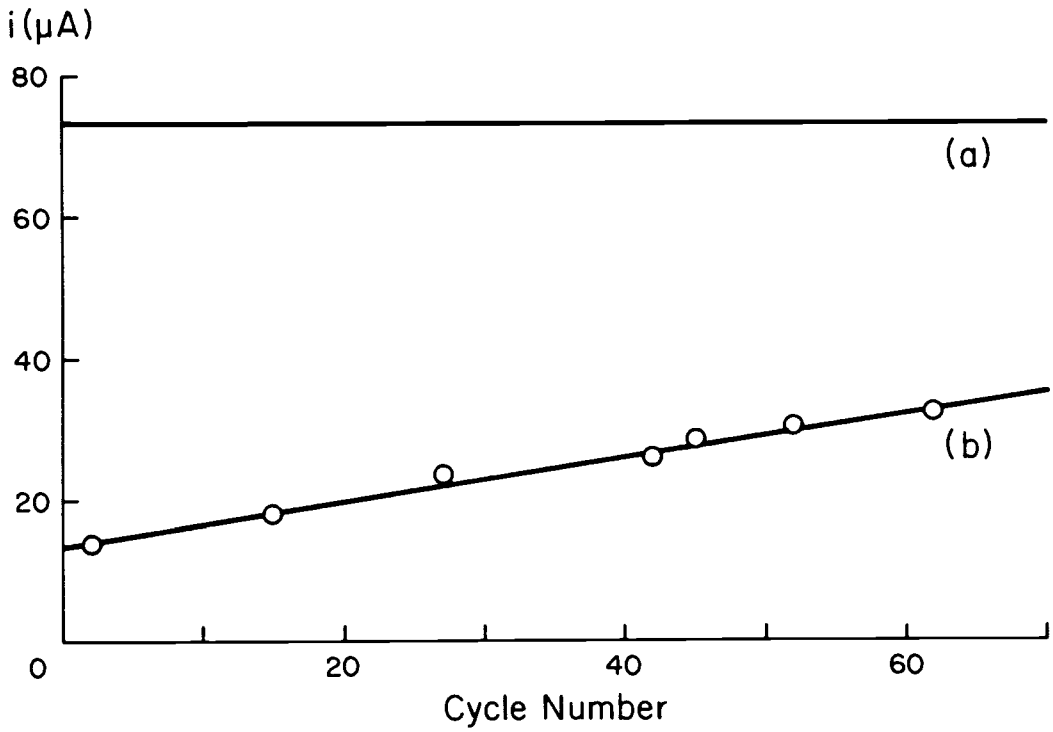

Figure 8. RVC Electrode Pretreatment. RVC microelectrode operated continuously for 60 CV cycles. 3.3 mM Cd^{2+} in 33% SCABE. Scan speed 50 mV/s, 68 s/cycle. (a) Manual polishing on film sheets, and (b) metallurgical polishing equipment.

Aluminum Oxide Lapping Film Sheets (Mark V. Laboratory, Inc., East Granby, Conn. 06026). The lapping sheets were laid flat on a table top and the electrode surface was immersed in a puddle of distilled water on the sheets. The electrode was moved by hand over an imaginary one to two inch diameter circle. A slight down force was applied to the electrode during polishing, and the electrode was kept wet during all polishing. The progression of abrasive sizes used in manual polishing was 30, 12, 3 and 0.3 microns.

This method of polishing consistently gave an electrode surface which was immediately and reproducibly more responsive than the electrode surface which was polished with slurried alumina. The electrode response shown as line **a** in Figure 8 was constant for over 90 minutes.

We believe that the two important factors responsible for the dramatic difference in the response of the electrode are 1) the clean environment and 2) the lower force and velocity of the manual polishing method. The manual method is cleaner because it does not have the unbound abrasive and silk fibers inherent in metallurgical polishing. Since the manual method requires the person doing the polishing to a) coordinate maintaining a vertical orientation and moving the electrode around the imaginary circle, b) provide a downward force and c) avoid fatigue, the tendency is to apply only a slight downward force and move the electrode at about 120 RPM. In contrast, the metallurgical polishing wheel rotates at 550 RPM and all the operator has to do is maintain vertical alignment, so the tendency is to provide a large downward force. The net result, we speculate, is that the electrode

surface is contaminated with abrasive and silk fiber particles during metallurgical polishing. This contamination does not occur during manual polishing because the method is inherently cleaner and does not involve as much force. This explanation is supported by Kazee et al (1985), who discuss incorporation of "deagglomerating" agents and contaminants from abrasion of polishing cloths into a carbon microparticle layer. Their article is recommended as a starting point for further study of the subject of electrode conditioning.

1.4.4. Appropriate Electrolytes. Cadmium reduction tends to occur toward the negative limit of most aqueous electrolyte systems; the reduction potential for cadmium approaches or exceeds the reduction potential for hydrogen ion under some circumstances. This section reports the suitability of several common aqueous electrolytes for the reduction of low concentrations of cadmium.

1.4.4.1. Sodium Chloride Acetate Buffer Electrolyte (SCABE). This is categorically the best electrolyte found. Typical concentrations were 33% SCABE, ie 0.33 M chloride, 0.33 M total acetate, and over 0.33 M sodium. This electrolyte is a pH buffer (pH 5.0 – 5.5).

1.4.4.2. Sodium Fluoride. Fluoride concentrations of 0, 10, 50, 100, 500, 1000 mM showed no measurable effect on the response to cadmium in SCABE, indicating that fluoride is not influencing the reduction of cadmium by complexation.

1.4.4.3. Potassium Nitrate. Potassium nitrate solutions are unacceptable electrolytes for work with cadmium because the *nitrate completely*

depolarizes the RVC electrode at about −0.8 V vs SCE, obscuring any reduction of cadmium. The nitrate electrolyte does not seem to damage the electrode because the response returns in SCABE. The use of nitrate ion as an electrode depolarizer is discussed further by Bard and Faulkner (1980, Figure 10.4.3 and page 386).

1.4.4.4. Negative Potential Extreme. The nucleation overpotential for cadmium forces the reduction of cadmium at the RVC electrode towards the negative limit for this electrode. As the concentration of cadmium is reduced, the cadmium reduction potential approaches the negative limit at a rate of −59/2 mV per decade. Under this scenario, the limiting factor in detection of cadmium at a RVC electrode will be the negative limit to which the electrode can be operated in a given electrolyte. Figure 9 is a demonstration that an RVC microelectrode can be operated at −1.1 V vs SCE.

1.4.5. Dissolved Zirconium Matrix. The only acid which dissolves zirconium is hydrofluoric acid. Typical alloys of zirconium contain 1.5% tin, which forms an oxide coating in HF and does not dissolve. This oxide coating is removed by the addition of nitric acid or hydrogen peroxide to the solution when the dissolution reaction rate slows or stops. Hydrogen peroxide was the reagent of choice because of the known problems with nitrate. The unexpected result of hydrogen peroxide addition was a very high background in CVs of these solutions. We will see that only the minimum amount of hydrogen peroxide should be used to facilitate the dissolution of zirconium alloys.

1.4.5.1. Excess Hydrogen Peroxide. A zirconium alloy was dissolved as

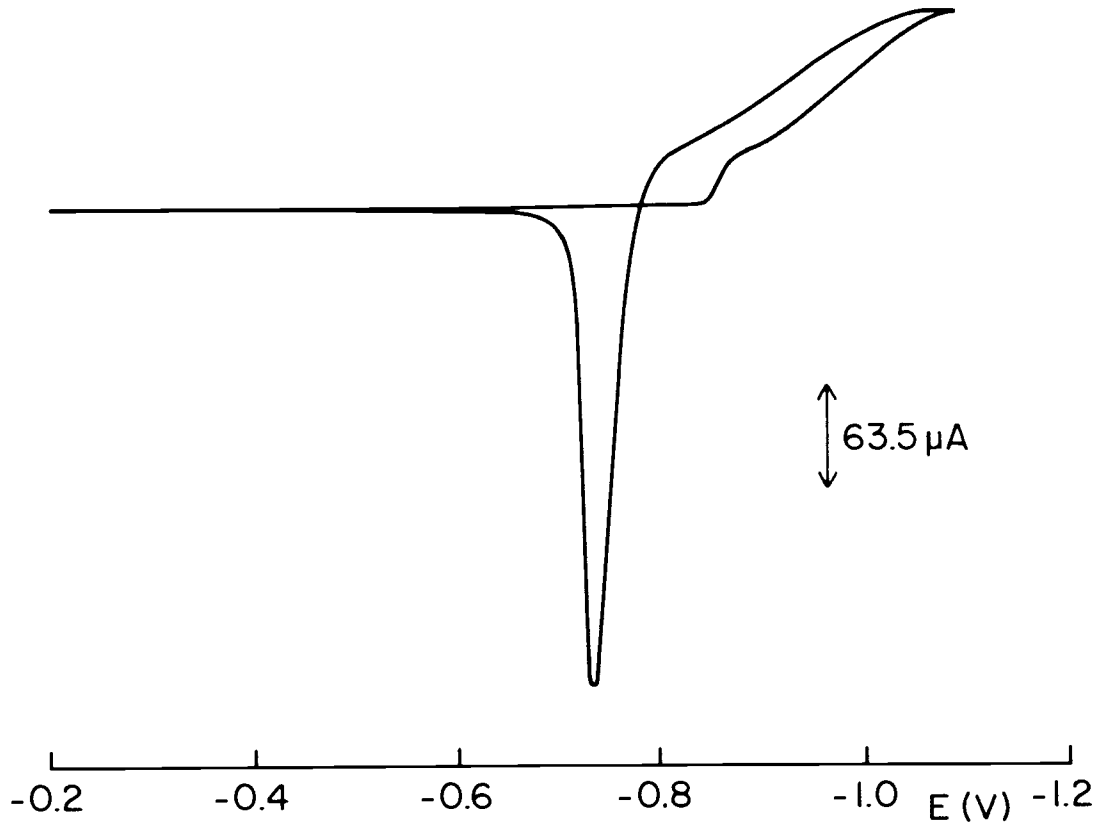

Figure 9. RVC Cyclic Voltammogram at Negative Limit. 3.3 mM Cd^{2+} in 33% SCABE, 50 mV/s, RVC Microelectrode.

described in section 1.1.3.1, with the exception that excess hydrogen peroxide was added to complete the dissolution of tin. The pH of the solution was then raised to about pH = 3, as discussed in section 1.1.3.1.

A very high background current from this electrolyte masked 20 mM cadmium CV peaks. One could observe cadmium stripping peaks with Anodic Stripping Voltammetry (ASV) with a 40 second plate time at −0.8 V vs SCE and a 20 mV/s stripping sweep, as shown in Figure 10. The small peak near −0.74 V and the very high background are attributed to excess hydrogen peroxide.

1.4.5.2. Minimal Hydrogen Peroxide. A second zirconium electrolyte was prepared as described in the previous section except that only a minimum amount of 20% hydrogen peroxide was added. The slow, dropwise addition of hydrogen peroxide ceased as soon as all of the black tin−oxide particles were dissolved. Figure 11 shows the CV response to 20 mM cadmium in this electrolyte. The reader should note that Figure 11 shows CVs and Figure 10 shows ASVs: The conservative addition of hydrogen peroxide allows us to see a cadmium stripping peak with CV rather than ASV. The conservative addition also reduced the background enough to allow the cathodic sweep to continue −0.1 V more negative.

1.4.6. Mercury Coated RVC. As discussed in the introduction, hydrogen reduction at a mercury coated RVC electrode is expected to occur a potential which is more negative than for a bare RVC electrode. The potential for reduction of cadmium and other amalgam forming metals is expected to be more positive for a mercury coated

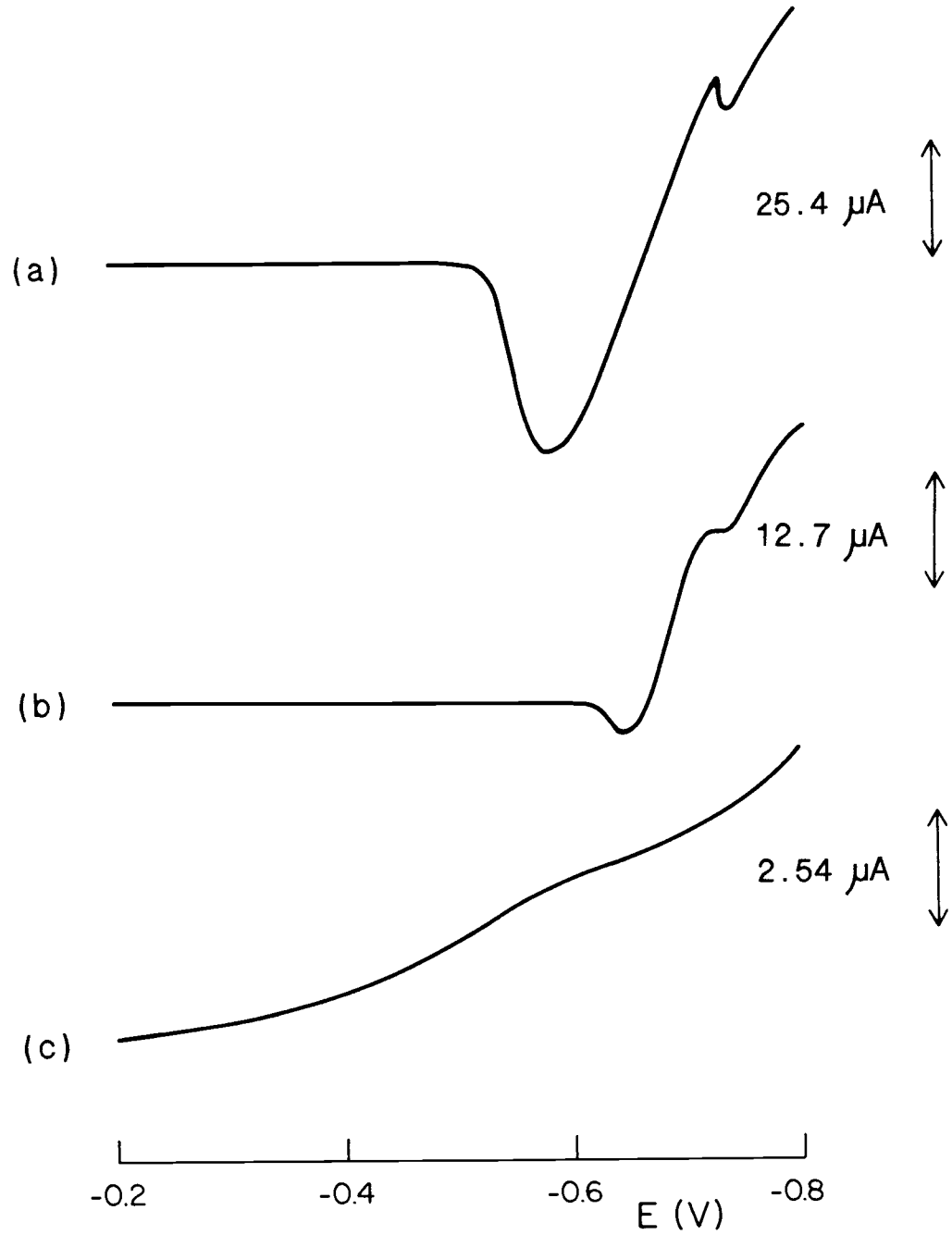

Figure 10. RVC Anodic Stripping Voltammograms, Cd in Zr. Electrolyte: 0.12 M Zr, 0.7 M HF, 0.092M NaOH + H_2O_2 (see text). 40 s plate, 20 mV/s strip. (a) 20 mM Cd^{2+}, (b) 10 mM Cd^{2+}, (c) Cd^{2+} blank.

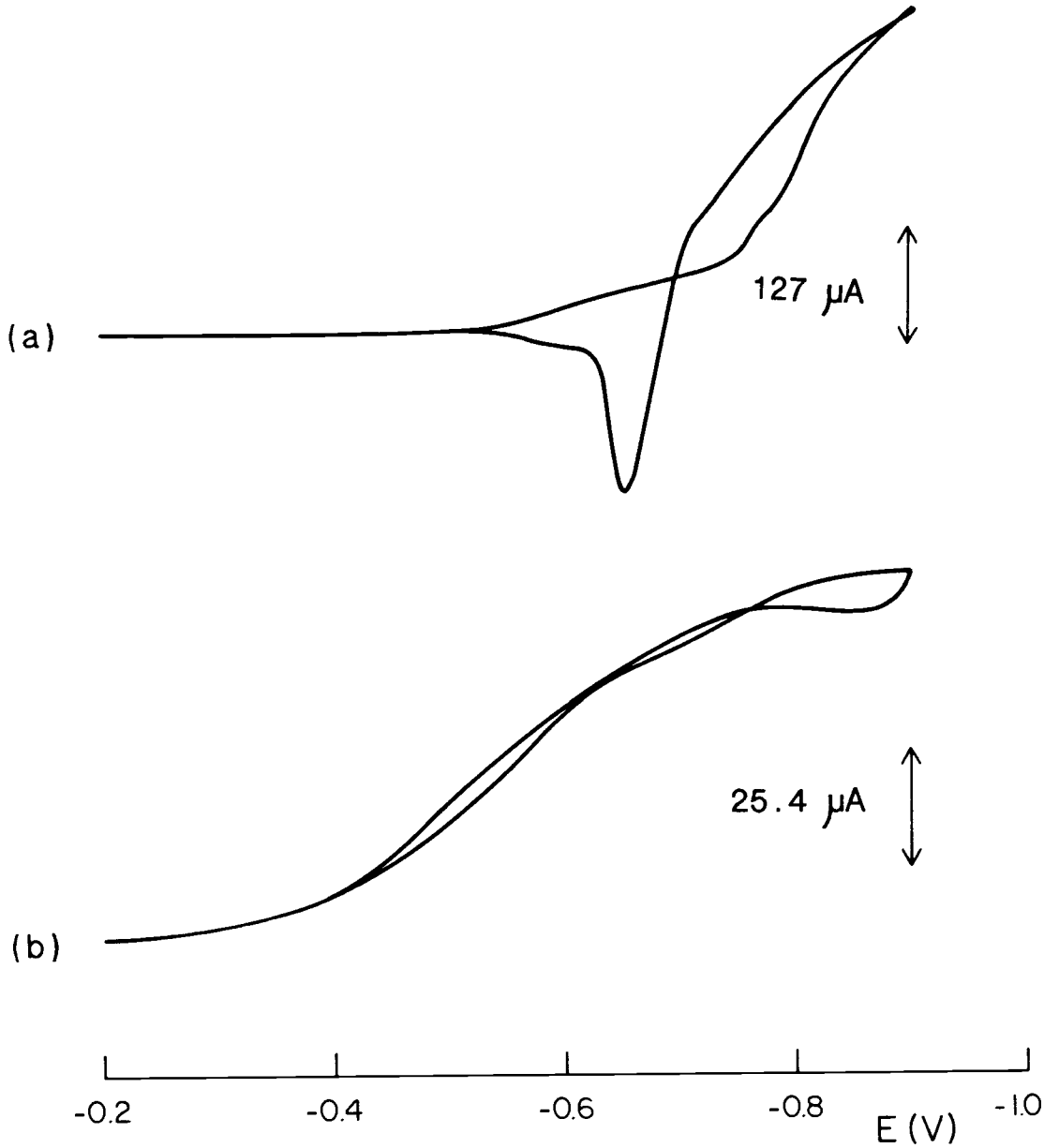

Figure 11. RVC Cyclic Voltammograms, Cd in Zr. Electrolyte: 0.12 M Zr, 0.7 M HF, 0.092M NaOH + minimum H_2O_2 (see text). 20 mV/s scan. (a) 20 mM Cd^{2+}, (b) Cd^{2+} blank.

electrode than for a bare RVC electrode. We will see that the reduction potential for cadmium and lead are lowered by coating an RVC surface with mercury. We will also see that the mercury coating forms as droplets rather than a thin film. The hydrogen overpotential we expect from mercury coating is not observed for RVC coated with droplets of mercury.

1.4.6.1. Shifts in Potential With a Mercury Coated RVC. Reduction potentials for cadmium in SCABE were observed to be 100 mV more positive at a mercury coated RVC electrode than at a bare RVC electrode. The same 100 mV shift towards the positive is seen for reduction of cadmium in a zirconium–fluoride matrix. Figure 12a, b and c are mercury coated RVC CVs of 3.3, 10 and 3.3 mM cadmium, respectively, in a dissolved zirconium matrix. Note that at the higher concentration of cadmium, the CV reverts to the nucleation overpotential crossover character of the non–mercury coated RVC. Apparently the majority of the reduction occurs on RVC rather than mercury at the higher concentration. This observation suggests either a concentration related nucleation phenomena or that the solubility of cadmium in the mercury was exceeded and further nucleation occurred at RVC rather than at saturated mercury. Note also that there is little if any evidence for a more negative reduction potential for hydrogen.

1.4.6.2. The Nature of the Mercury Coating. Figures 13 and 14 are scanning electron microscope (SEM) images of RVC before and after mercury plating, respectively. These pictures show mercury deposited as droplets on the RVC surface, confirming the many individual

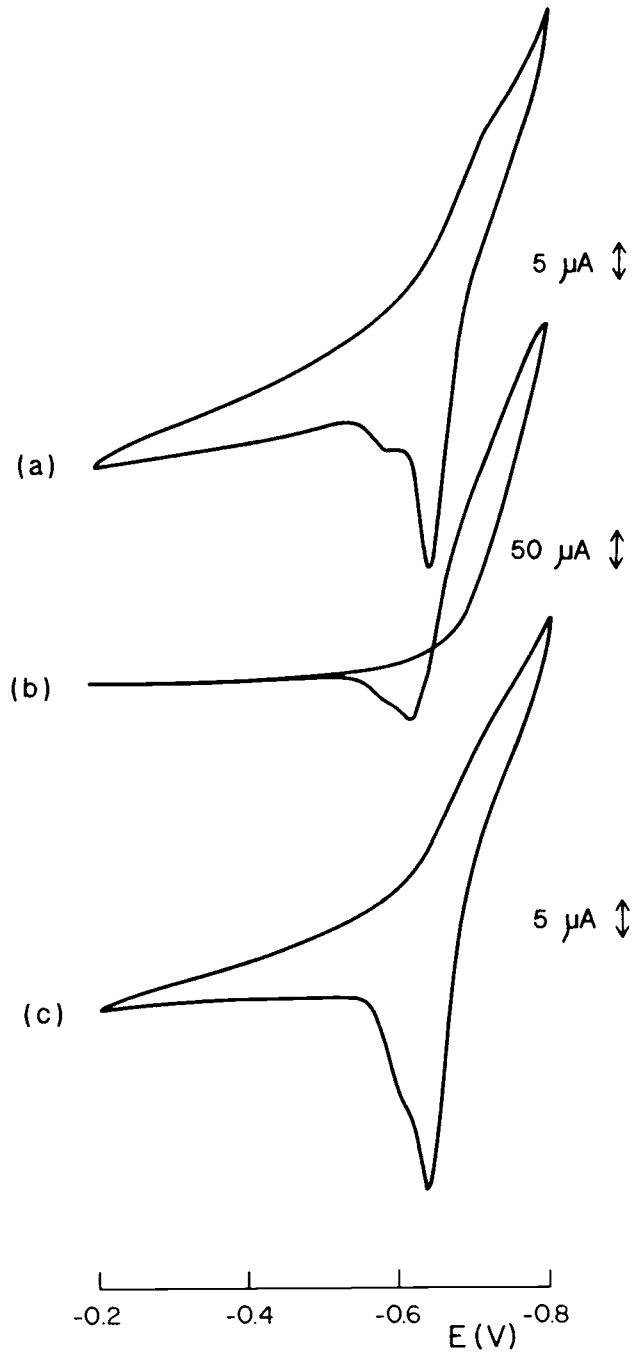

Figure 12. Mercury Plated RVC Cyclic Voltammograms, Cd in Zr. Electrolyte: 0.12 M Zr, 0.7 M HF, 0.092M NaOH + minimum H_2O_2 (see text). 50 mV/s scan. (a) 3.3 mM Cd^{2+}, (b) 10 mM Cd^{2+} and (c) 3.3 mM Cd^{2+}.

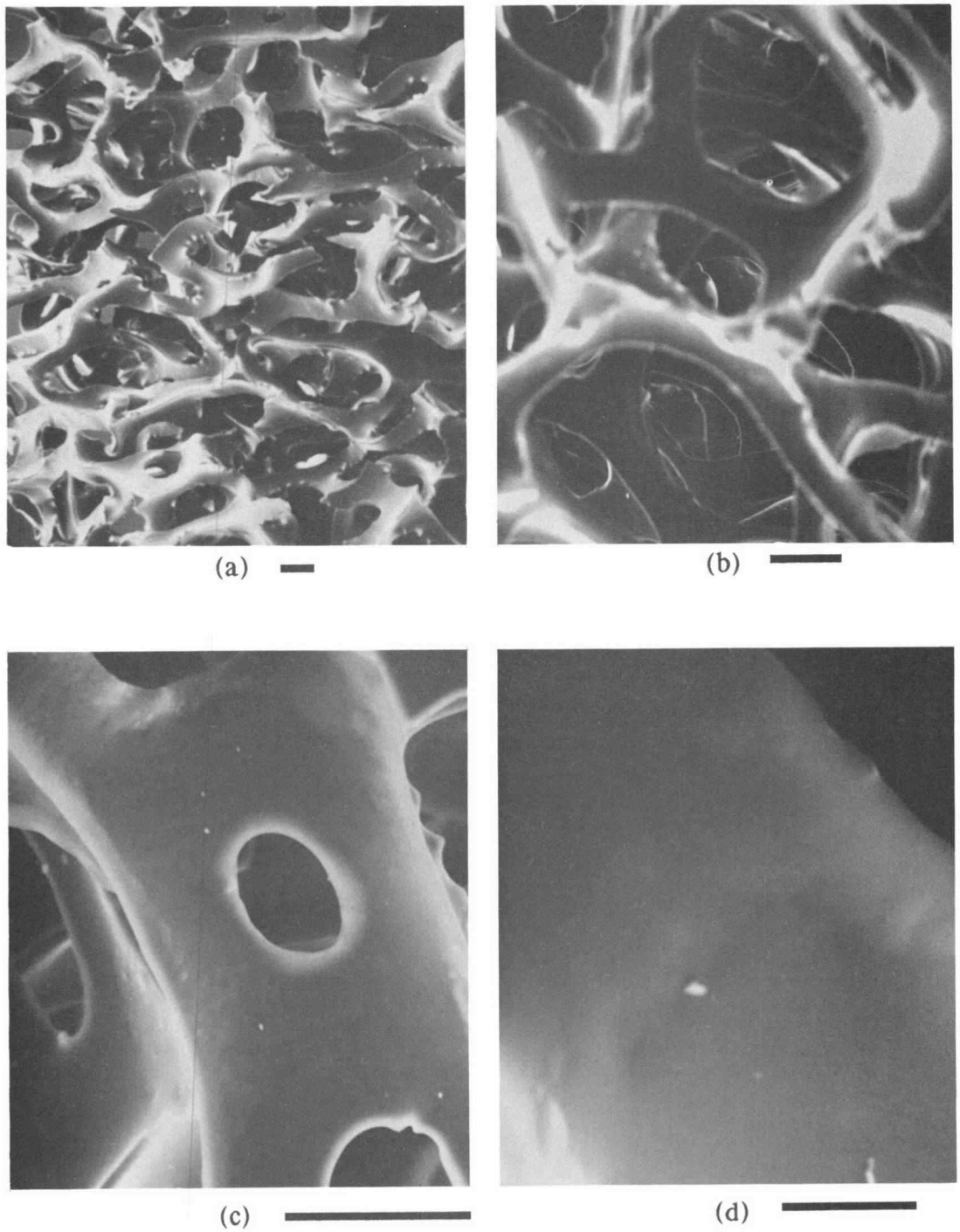

Figure 13. Scanning Electron Micrograph of Bare RVC. Magnification and bar length, microns respectively are (a) 52X, 100, (b) 108X, 100, (c) 280X, 100 (d) 2000X, 10.

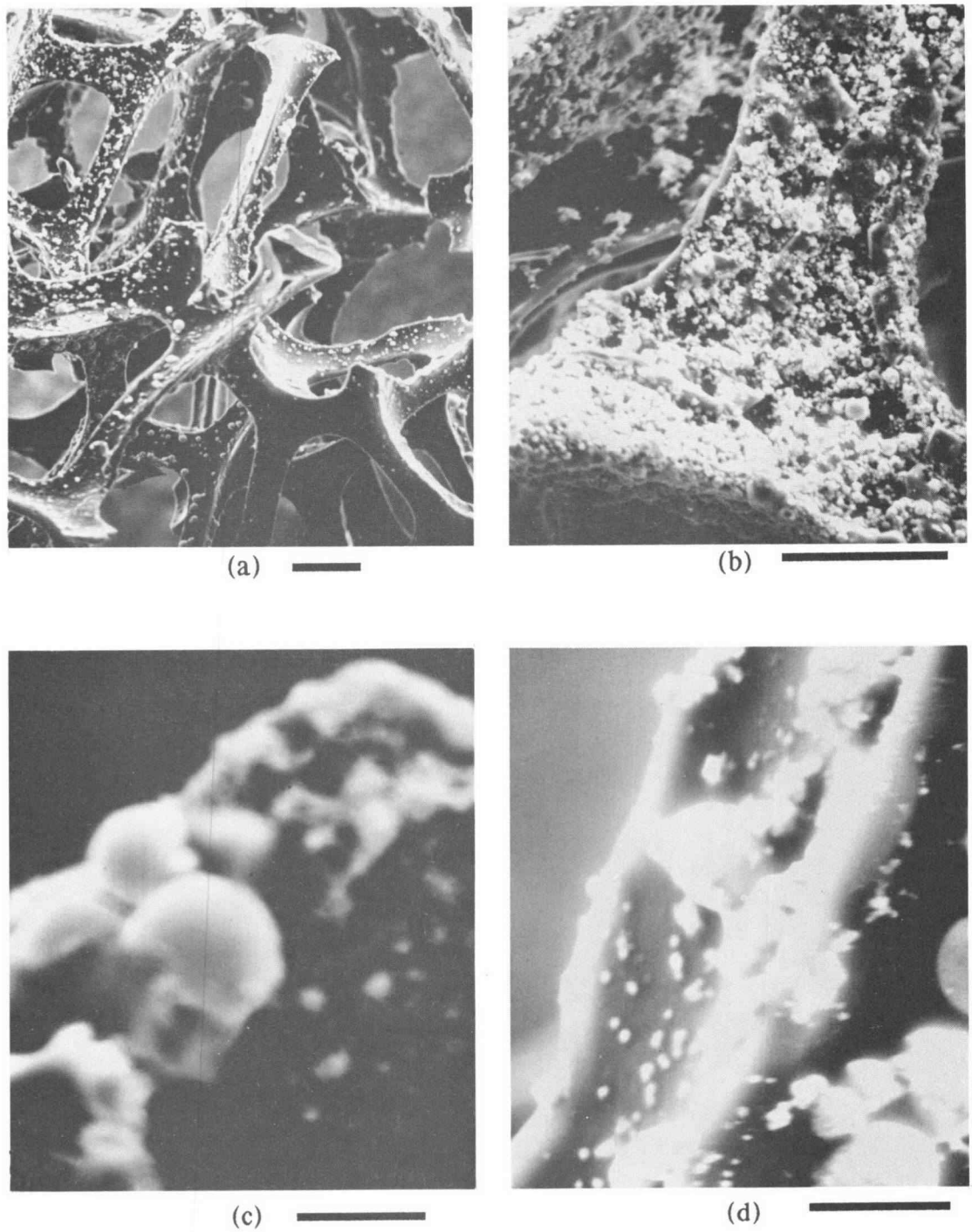

Figure 14. Scanning Electron Micrograph of Mercury Plated RVC. Magnification and bar length, microns respectively are (a) 103X, 100, (b) 492X, 50, (c) 1920X, 10, (d) 2040X, 10.

nucleation sites concept reported by Hills et al (1974). Hoyer et al (1987), Wang et al (1987), Sottery et al (1987) and Stulikova (1973) have also reported that mercury plated on carbon substrates forms as droplets. It is thus reasonable for nucleation of cadmium to take place at RVC as well as at mercury, and there is no guarantee that mercury droplets on a RVC electrode will retard hydrogen reduction from the RVC surface. Obviously the concept of a thin mercury film does not apply until the RVC surface is completely covered. Further investigation is indicated.

1.4.7. Copper and Lead CVs. Before we leave the discussion of the micro–RVC electrode, it is worthwhile to report the CVs obtained from copper, lead and lead plus cadmium, Figure 15, each in 33% SCABE. The copper CV, Figure 13a, is interesting because it exhibits both soluble and insoluble reduction product characteristics; the oxidation of copper metal to Cu[I] shows the characteristic sharp peak (and nucleation overpotential related crossover), while the oxidation of Cu[I] to Cu[II] shows the typical rounded shape attributed to diffusion limited current arguments in the theory. This CV is also an excellent example of hemispherical diffusion limited reduction current because of the two distinct plateaus. The lead CV, Figure 13b, is another example of the typical shape attributed to deposition of a solid reduction product. The mixture of cadmium and lead CV, Figure 13c promotes speculation about lead nucleation sites and separate cadmium nucleation sites, the activity of lead at a cadmium nucleation site and vice versa, and the significance of intermetallic effects.

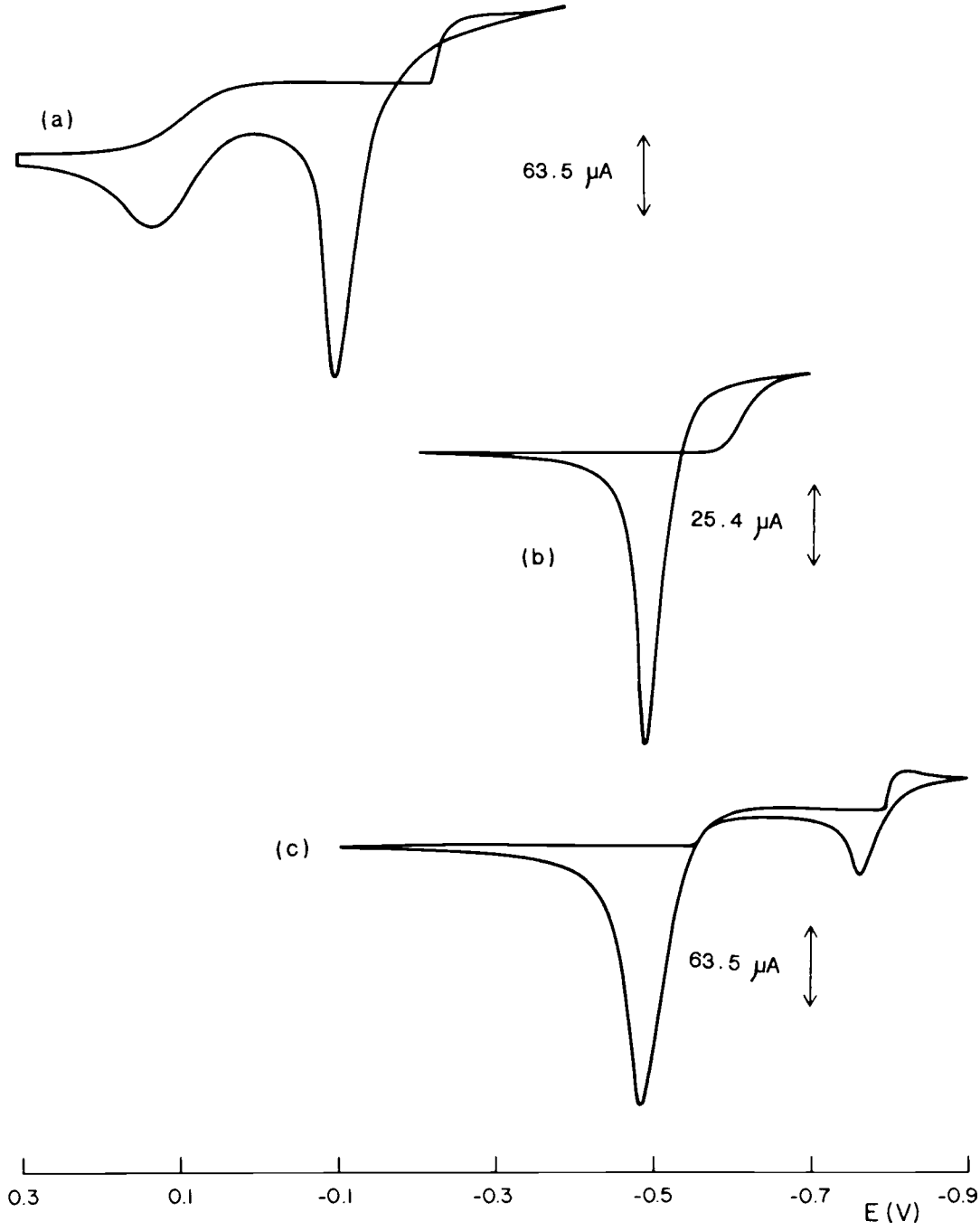

Figure 15. RVC Cyclic Voltammograms, Cu, Pb and Pb+Cd. Electrolyte is 33% SCABE. (a) 3.3 mM Cu^{2+}, 2 mV/s, (b) 3.3 mM Pb^{2+}, 20 mV/s, (c) 3.3 mM Pb^{2+} + 3.3 mM Cd^{2+}, 50 mV/s.

1.5. CONCLUSIONS

The microelectrode fabricated here from RVC is suitable for the reduction of cadmium in a number of electrolytes, including a sodium–chloride–acetate buffer and zirconium dissolved in hydrofluoric acid. The cyclic voltammetry studies which resulted in the formation of solid products at this electrode agree with the CV theory developed by Schiffrin (1986) with two notable exceptions. Schiffrin assumes in his theory that the transition from bare electrode to an electrode with a monolayer of reduced species occurs instantaneously, and that there is no nucleation overpotential at the solid electrode. The work here demonstrates that for RVC, there is a significant nucleation overpotential and the nucleation is relatively slow. The slow nucleation process explains why current can continue to increase after CV scan reversal, and why the CVs can cross the themselves.

The potential at which the reduction current of cadmium at RVC is significantly above the baseline follows a Nernstian concentration dependence (Figure 6). The slow nucleation kinetics observed at RVC mean that reduction potentials appear to be scan rate dependent. At a scan rate of 10 mV/s, the overpotential for cadmium is −30 mV more negative at the RVC electrode than for the platinum electrode, Table 1. The reduction of water at both platinum and RVC starts at about the same potential (−870 mV) in 33% SCABE, Table 1.

A method of electrode pretreatment has been discovered which is simple, quick and does not require any electrochemical pretreatment. The pretreatment is simply to manually polish the electrode with commercially available lapping film papers.

Potassium nitrate solutions are unacceptable as electrolytes because of electrode depolarization near the cadmium reduction potential. Similarly, hydrogen peroxide is electroactive at RVC, producing background currents in the area of cadmium reduction. A sodium chloride acetate buffer electrolyte (SCABE) allows the RVC microelectrode to be used up to a negative limit of about −1.1 V vs SCE, Figure 9, but this *limit* is loosely defined.

The RVC electrode is suitable for reducing cadmium at millimolar concentrations in properly prepared aqueous acidic zirconium-fluoride solutions. The concentration of zirconium in the properly prepared solution is 0.11 M, which is a concentration suitable for use in plasma emission spectrochemical equipment. In addition the solution should be prepared without nitric acid, with a minimum of hydrogen peroxide, and the pH should be raised to about 3.

If the RVC is coated with mercury, the response to cadmium is improved because of the reduced interference from hydrogen reduction. In this particular application, the potential for reducing cadmium at a mercury surface is about 100 mV more positive than for the RVC surface. Since the negative potential required for cadmium reduction is lower for mercury coated RVC than it is for bare RVC, the hydrogen reduction is less of an interference at the mercury coated RVC electrode.

We have found no evidence that the reduction potential for hydrogen is changed by a mercury coating on an RVC electrode. The mercury coatings observed in this work were individual hemispheres on the mercury surface rather than a uniform, thin film. Since our mer-

cury coated RVC still had bare RVC exposed to the electrolyte, we are not surprised that the reduction potential for hydrogen was unchanged by the mercury coating.

The proper ratio of mercury to cadmium and the degree of mercury coverage over the RVC surface are non–trivial and closely related considerations.

PART 2: DEVELOPMENT OF A FLOW-CELL

2.1. INTRODUCTION

The ideal flow-cell for preconcentration of cadmium would plate 100% of the cadmium in a flowing stream, occupy a minimum volume, and allow all the plated cadmium to be stripped into a minimum volume of electrolyte to produce a high concentration plug of cadmium in the electrolyte. Unfortunately, this author was unable to find a comprehensive description of the theory of flow-cell design which directly addresses these issues or which discusses practical flow-cell operation.

The reduction of cadmium but not hydrogen requires *first* of all an appropriate set of conditions, one of which is that we have more than the minimum detectable concentration of cadmium[II] and less than the maximum allowable concentration of the interfering hydrogen ion. These concentration limits are dependent on the formal reduction potentials for cadmium and hydrogen. Another condition is that we have a working electrode which is compatible with our analyte and electrolyte. We are considering RVC or mercury coated RVC for the working electrode material, and we have already seen that these two electrode materials introduce overpotential and underpotential phenomena which affect the selection of appropriate conditions.

Assuming we have a set of appropriate conditions as outlined above, we soon discover the *second* problem in reducing cadmium but not hydrogen: uncompensated potential drop, iR_u, which results from three things: 1) the cell's current; 2) the electrolyte's resistance, and 3)

the many different current *paths* inherent in a three dimensional working electrode. As an introductory illustration, we borrow a common conceptual development made for a three electrode cell with a planar working electrode. In the planar electrode case, the source of uncompensated potential drop is shown in Figure 16. We see from this diagram that to obtain the minimum uncompensated potential iR_u, the reference electrode should be placed *as close as possible* to the planar working electrode. This strategy for obtaining the minimum iR_u is conveniently described as placing a point (the reference electrode) as close as possible to a plane (the working electrode).

Reducing the uncompensated potential drop in a three dimensional flow-cell is a non-trivial problem because the solution to the problem can no longer be described as "placing a point close to a plane". The plane has become a three dimensional object. The *point* can still be placed close to the three dimensional object, but that geometrical arrangement will describe only one electrolyte path with a minimum uncompensated potential drop. Since the working electrode is three dimensional, there will be an infinite number of electrolyte paths between the auxiliary electrode and the working electrode. All of these paths have *different* lengths. The extremes of these different path lengths are defined by the geometry of the flow-cell.

In terms of the degree to which we can control the potential applied to the interface between the electrolyte and the three dimensional working electrode, the reference electrode can be placed so that it monitors the shortest or the longest path length in the set of electrolyte path lengths between the auxiliary and working electrode. In

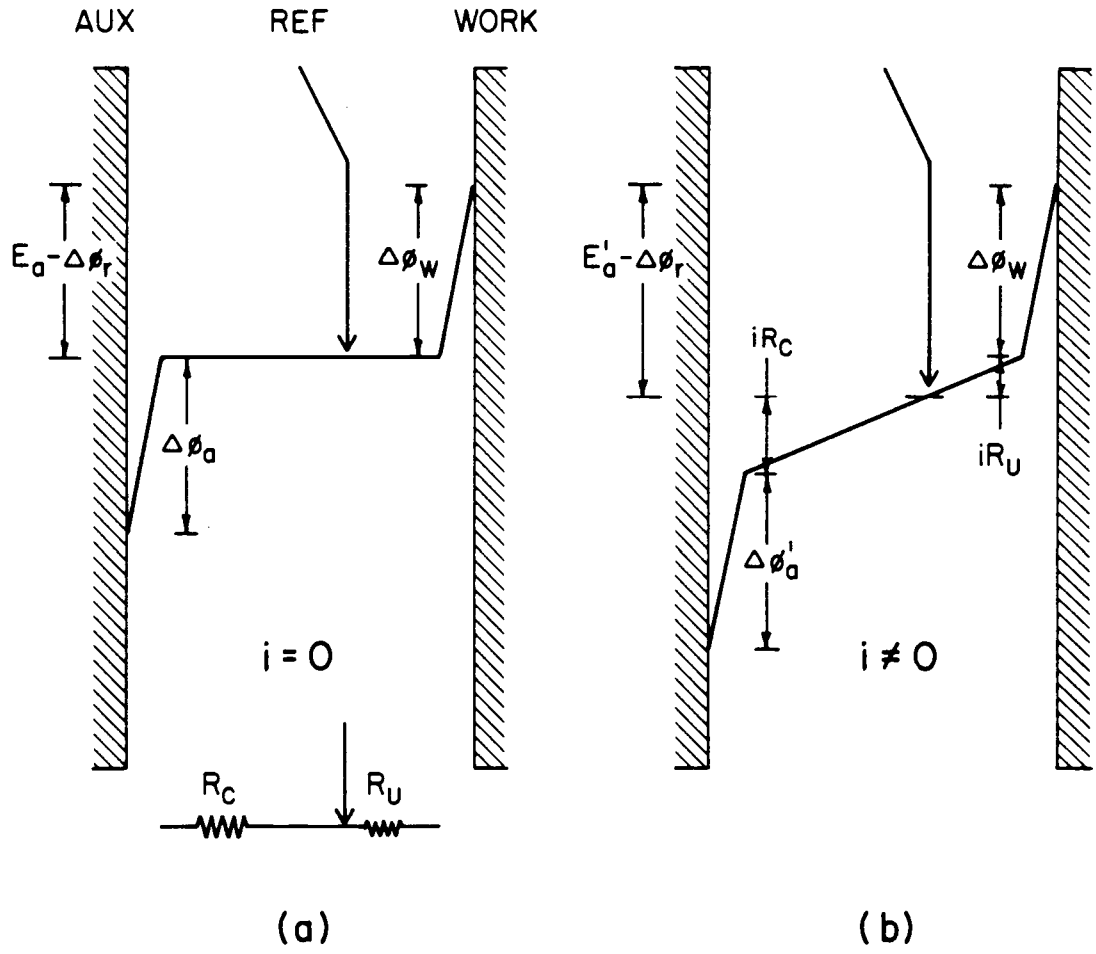

Figure 16. Potential Profiles in Planar Electrode System. (a) No uncompensated potential for no current. (b) When cell current flows, uncompensated iR drop becomes significant. Diagram after Hawkridge as Figure 6.5 in Kissinger & Heineman (1984).

either case, the potential of the electrolyte – working electrode interface will be distributed between the control potential at the reference electrode site and the control potential plus or minus the iR drop across the electrolyte. The magnitude of this difference in potential is a complicated function of the distribution of potential in the electrolyte and the distance from the "point" which the reference electrode is monitoring to the "point" on the working electrode surface. We will see that the magnitude of the difference in potential extremes of the electrolyte – working electrode interface is often large enough to cause reduction of hydrogen at one place when the potential for cadmium reduction has just been reached at another place.

We will find that the geometrical relationship between the auxiliary and the working electrode defines the limit to which we can control the potential at the working electrode – electrolyte interface in a three dimensional flow–cell. The actual position of the reference electrode has a much smaller effect on controlling this potential than the auxiliary – working electrode geometry.

In order to demonstrate the significance of iR_u, Part 2 reports on an evolution of flow–cell designs. Some negative results are reported in this section because they illustrate the difference in operation when one changes from *two–dimensional* planar electrodes to *three–dimensional* flow electrodes.

The initial approach to flow–cell design was to build a simple cell, evaluate it, then modify the design until the cell produced the desired results. After several design/evaluation cycles, it was evident that a theoretical analysis of the various sources of uncompensated potential

drop in the flow–cell would be necessary before further progress could be made.

The theoretical work suggested that a cell with cylindrical symmetry would significantly reduce iR_u in the electrolyte. Cylindrically symmetric electrodes were fabricated and improved cell performance was demonstrated. Additional testing of these cells indicated that the plumbing on the inlet and outlet ends of the flow–cell made a very significant contribution to the stability of the flow rate of electrolyte. Since the flow rate of the solution through the cell is one of the variables in the function which determines the current flowing through the cell, modifications to the flow system which made a more stable flow also made a more stable current output from the cell: "noise" in the current response of the cell was reduced by the improved plumbing.

2.2. EVOLUTION OF THE FLOW-CELL

2.2.1. Reference Electrode. The reference electrode was an Orion model 900100 single junction reference electrode operated with Orion's filling solution. The potential of this electrode is similar to that of a Saturated Calomel Electrode (SCE). Details of the electrode holder are presented in section 2.4.2.3: The Reference Electrode Holder.

2.2.2. Flow-Cell With Flag Auxiliary Electrode. The first flow–through working electrode, sketched in Figure 17, was designed to be compatible with available plumbing fittings. The RVC cylinder was nominally 3.2 mm diameter by 6 cm long. The fitting on one end was a hose barb (10–32 threads on one end, hose barb on the other) and

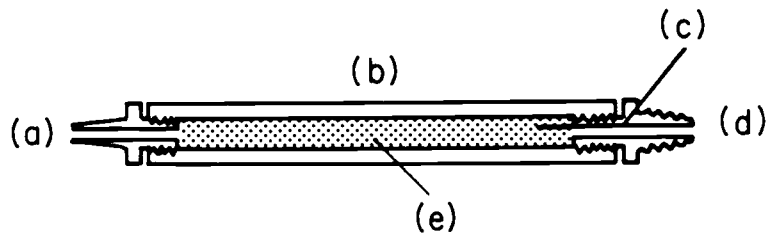

Figure 17. First Flow–Through Working Electrode. (a) Hose barb X 10–32 thread, (b) Teflon sheath, (c) Pt wire contact / connection to RVC, (d) 10–32 nipple, (e) RVC cylinder 3.2 mm X 6 cm.

the fitting on the other end was a nipple (10–32 threads on both ends). These two fittings and the RVC cylinder were connected with heat shrink FEP teflon tubing. Electrical contact with the RVC was made with a platinum wire inserted into one end of the RVC through a pre–drilled off–axis hole in the nipple. Continuity was checked by measuring the resistance between the platinum and a probe which was inserted through the hose barb to make contact with the RVC. This flow–through working electrode was connected on the nipple end to the reference electrode holder and on the barb end to a test solution reservoir, Figure 18. A platinum wire auxiliary electrode was connected on the other side of the reference electrode assembly.

A solution of 3.3 mM Cd^{2+} in 33% SCABE flowed through this cell while attempts were made to obtain CVs within a potential range of 0 to −1 V vs SCE. We expected cadmium reduction and stripping under these operating conditions because of previous demonstrations with the microelectrode, as shown in Figure 9. Unfortunately, no indication of cadmium reduction or stripping was observed.

We did not observe cadmium reduction because we inadvertently assembled a voltage divider which precluded reaching the cadmium reduction potential at the working electrode. The voltage divider was the result of electrolyte resistance and small–bore plumbing parts. The equivalent circuit in Figure 18 lists the resistance values which were calculated for each cell part in Appendix 1. The voltage divider sets the potential of the working electrode at 440/19700+440 = 0.022 of the potential applied by the potentiostat. Since the potentiostat is limited to 30 V, the maximum available potential at the working electrode would

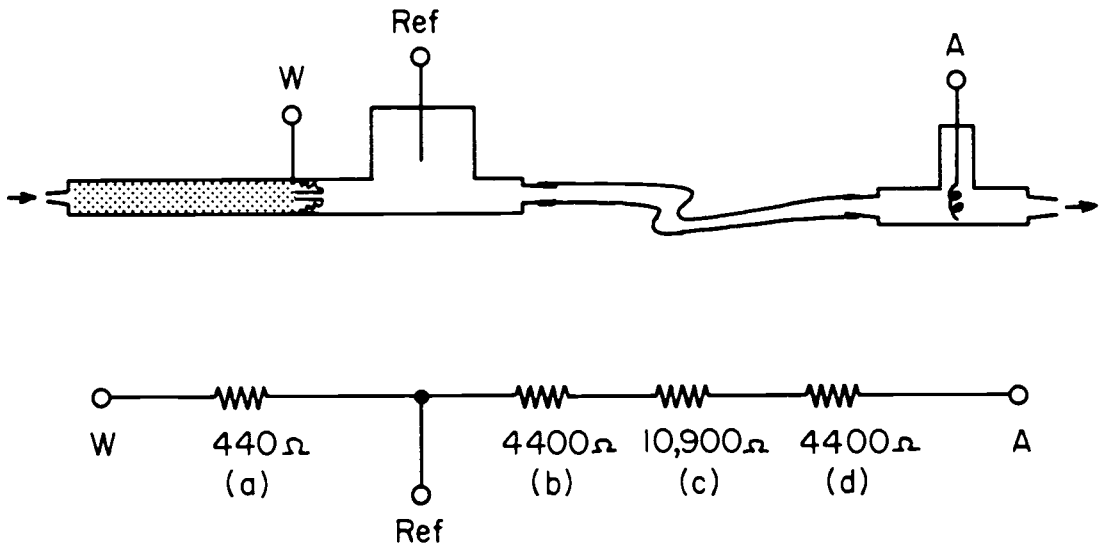

Figure 18. Initial Flow–Cell System and Equivalent Circuit. (W) is the flow–through working electrode of Figure 17, (Ref) is the reference electrode described in text, (A) is a coiled platinum wire auxiliary electrode. The numbers below the resistors are the resistances of the solution element computed from dimensions of the various parts and the electrolyte composition. (a) nipple, (b) and (d) hose barb, (c) tubing. Example dimensions and solution resistance calculations are shown in Appendix 1.

have been 0.659 V. Direct verification of this explanation is impossible at this time because information on the output voltage of the potentiostat was not recorded. It is evident from these calculations, however, that closer coupling of the working and auxiliary electrodes is necessary to reduce the iR drop from the electrolyte.

2.2.3. A Beaker Test-Cell for Diagnosis. When no electrochemical activity was observed from the cell described above, experiments were made with a controlled number of components in the electrochemical experiment. The objective was to isolate the problem by progressing from a simple case to the failure case and observing the cell response as the system grew.

In the *first* experiment, CVs of 3.3 mM Cd^{2+} in 33% SCABE from a bare 3.2 mm diameter RVC rod were obtained. The un-stirred test cell, Figure 19a, was a beaker containing the reference electrode, a coiled platinum wire auxiliary electrode, and the RVC rod working electrode. The equivalent circuit for this cell, also shown in Figure 19a, includes a bulk solution resistance and an uncompensated resistance similar to those shown in Figure 18. The mass transfer resistance, which is distributed throughout the three dimensional structure of the working electrode, is depicted as a parallel combination of mass transfer resistors. This distributed resistance is insignificant in this case, but we introduce the model here so that we may lay the foundation for understanding future problems in three dimensional cells. The operational variable in this experiment was the insertion depth of the RVC working electrode; four different RVC insertion depths produced the four different CVs shown in Figure 20. The stripping peak heights

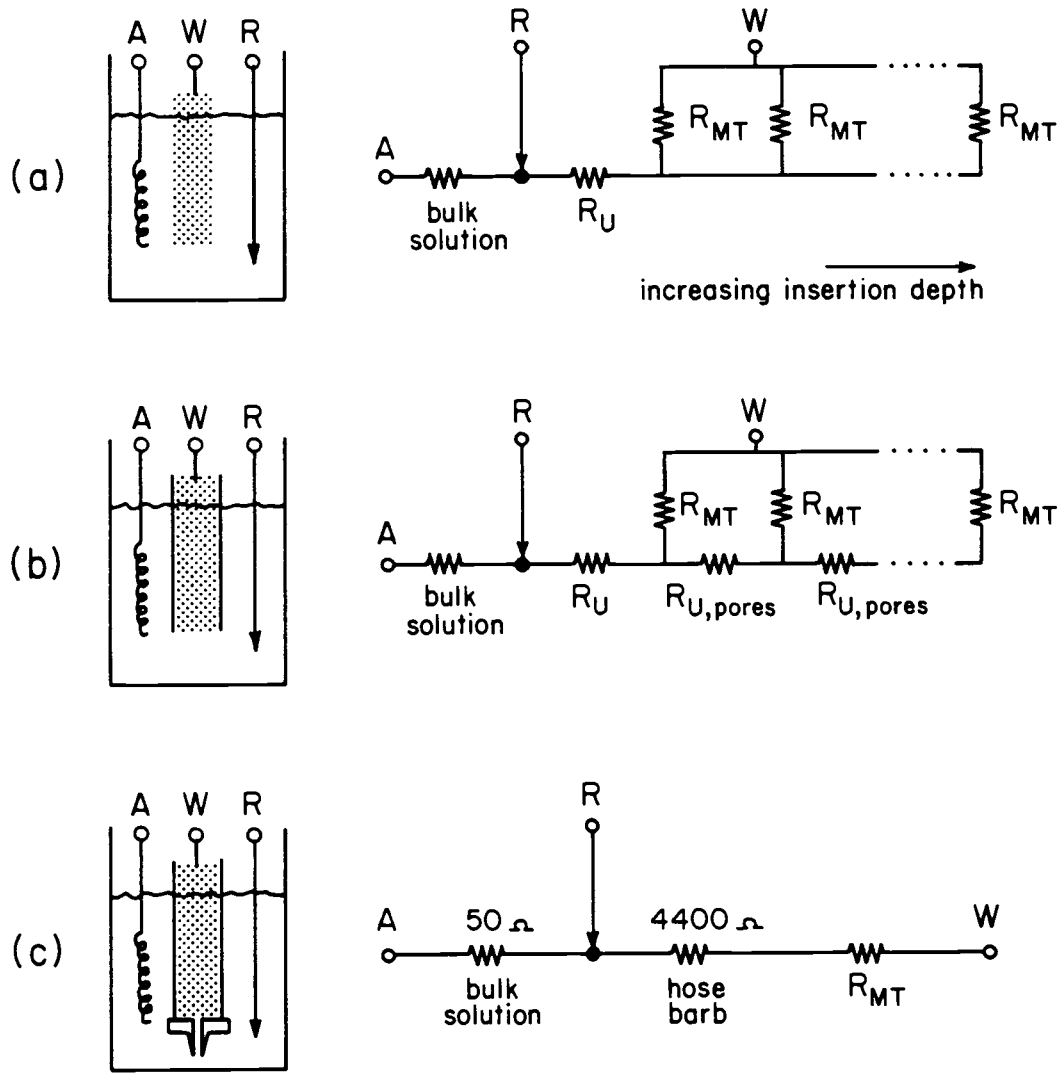

Figure 19. Three Configurations of Bulk RVC Electrode. (a) RVC cylinder only, response is depth dependent; (b) RVC walls sheathed, response independent of depth; (c) same as (b) with added hose barb, no Faradaic response. Example resistance calculations may be found in Appendix 1.

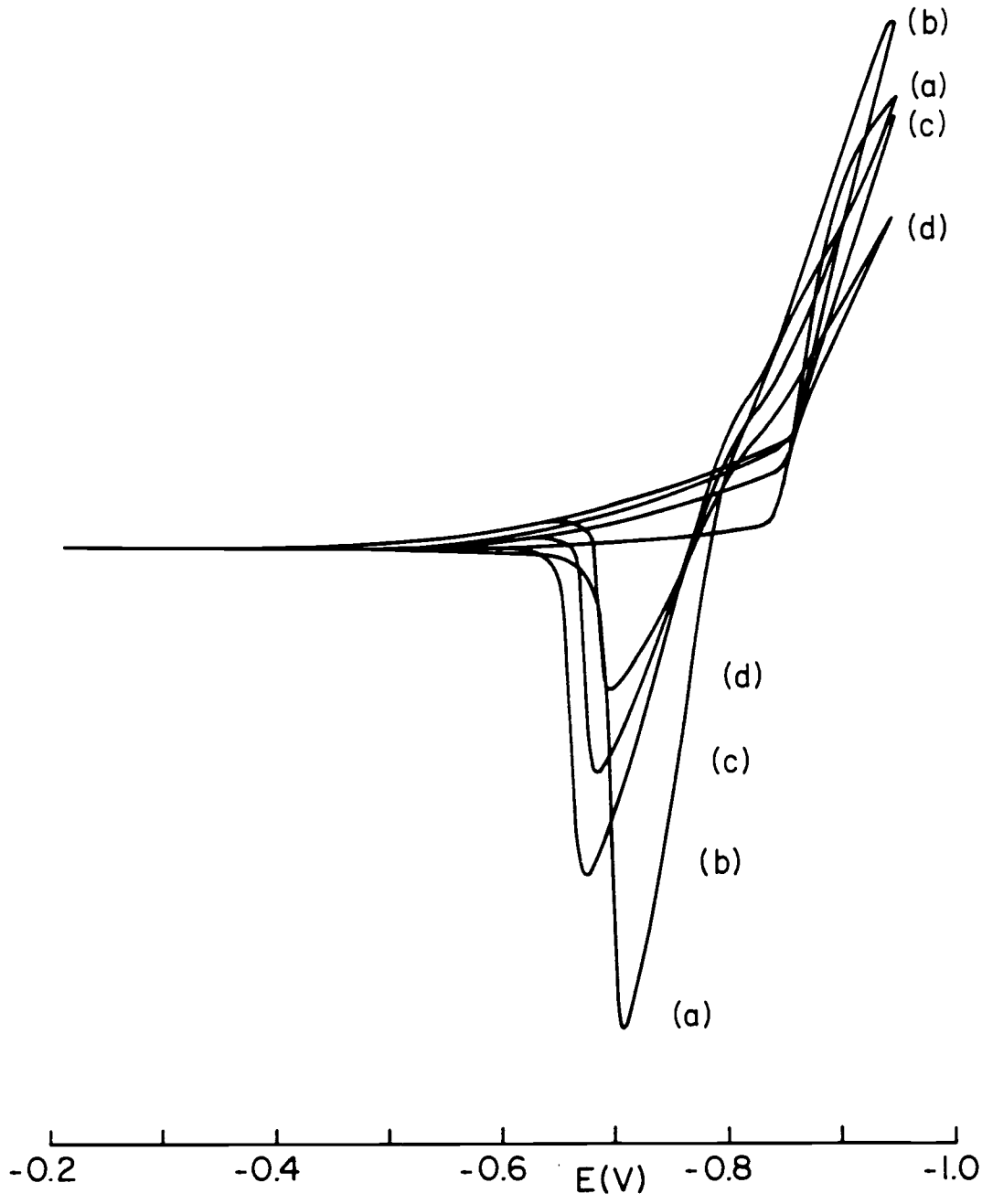

Figure 20. Depth Dependent CVs. Cell geometry of Figure 19 (a). Insertion depth and stripping peak current, microamps/cm respectively are (a) Barely inserted, 1.7, (b) 12 mm, 2.7, (c) 33, 2.6, (d) 50, 1.2. Solution was 3.3 mM Cd^{2+} in 33% SCABE. 100 mV/s.

agree with each other within a factor of two when normalized for scale factor and insertion depth, which means that the observed response is simply a function of working electrode surface area.

In the *second* experiment the RVC rod was encapsulated in Teflon, Figure 19b. Faradaic activity was observed, but there was no variation in peak height with insertion depth. This depth independence is caused by the uncompensated electrolyte resistance within the pores of the RVC, depicted in the equivalent circuit as $R_{u,\ pores}$. The reference electrode and potentiostat control the potential between the auxiliary and the *END* surface of the RVC working electrode. The iR drop in the electrolyte path within the pores of the sheathed RVC reduces the potential as a function of distance from the open end of the electrode. The only Faradaic activity occurs at or near the end of the working electrode, and this activity is independent of insertion depth.

In the *third* experiment, Figure 19c, *all Faradaic activity from cadmium was eliminated* by adding a hose barb to the solution end of the encapsulated RVC rod. Faradaic activity disappeared because the reference electrode is sampling the system in the middle of a voltage divider. The hose barb, because of its small inside diameter, introduces a resistance ten times greater than the resistance of the bulk solution between the auxiliary and working electrodes. From the resistances noted in Figure 19c, the potential applied to the end surface of the working electrode will be a factor of 50/4400+50 = 0.011 times the potential that the potentiostat is applying. If a 1 volt potential is desired at the working electrode, the potentiostat would have to apply

89 V, but its maximum rating is 30 V. The maximum potential available at the working electrode is 0.33 V. Unfortunately, the records for this experiment do not indicate whether or not the potentiostat was potential limited, so this explanation is not directly verified.

2.2.4. Flow-Cell With Closely Coupled Auxiliary. The resistance of the electrolyte path and associated iR drop identified above is the largest problem in controlling the potential within a flow-cell. In an attempt to reduce electrolyte iR drop, the design was changed by shortening the working electrode from 6 cm to 2 cm and by moving the platinum wire auxiliary electrode very close to the RVC, Figure 21a. The method of construction was to place the Teflon encapsulated RVC between two Luer lock tees. The assembled cell had the shape of the character "pi" with the horizontal portion carrying solution and the vertical "legs" (after sealing with epoxy resin) containing the platinum working and auxiliary leads.

When a solution of 3.3 mM Cd^{2+} flowed through the shortened cell at 1 ml/min, so much hydrogen was reduced that cadmium reduction was not observed, Figure 22. Gas generation within the cell was observed and the maximum current decreased with time. The data in Figure 23 support the hypothesis that the current was primarily from hydrogen reduction, since the logarithm of the cell current is proportional to pH. The fact that gas is being generated at all indicates an uncompensated potential drop is causing a loss of control of the potential at the electrolyte – working electrode interface.

When the potentiostat applies voltage between W and A, Figure 21b, to maintain W–Ref at the selected value, a current flows

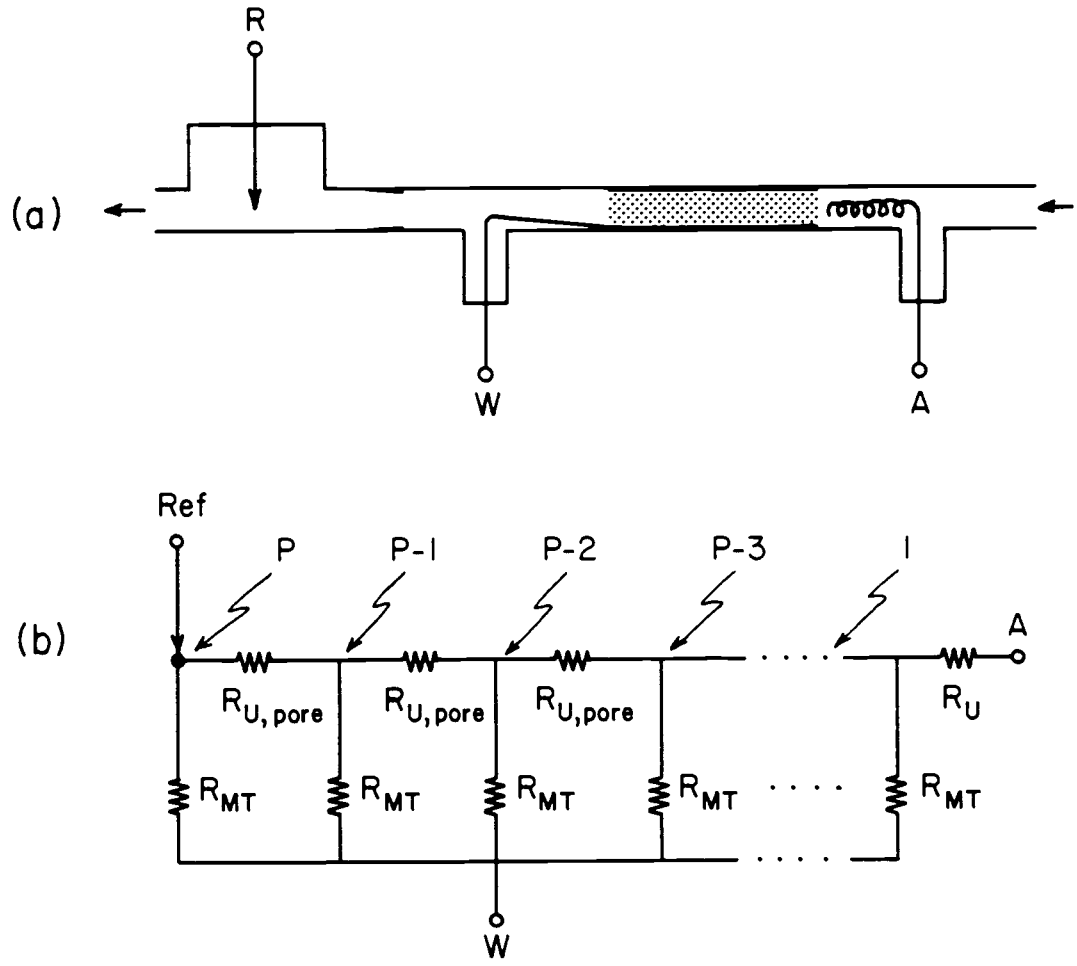

Figure 21. Short Flow–Cell, Flag Auxiliary. Revision of cell from Figures 17 and 18. RVC segment is 2 cm long; reference electrode relocated.

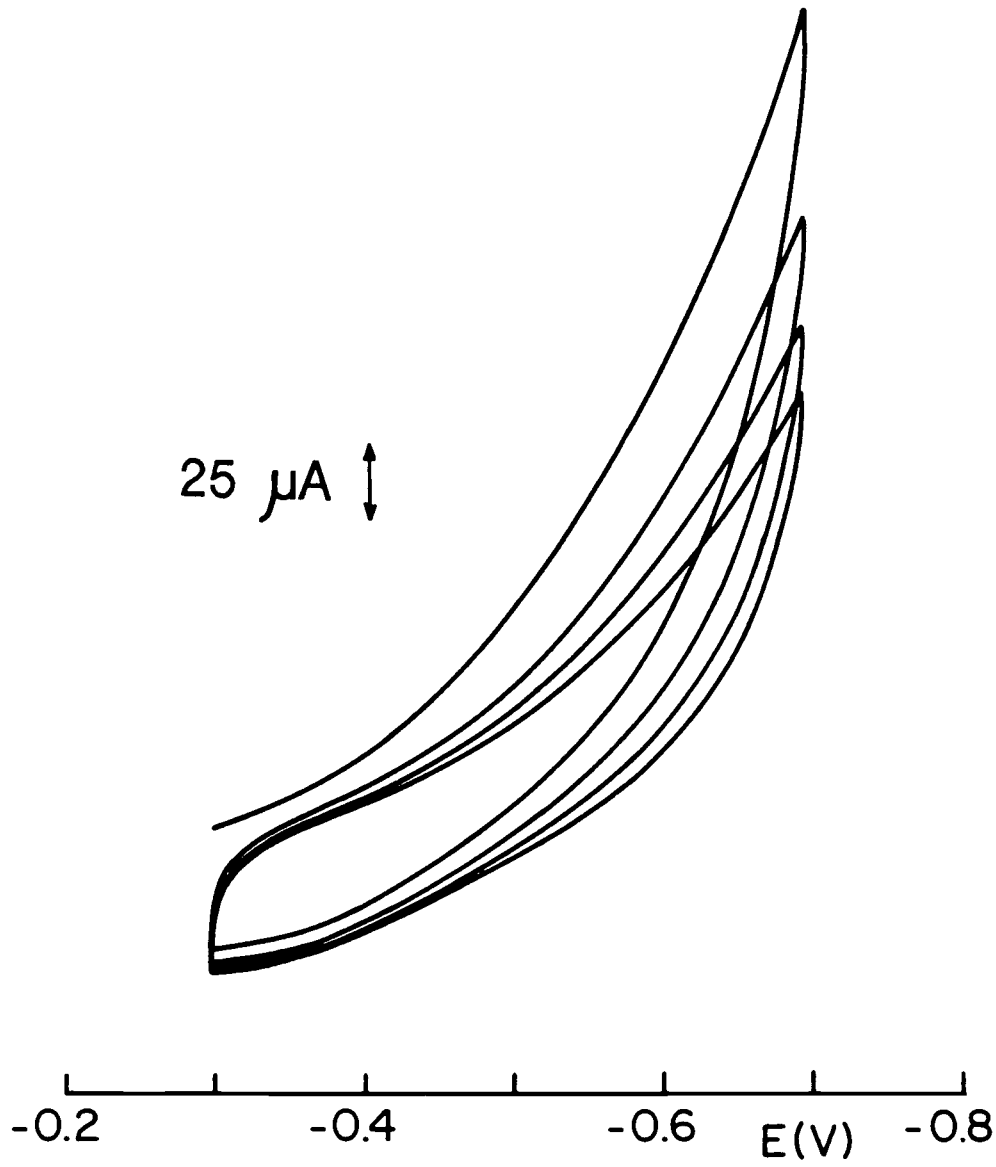

Figure 22. Hydrogen Reduction in Cell of Figure 21. Cadmium reduction is not observed in this CV scan of 3.3 mM Cd^{2+} in 33% SCABE adjusted to pH 6.1, 1 ml/min, 50 mV/s.

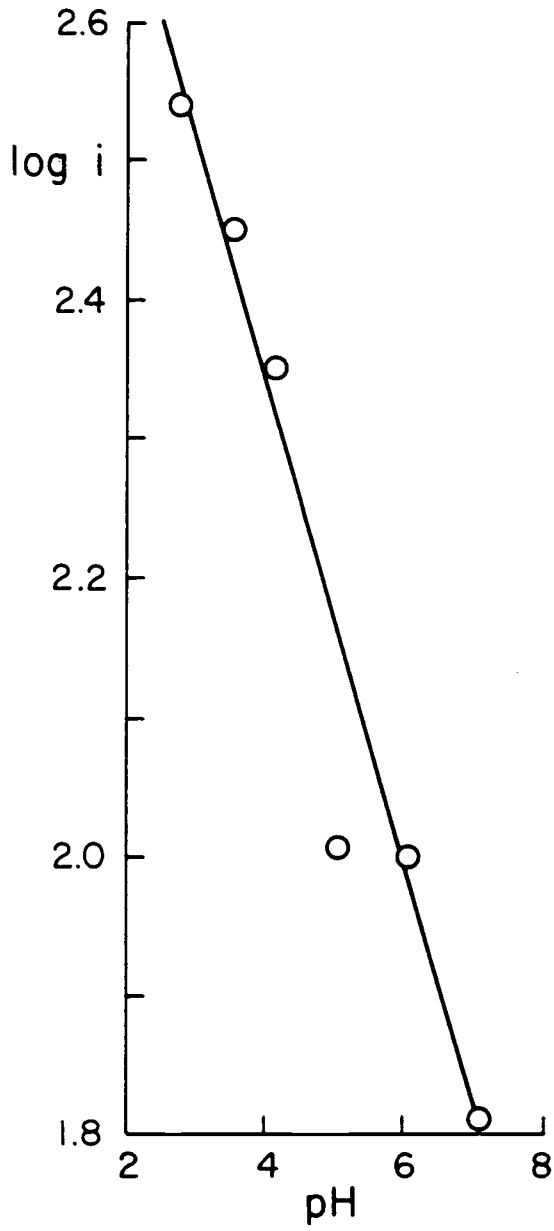

Figure 23. Dependence of Current on pH. Values for current were taken from current at −0.7 V on the second CV sweep at indicated pH.

from A, through the network of resistors (labeled $R_{u,pore}$ and R_{mt}) to W. While the potential at point P is maintained at the desired value, the potentials at points P–1, P–2, ..., 1 are successively greater due to the iR drop across the resistors labeled $R_{u,\ pore}$. Thus while only reduction of cadmium would occur at point P, hydrogen could be reduced at point 1.

Gas generation will always reduce cell current over time. Gas generation displaces electrolyte which forces an increase in resistance of the cell because of the decreased diameter of the conducting column of electrolyte. The increased resistance will increase the iR drop, resulting in increased potential applied by the potentiostat. The increase in potential then generates even more hydrogen, which displaces more electrolyte, and so on. The decreasing volume of electrolyte obviously means a decrease in the current the cell can generate, the limit being a dry cell and no current.

2.2.5. Helical Auxiliary Electrode. A series of quick experiments on the physical configuration of the flow–cell of Figure 21 indicated that the electrolyte path length within working electrode was a significant parameter of electrode design. Briefly, the RVC segment was shortened to 1 mm before cadmium could be reduced without hydrogen also being reduced.

We will see in Part 3 that the conversion efficiency of a porous flow–through electrode generally increases with its length. We therefore desire a cell design with a long working electrode but with a short path length from the auxiliary electrode to all points on the working electrode. One way to achieve this design is with a cylindrical

auxiliary electrode which surrounds a cylindrical working electrode. For the sake of simplicity and in the interests of proof of principle, we assumed that a platinum wire in the shape of a helix could approximate a cylindrical auxiliary electrode.

The inner–most part of the cell with the helical auxiliary electrode, shown in Figure 24, is a cylinder of RVC 0.32 cm diameter by 2 cm long. A platinum wire (36 gauge, 0.01 cm diameter) contacts the RVC along the length of the RVC and continues beyond to form the working electrode lead. The RVC cylinder and the platinum lead are wrapped in 7.5 mil thick polypropylene non–woven cloth (Webril–M 1003) to form a porous separator between the working electrode and the auxiliary electrode. The auxiliary electrode is a second piece of platinum wire (36 gauge) wrapped around the cloth about five times in a helical configuration, then past the end of the RVC cylinder and beyond to form the auxiliary lead. These four pieces are held together by heat shrink FEP teflon tubing, resulting in a tube with an electrode lead at each end. This tube is completed by adding two Luer lock tees to form the shape of the character "pi" as shown in Figure 21.

Figure 25 is a CV obtained from the cell with the helical auxiliary electrode. This is the *first* CV obtained from a flow–cell with a 2 cm long working electrode. This result reflects the success of the helical auxiliary electrode in reducing the iR drop through the porous working electrode. However, with additional cycles, gas bubbles appeared and the response degraded. We conclude that we still do not have sufficient control over the potential drop at all points on the electrode – electrolyte interface. In the next section we analyze iR

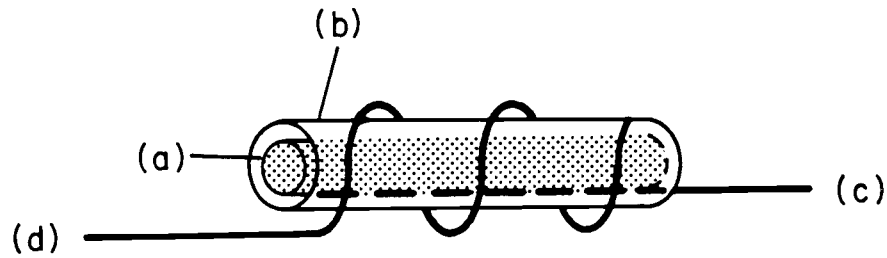

Figure 24. Flow–Cell with Helical Auxiliary Electrode. (a) 0.32 X 2 cm RVC, (b) polypropylene cloth, (c) Pt working electrode lead, (d) 0.01 cm dia Pt auxiliary electrode lead. Not shown is the teflon sheath around (a–d).

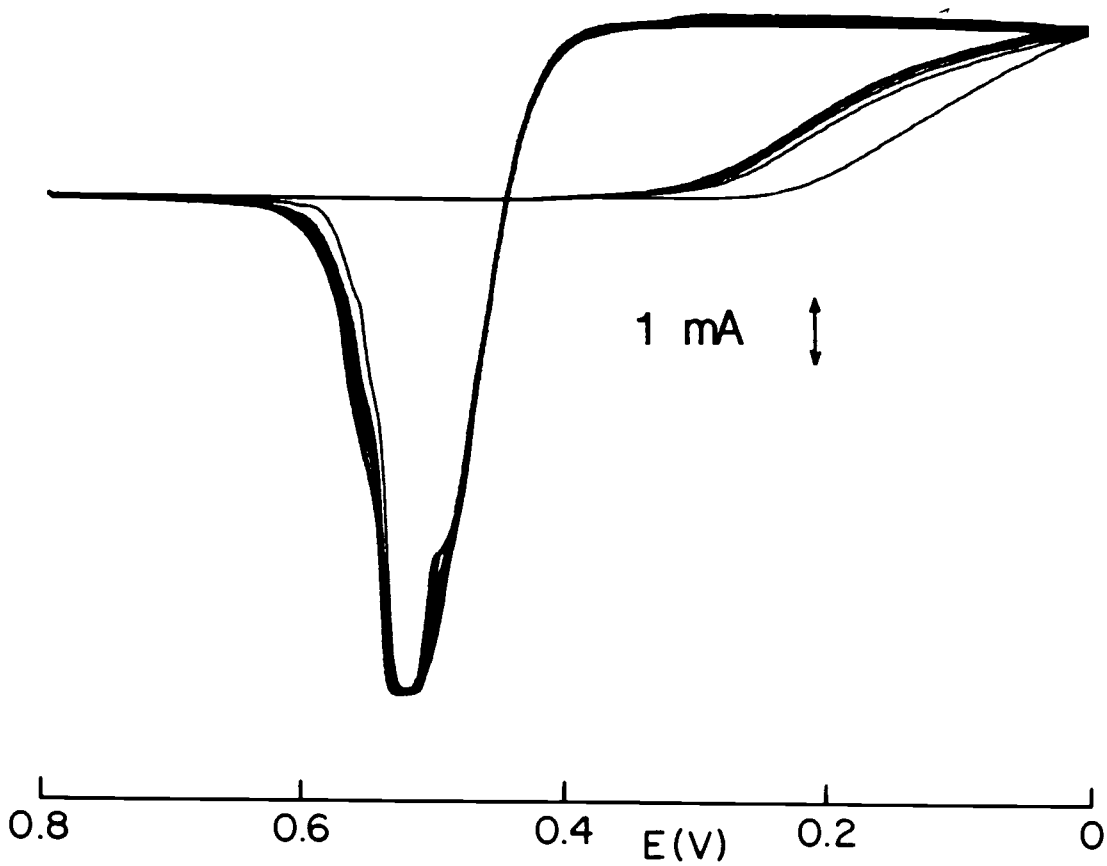

Figure 25. CV from the Flow–Cell of Figure 24. The analyte is 1 mM $Hg(NO_3)_2$ in 0.1 M KNO_3. 50 mV/s, 1 ml/min.

drops throughout all components of the flow–cell: contacts, electrodes, and electrolyte. On the basis of this analysis, we arrive at the final design for the flow–cell. We will see that the helical auxiliary electrode was a poor approximation of a cylindrical auxiliary electrode. A flow–cell with a cylindrical auxiliary and working electrode is a viable method for reducing the iR drop in the electrolyte.

2.3. FINAL DESIGN OF THE FLOW-CELL

Through an evolutionary process, we have arrived at a promising design based on cylindrical symmetry. Previous cell designs were unsatisfactory mainly because of large potential drops within the flow–cell. These potential drops were the result of placement of the auxiliary electrode at one end of the flow–cell.

The positive results obtained from the cell with the helical auxiliary electrode invite further analysis of the sources of uncompensated potential drop. The first step in this analysis is a more complete equivalent circuit with distributed resistances such as those used in Figures 19 and 21. The next step is an analysis of the relative contributions of the resistances identified in the equivalent circuit. Our intent in this analysis is to determine how to reduce the uncompensated potential drops within the cell. Finally we consider the effects of the radial and longitudinal placement of the reference electrode on the performance of the flow electrode.

2.3.1. Equivalent Circuit. In Figure 26 is an equivalent circuit for a cylindrically symmetric flow–cell. The resistance from the RVC working electrode is denoted R_w. We ignore the small resistance from

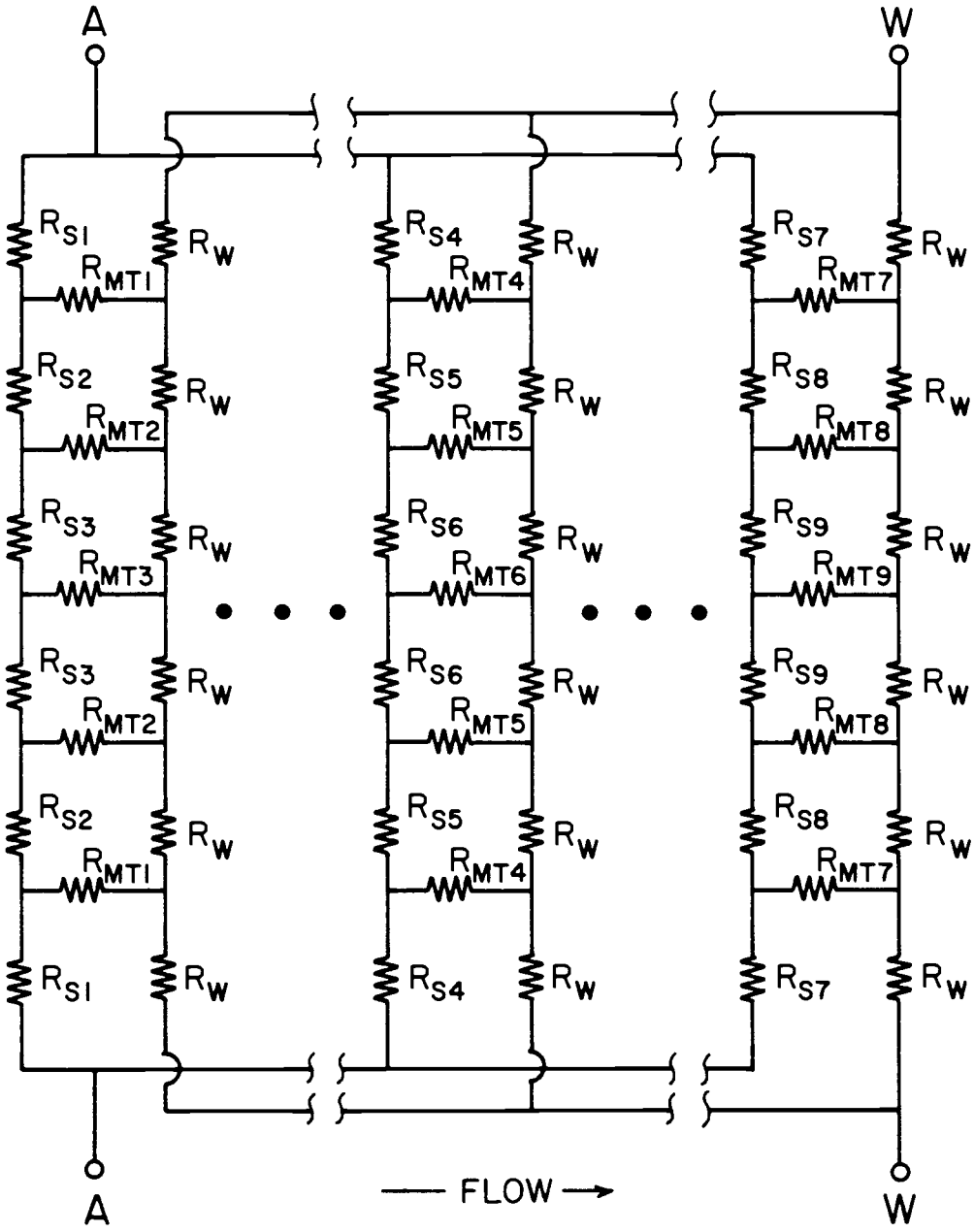

Figure 26. Equivalent Circuit of Cylindrically Symmetric Flow Electrode. R_s = resistance of solution (electrolyte). R_{mt} = resistance to mass transfer. R_w = resistance of the RVC working electrode. The resistance of the Pt auxiliary electrode is assumed to be negligible.

the platinum auxiliary electrode, as will be justified in section 2.3.2.1. Electrolyte resistance is represented as R_s, and R_{mt} is the resistance to mass transfer. A detailed analysis of the significance of these resistances follows, and a detailed circuit analysis is given in Section 2.3.4.3.

2.3.2. The iR Drop Through the Flow-Cell Materials. In the following two sections, the resistance contribution from the materials of construction of the flow cell are considered. The materials we consider here are platinum and RVC. The objective is to estimate the contribution of each to the cell's resistance and resultant iR drop. We will consider the iR drop from the electrolyte in the cell after this discussion of the materials of construction.

2.3.2.1. The iR Drop through the Platinum Lead. Platinum has a resistivity of 11 microohm cm, and the 36 gauge wire used is 0.01 cm diameter. With this data, we can calculate the resistance of this platinum wire according to

$$R = \frac{\text{rho} * l}{A} \tag{4}$$

where

rho	is the resistivity of the material
l	is the length of the material
A	is the cross sectional area of the material

To compute the iR drop, we need to choose a worst case maximum

current. We expect the maximum current will be from mercury plating the electrode, if that procedure is used. The current levels observed for this process are on the order of 1 mA, as noted in Figure 25.

The length of the platinum wire leads, Figure 24, which are not in contact with the electrolyte and/or the RVC is about 2.3 cm. The calculated resistance for this platinum lead is 0.32 ohm. The potential drop from the platinum wire lead carrying 1 mA is 0.32 millivolts, which is too small a potential error to warrant further consideration.

The helical auxiliary electrode, Figure 24, is assumed to be 10 wraps of platinum wire around the RVC electrode. The length of the auxiliary electrode is estimated as $10\pi d$ = 10 cm and the resistance is 1.4 ohm, thus generating an insignificant 1.4 millivolt iR drop when operated at 1 milliamp.

2.3.2.2. The iR Drop Through the RVC. Current must be conducted through the cylindrical RVC electrode. The distance that the current must travel and the resultant iR drop depend on how the platinum lead is attached to the RVC cylinder. If the lead is connected only at one end of the RVC, then the current must travel through the entire length of the RVC cylinder. Any extension of the contact will shorten the current path and reduce the iR drop. Here, as a limiting case, we consider the iR drop when current flows through the entire length of the RVC cylinder. The iR drop will be shown to be small, but significant; however, in a later section, we will show that the resistivity and iR drop of the RVC will generally still be insignificant in comparison to those of the electrolyte.

The longitudinal resistance of representative RVC cylinders is

between 10 and 100 ohms as measured with a multimeter. We can use these values and the dimensions of the cylinders to calculate the bulk resistivity of RVC, thereby obtaining a value to compare with literature values. The bulk resistivity *rho* of a material can be calculated from the measured resistance *R* and the area *A* to length *l* ratio of the bulk material

$$\text{rho} = \frac{R \cdot A}{l} \tag{5}$$

The resistivity calculations for three RVC cylinders are shown in Table 2. The resistivities agree with the value of 0.3 ohm cm reported by Iacovangelo & Will (1985) and the range from 0.47 to 0.69 ohm cm quoted by Ladda (1987). Significant errors in the resistance measurement of porous RVC are possible because the measurements were made with a multimeter which had pointed test probes. The RVC material breaks apart with significant contact pressure, causing a variable surface area of contact and possible added resistance due to a layer of broken particles between the probe and the bulk RVC. Ideally, the probes should have been planes covering the ends of the RVC. Because we are interested in demonstration of principle, we will use the approximate value of 1 ohm cm for future calculations. Thus the longitudinal resistance of a 0.32 cm diameter by 2 cm long cylinder of RVC is 25 ohms, and the iR drop along the length for a one milliamp current will be 25 millivolts.

This iR drop of 25 millivolts is not negligible, but it can be

Resistance ohms	Diameter cm	Length cm	Resistivity ohm-cm
30	0.32	2.25	1.1
80	0.31	7.50	0.85
60	0.37	7.95	0.83

Table 2. RVC Resistivity Calculation. Resistivity is calculated from the values measured in the other three columns according to equation (5).

reduced easily by extending the Pt contact along the length of the cylinder. The more serious problems with iR drop come from the electrolyte, which will be considered next.

2.3.3. The iR Drop in the Electrolyte. The resistance of the electrolyte in a cylindrical flow-cell can be considered in the longitudinal and radial directions. If a "flag at one end" auxiliary electrode is used, the longitudinal resistance is of maximum significance, and must be considered. If a concentric cylindrical auxiliary electrode is used, only the resistance in the radial direction needs to be considered. A brief review of the literature and these two cases are considered below.

2.3.3.1. Typical Flow-Cell Models in the Literature. The literature suggested by Bard and Faulkner (1980) provides detailed models of flow-cells in which the direction of electrolyte flow is from one electrode to the other, analogous to our electrode designs in which the auxiliary electrode was at *one end* of the flow-cell (Trainham and Newman (1977), Ateya and Austin (1977), Alkire and Gould (1976) and Sioda (1971)). In none of these studies was the auxiliary electrode placed parallel to the direction of flow as we have shown in Figure 24. Further, they assume uniform values of current, potential and concentration in all directions except the direction of flow.

Several of these articles give profiles along the direction of flow for potential, current, concentration and side reactions (generation of dissolved hydrogen). Unfortunately, as we will see in the next section, we do not have uniform conditions across the diameter of our

flow–cell, so the developments made in the literature discussed above do not apply to our case. It is not surprising that two–dimensional solutions are rare. As stated by Alkire and Gould (1976), "Attempts to model complex porous electrode systems must rely on restrictive assumptions and perhaps artificial visions of physical reality in order to render the problem amenable to mathematical treatment."

2.3.3.2. Longitudinal iR Drop in Cylinder of Electrolyte. Details of the calculation of the longitudinal resistance of a 0.32 cm diameter by 2 cm long cylinder of 33% SCABE can be found in Appendix I. The result is 350 ohms, which means that a cell conducting 1 milliamp from one end to the other will have a 350 mV iR drop in the electrolyte. This very significant potential drop along the length of the cell is unavoidable for the "flag at one end" configuration of the auxiliary electrode, but can be reduced by use of a concentric cylindrical auxiliary electrode.

2.3.3.3. Radial iR Drop in Cylinder of Electrolyte. Calculation of the radial iR drop in the electrolyte of a cylindrical flow–cell is not a simple matter. Here we approach the problem through a series of approximations, in order to: 1) facilitate solution of the problem, and 2) allow us to evaluate the effectiveness of several *physical approximations* of a true cylindrical auxiliary electrode. We will use three different physical approximations of the cylindrical auxiliary electrode. They are 1) a single wire, 2) two wires and 3) four wires, all of which are parallel to the axis of the working electrode cylinder. We will see that the closer the auxiliary electrode comes to cylindrical symmetry,

the lower the radial iR drop in the cell.

First we consider the case of the flow cell with a single wire auxiliary electrode. As an upper bound to the radial iR drop, we calculate the potential drop across the *diameter* of the flow cell. To simplify the problem we represent the cylindrical RVC electrode as a rectangular box, which just fits within the the cylindrical RVC electrode. The length of the box is L = 2 cm, and the length of the diagonal across the square end of the box is D = 0.32 cm, as shown in Figure 27. The electrolyte in the box is divided into longitudinal cross-sectional volume elements, as shown in the figure. If the dimensions and current of each volume element are known, the iR drop can then be calculated from Equation 6.

The dimensions of any volume element can be calculated by straightforward geometry. The box, from one corner to the other, is divided into n = 20 volume elements. An end view of the box with one of the volume elements is shown in Figure 28. The width, *w*, of each element is

$$w = \frac{D}{n} \tag{6}$$

and the height, h_i, of any volume element i (with i=1 at the platinum auxiliary electrode and i = n at the opposing corner) is:

$$h_i = 2w \cdot i \qquad \text{for } i \leq n/2 \tag{7}$$

$$h_i = 2w \cdot (n-i+1) \qquad \text{for } i > n/2 \tag{8}$$

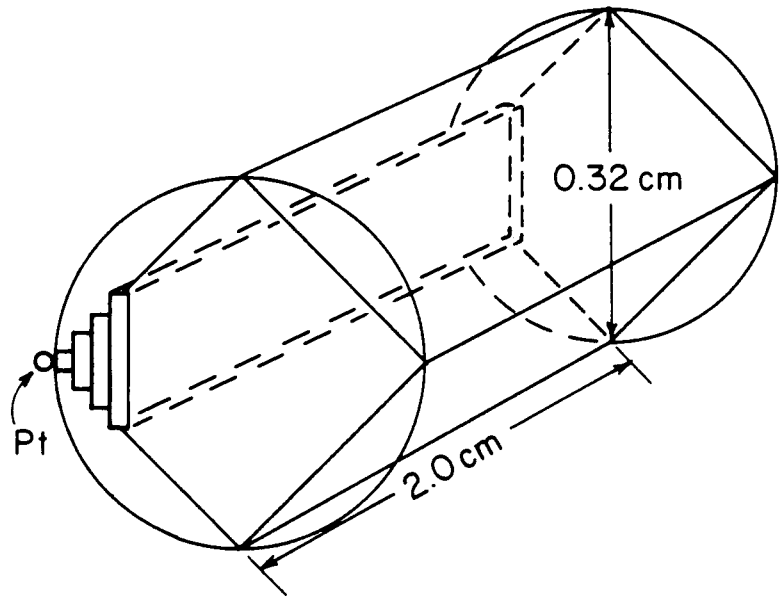

Figure 27. Volume Elements in Box Electrode. Current flows from Pt auxiliary electrode towards the right edge of the box. The volume element next to the Pt wire has both the highest current density and the lowest cross sectional surface area. Total current passing through each volume element decreases from left to right.

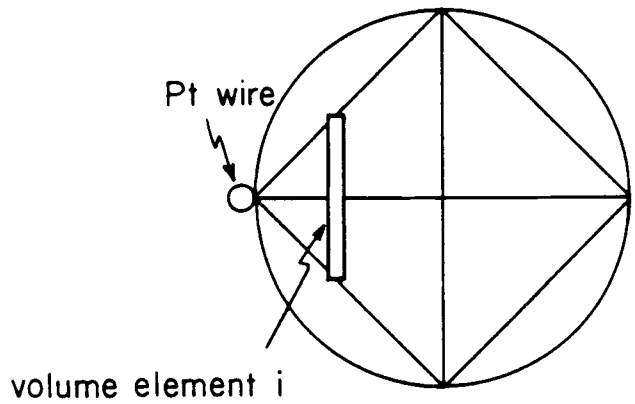

Figure 28. End View of the Box Shaped Electrode in Figure 27. One Pt auxiliary electrode runs along a corner. The width w of each volume element is given by Equation 6 in the text. The height of each volume element may be calculated with Equations 7 or 8 in the text.

The area A_i of the face of any volume element is

$$A_i = h_i \cdot L \tag{9}$$

The total current passing from volume element i+1 to i can be calculated from the following observations and assumptions: 1) All of the cell current must pass through the auxiliary electrode. Current density is highest at the auxiliary electrode, and zero at the opposite side of the RVC cylinder. 2) There is only one electrochemical reaction occurring in the cell, and the potential applied to the electrodes is high enough that the electrochemical reaction takes place throughout the volume of cell. 3) We suppose that Faradaic current density is uniform throughout the cell, therefore the total current from volume elements i+1 ... n is proportional to the total volume of those volume elements i+1 ... n. The total volume of the elements i+1 ... n can be calculated directly from the total volume of the box, V_t, and the location of the i/i+1 face of volume element i:

$$V_{(i+1 \ldots n)} = V_t - i \cdot w \cdot h_i / 2 \qquad \text{for } i \leq n/2 \tag{10}$$

$$V_{(i+1 \ldots n)} = D - i \cdot w \cdot h_{(i+1)} / 2 \qquad i > n/2 \tag{11}$$

The current passing from volume element i+1 to i is then

$$i_{(i+1,i)} = k \cdot V_{(i+1 \ldots n)} \tag{12}$$

where k is a proportionality constant.

The iR drop in any volume element *i* can now be calculated

from Equation 12 and 1) the area A_i and the current path length w of the volume element; 2) the resistivity of the electrolyte (Appendix 1); and 3) the total current entering volume element i from volume elements i+1, ... n. These calculations were made with a computer, and the results of the BASIC program *BOX1*, which is listed in Appendix 2, are presented in Table 3.

Inspection of the *current* column in Table 3 reveals that both halves of the cell (proximal and distal to the auxiliary electrode) contribute equally to the total current flowing from the cell. However, further inspection of the *sum iR* column reveals that only 1/13 of the total iR drop in the cell is generated in the distal half of the cell. Indeed, over 50% of the iR drop in the cell occurs in the 10% of the cell nearest the auxiliary electrode. These observations suggest that the potential distribution in the cell could be improved by adding a second auxiliary electrode, as shown in Figure 29.

The characteristics of the two–auxiliary–electrode cell shown in Figure 29 were calculated with the program *BOX2* (Appendix 2) and are presented in Table 4. Note here that the path length is only half that of the previous cell, and the current carried by each leg of the auxiliary electrode is half that of the single auxiliary electrode lead, yet the total iR drop across this electrode is only 41% that of the previous electrode. The characteristics of the four–auxiliary–electrode cell of Figure 30 are shown in Table 5 (BOX4, Appendix 2). Note that the sum of the iR drop column is 25% of the same column in Table 3, as one would expect from geometry considerations.

It is now apparent that there are three factors to optimize in

volume element number	current path area	current i	path resistance R	iR	sum iR
1	0.20	1.99	0.500	0.995	0.995
2	0.40	1.96	0.250	0.490	1.485
3	0.60	1.91	0.167	0.318	1.803
4	0.80	1.84	0.125	0.230	2.033
5	1.00	1.75	0.100	0.175	2.208
6	1.20	1.64	0.083	0.137	2.345
7	1.40	1.51	0.071	0.108	2.453
8	1.60	1.36	0.062	0.085	2.538
9	1.80	1.19	0.056	0.066	2.604
10	2.00	1.00	0.050	0.050	2.654
11	1.80	0.81	0.056	0.045	2.699
12	1.60	0.64	0.063	0.040	2.739
13	1.40	0.49	0.071	0.035	2.774
14	1.20	0.36	0.083	0.030	2.804
15	1.00	0.25	0.100	0.025	2.829
16	0.80	0.16	0.125	0.020	2.849
17	0.60	0.09	0.167	0.015	2.864
18	0.40	0.04	0.250	0.010	2.874
19	0.20	0.01	0.500	0.005	2.879
20	0.00	0.00	–	–	–

Table 3. Results of Basic program *BOX1* simulating resistance, current and potential profiles of electrode in Figure 28.

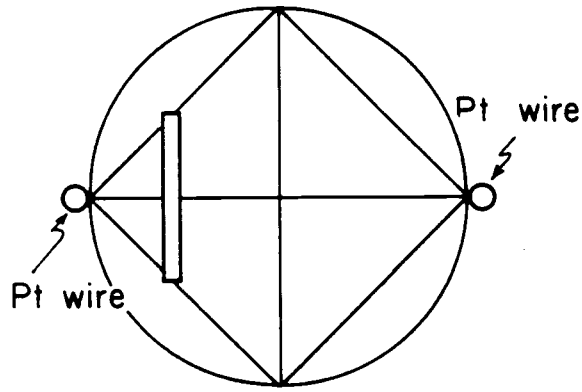

Figure 29. End View, Box Shaped Electrode. Two Pt auxiliary electrodes run along opposite corners.

volume element number	current path area	current i	path resistance R	iR	sum iR
1	0.20	0.99	0.500	0.495	0.495
2	0.40	0.96	0.250	0.240	0.735
3	0.60	0.91	0.167	0.152	0.887
4	0.80	0.84	0.125	0.105	0.992
5	1.00	0.75	0.100	0.075	1.067
6	1.20	0.64	0.083	0.053	1.120
7	1.40	0.51	0.071	0.036	1.156
8	1.60	0.36	0.062	0.022	1.179
9	1.80	0.19	0.056	0.011	1.189
10	2.00	–	–	–	–

Table 4. Results of Basic program *BOX2* simulating resistance, current and potential profiles of two–auxilliary lead electrode in Figure 29.

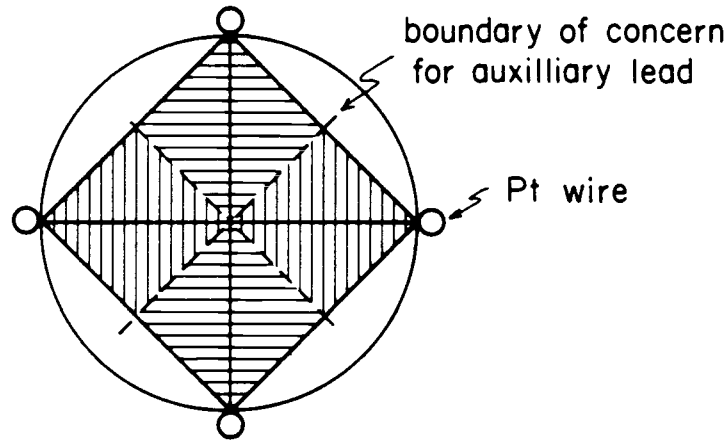

Figure 30. End View, Box Shaped Electrode. Four Pt auxiliary electrodes, one for each corner.

volume element number	current path area	current i	path resistance R	iR	sum iR
1	0.10	0.50	0.500	0.249	0.249
2	0.20	0.49	0.250	0.123	0.371
3	0.30	0.48	0.167	0.080	0.451
4	0.40	0.46	0.125	0.058	0.508
5	0.50	0.44	0.100	0.044	0.552
6	0.60	0.41	0.083	0.034	0.586
7	0.70	0.38	0.071	0.027	0.613
8	0.80	0.34	0.062	0.021	0.634
9	0.90	0.30	0.056	0.017	0.651
10	1.00	0.25	0.050	0.012	0.663
11	0.90	0.20	0.056	0.011	0.675
12	0.80	0.16	0.063	0.010	0.685
13	0.70	0.12	0.071	0.009	0.693
14	0.60	0.09	0.083	0.007	0.701
15	0.50	0.06	0.100	0.006	0.707
16	0.40	0.04	0.125	0.005	0.712
17	0.30	0.02	0.167	0.004	0.716
18	0.20	0.01	0.250	0.002	0.718
19	0.10	0.00	0.500	0.001	0.720
20	0.00	0.00	–	–	–

Table 5. Results of Basic program *BOX4* simulating resistance, current and potential profiles of four–auxilliary lead electrode in Figure 30.

the auxiliary electrode design. The *current path length* within the electrolyte needs to be short, the *area of the auxiliary electrode* needs to be large, and the auxiliary electrode needs to be *highly symmetrical* about the working electrode. For a cylindrical working electrode, the easiest way to reduce path length and increase both the auxiliary electrode area and symmetry is to use a concentric auxiliary electrode. The concentric auxiliary electrode has the added benefit of not restricting the length of the cell. The easiest way to achieve a high surface area in the auxiliary electrode is to use a high surface area material like a fine mesh gauze.

2.3.4. Reference Electrode Considerations. The strategy for proper placement of the reference electrode is to minimize the uncompensated iR drop between the reference and working electrodes. Our previous discussions have dealt with the factors that affect the iR drop along the length of and across the diameter of cylindrical cell. In the next section we will describe the uncompensated iR drop in relation to the cylindrically symmetric potential profile within in the cell. We then use the cylindrical profile to discuss the implications of the radial and longitudinal placement of the reference electrode.

2.3.4.1. Cylindrically Symmetric Potential Profile. The case of a cylindrical working and auxiliary electrode pair operating at an applied potential such that Faradaic activity occurs all the way across the diameter of the working electrode is shown in Figure 3la. A cross section of this cell is shown in Figure 3lb. If the potential across the cell is large enough to produce Faradaic activity at the center (r=0)

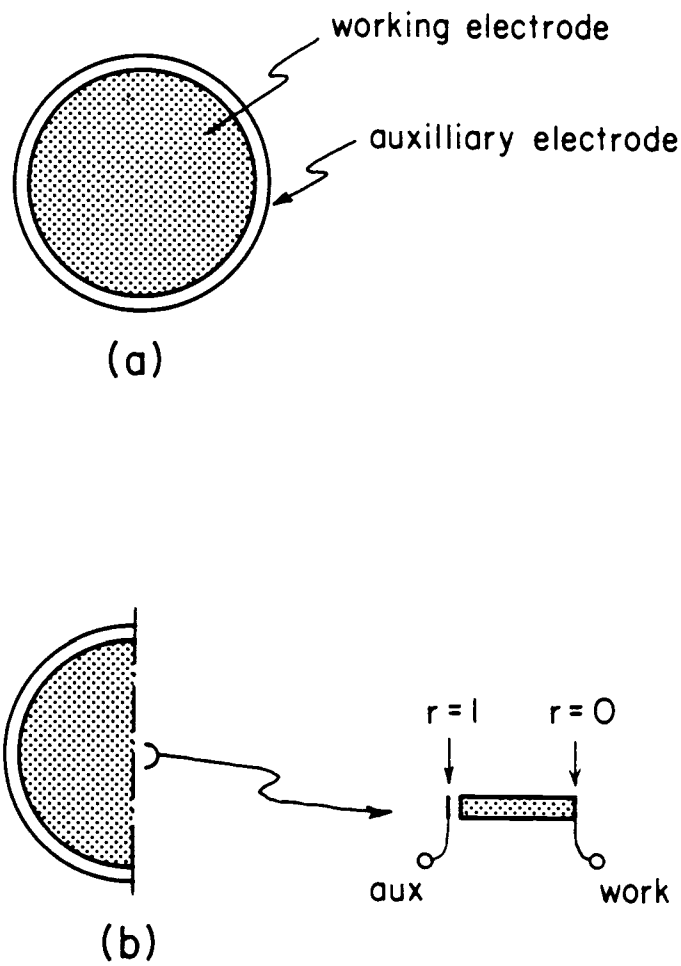

Figure 31. Cylindrically Symmetric Potential Profile. (a) Geometrical relationship of working and auxiliary electrode. (b) Current path. The potential at r = 0 will differ from potential at r = 1 by the **iR** drop along the radius.

then the absolute value of the difference in potential between the circumference (r=l) and the center (r=0) will be *iR*.

2.3.4.2. Radial Placement of the Reference Electrode. If a very small reference electrode were placed at the center of the working electrode and the applied potential were such that Faradaic activity occurred at the center of the electrode, the absolute value of the difference in potential between the center and the edge (circumference) would be *iR*. In this case there is the risk that the overpotential at the circumference will cause interfering reactions, such as the reduction of hydrogen ion, to occur. If the small reference electrode were placed at the circumference of the working electrode, a similar *iR* drop over the radius would occur. In this case, there is the risk that the potential would not be set high enough to overcome the iR drop and cause Faradaic activity to occur in the interior of the electrode. There is no way to avoid an *iR* drop along the radius of the electrode. The best situation is to arrange for the iR drop to be small enough along the radius to be of little consequence. One major factor influencing the radial iR drop is where along the *length* of the cylindrical electrode the iR drop occurs. This concept is elucidated in the next section.

2.3.4.3. Longitudinal Placement of the Reference Electrode. A cylindrical auxiliary electrode does not ensure a uniform potential along the length of the cell. Indeed, in the case of a cell operating at 100% conversion efficiency, we expect considerable Faradaic activity at the inlet end and no Faradaic activity at the outlet end.

We can describe the potential, current and concentration dis-

tributions by assuming that the equivalent circuit of Figure 26 represents a cell with electrolyte and analyte flowing through it in the direction indicated. We further assume that the potential applied between the auxiliary leads *A* and the working leads *W* is enough to drive Faradaic current through the *two* mass transfer resistors which are labeled R_{MT1} in Figure 26. This applied potential A–W is not, however, large enough to drive Faradaic current through the *two* resistors R_{MT2} because of the potential drop iR_{S1}.

If we assume laminar flow, then the analyte concentration in the electrolyte near the points depicted by the two resistors R_{MT4} will be lower than the concentration near the locations of resistors R_{MT1}, therefore $iR_{S4} < iR_{S1}$ and Faradaic current will flow through the resistors R_{MT5}. We assume here that the potential drop $iR_{S4} + iR_{S5}$ is large enough to prevent Faradaic current from flowing through the resistor R_{MT6}.

With similar arguments, we see that there will be Faradaic current flowing through R_{MT9}, which is near the outlet end of the cell, but not through R_{MT6} near the middle and not through the resistors R_{MT2} or R_{MT3} at the inlet end of the cell.

Viewed from the inlet end, the potential distribution in the cell we just described will be extremely non–uniform: All the potential drop occurs at the edge of the cell. In contrast, for an cell operating at 100% conversion efficiency, there will be no Faradaic current flowing across the cell at the outlet end, and consequently no iR drop induced potential distribution. A reference electrode placed at the outlet end should see the potential A–W without the complications of potential

drop caused by Faradaic current. Therefore, the reference electrode should be placed in a position to monitor the potential at the outlet end of the cylindrical cell.

2.3.5. Summary. We have examined the potential drops arising in all of the materials in the flow cell: Pt, RVC, and the electrolyte. It is now apparent that the best cell design strives to reduce the potential drop in the electrolyte by optimizing the symmetry and reducing the path length between the auxiliary and the working electrodes. Optimization can be accomplished with a concentric auxiliary electrode around a cylindrical working electrode, and by reducing the diameter of the working electrode. The best location for a reference electrode with typical macro dimensions is at the outlet end of a flow-cell which is operating at 100% conversion efficiency. If the reference electrode is located at the inlet end, or if the the cell is not operating at 100% conversion efficiency, the potential sampled by the reference electrode will be perturbed by the potential distribution across the end of the cell.

2.4. CONSTRUCTION DETAILS OF FINAL CELL

2.4.1. Cell Module. The complete cell is an assembly consisting of inlet and outlet Luer lock fittings, working and auxiliary contact leads, and the working and auxiliary electrodes. Detailed stepwise construction of this cell is shown in Figure 32 and is described below.

2.4.1.1. Materials of Construction. During the course of this research, about 30 cells were constructed. The procedure described here requires

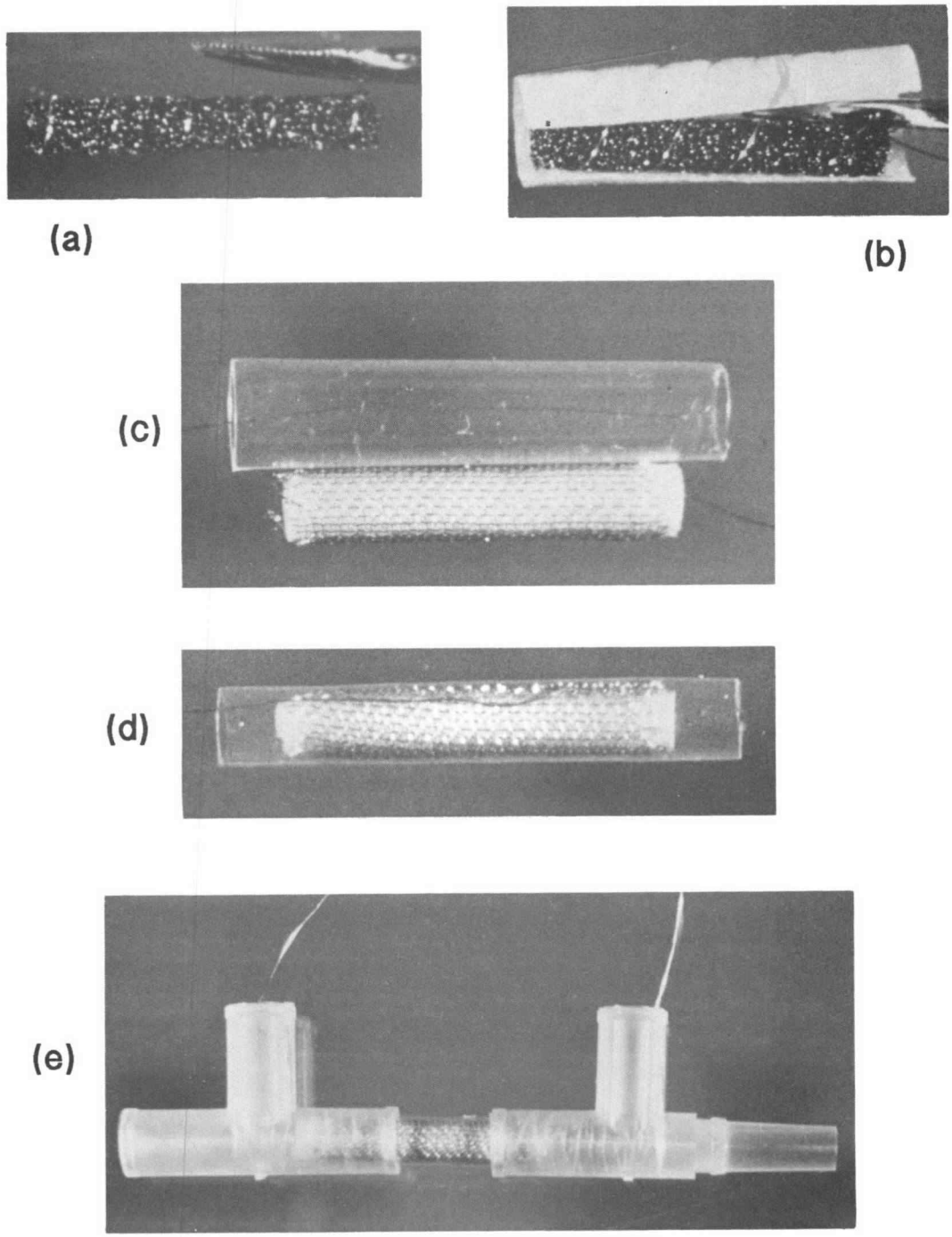

Figure 32. Stepwise Construction of Flow–Cell. (a) RVC cylinder, (b) wrapped in pre–bent polypropylene cloth, (c) and Pt gauze, sitting next to teflon heat shrink tube, (d) after heat shrinking, and (e) assembled electrode.

about four hours of work to produce one cell, and about six hours to produce 12 cells. The first step in construction is to gather all the individual pieces for the batch of cells to be produced.

2.4.1.1.1. RVC Cylinders. The RVC cylinders were cut from a block of 100 ppi RVC three inches thick, obtained from ERG, Inc., 952 – 57th Street, Oakland, CA 94608. The cutter used was a 12 inch long by 0.125 inch inside diameter by 0.155" outside diameter brass tube obtained from a hobby shop. Twelve flutes were made in one end of the tube, each 1/16 inch long, with a four inch side cutter (Diamalloy – USA, model MS54). The flutes were made so that the inside diameter of revolution was less than 0.125 inch and the outside diameter of revolution was greater than 0.155 inch, thereby ensuring clearance between the brass and the RVC both inside and outside the tube after the cutting operation by the flutes was complete. The brass tube was held by hand and fed through the RVC block with a nominal 30 revolutions per feed–inch. When the tube had been fed through the RVC block, it was withdrawn, and the RVC cylinder removed from the tube by pushing it out with a nominal 1/8 inch rod fed from the un–fluted end. These three inch by approximately 0.120 inch RVC cylinders were then cut to 2.0 cm in length with a single edged razor blade. Six such rods were weighed, in grams: 0.0082, 0.0082, 0.0083, 0.0081, 0.0084, 0.0088; mean 0.0083, relative standard deviation 3.9%.

2.4.1.1.2. Electrode Separator Material. The material used to separate the working from the auxiliary electrode is known as nonwoven polypropylene fabric. It is approximately 0.0075 inches thick and weighs about 43 grams per square yard. The trade name is Webril–M 1003. It

is available from The Kendall Company, P. O. Box 10, Boston, MA 02101–0010. Rectangles 2.1 by 1.5 centimeters were easily cut with a single edge razor blade and a cardboard template. The fabric has a definite grain, and must be cut to facilitate rolling into a tube approximately 1/8 inch diameter by 2.1 cm long. Construction of the cell is greatly simplified if this tubular shape is "remembered" by the material. Shaping can be accomplished by wrapping the material around a 1/8" diameter aluminum rod, holding it in place with about six helical wraps of soft copper wire, and placing the rod/fabric in an oven at 150 degrees Celsius for 30–45 seconds. Care must be taken to ensure that only hot air contacts the fabric, or it will soften too much and become useless.

2.4.1.1.3. Platinum Gauze. Since manufacturer's specifications for the platinum gauze were unavailable, the following measured characteristics are given. The gauze was 50 mesh, measuring about 0.0077 inches thick, with a single strand measuring about 0.0034 inches diameter. The gauze was work hardened in manufacture and was initially too stiff to be rolled to 1/8 inch diameter tubes. After the mesh was annealed at 800 degrees Celsius for 15 minutes, it was squared by twisting and then affixed to a piece of tablet cardboard with ordinary translucent "scotch" tape. Orthogonal grid marks had been drawn on the cardboard at 1.5 and 2.0 centimeter spaces. The rectangles of gauze were cut with a straight edge and a new single edge razor blade. The tape was subsequently peeled from each rectangle. As a measure of the consistency of this cutting method, six pieces were weighed, in grams: 0.2181, 0.2196, 0.2313, 0.2052, 0.2060, 0.2230; mean 0.2172, relative standard devia–

tion 4.6%.

2.4.1.1.4. Platinum Leads. The electrode leads were 36 gauge platinum wire, annealed as above for the gauze. The auxiliary leads were six and the working leads were nine centimeters long.

2.4.1.1.5. Luer Lock Tees. The tees used to connect the heat shrink teflon assembly to standard Luer lock plumbing fittings were model FTLT-6 female and FMTLT-6 female-male polypropylene Luer lock tees. All Luer lock parts except valves were obtained from Value Plastics, Inc., 3350 Eastbrook Drive, Fort Collins, CO 80525. As shown in Figure 33a, the bore of each tee (through one leg and the junction and just into the opposite leg) was enlarged to provide a shoulder against which the heat shrink teflon assembly could be installed. Since the tees were more than two centimeters from junction to junction, the mating legs of the two tees were cut to allow the heat shrink assembly to seat against the shoulder of each tee, as shown in Figure 33b.

2.4.1.1.6. Heat Shrink Teflon Tube. Pieces of heat shrink Teflon tubing were selected from an assortment of tubes (FIT 400 MS/2, FEP Teflon, minimum shrink temperature 149 degrees Celsius, Alpha Wire Corporation, available through major electronics supply houses). The kit contains six different sizes. The most appropriate size fit just snugly over a 3/16 inch rod. Pieces 2.6 centimeters long were cut with a razor blade.

2.4.1.2. Assembling The Cell Module. The process of assembling the pieces starts at the inside and works out. The first step is to affix the end of the nine centimeter platinum working electrode lead to the circumference near the end of the RVC cylinder with a small spot of

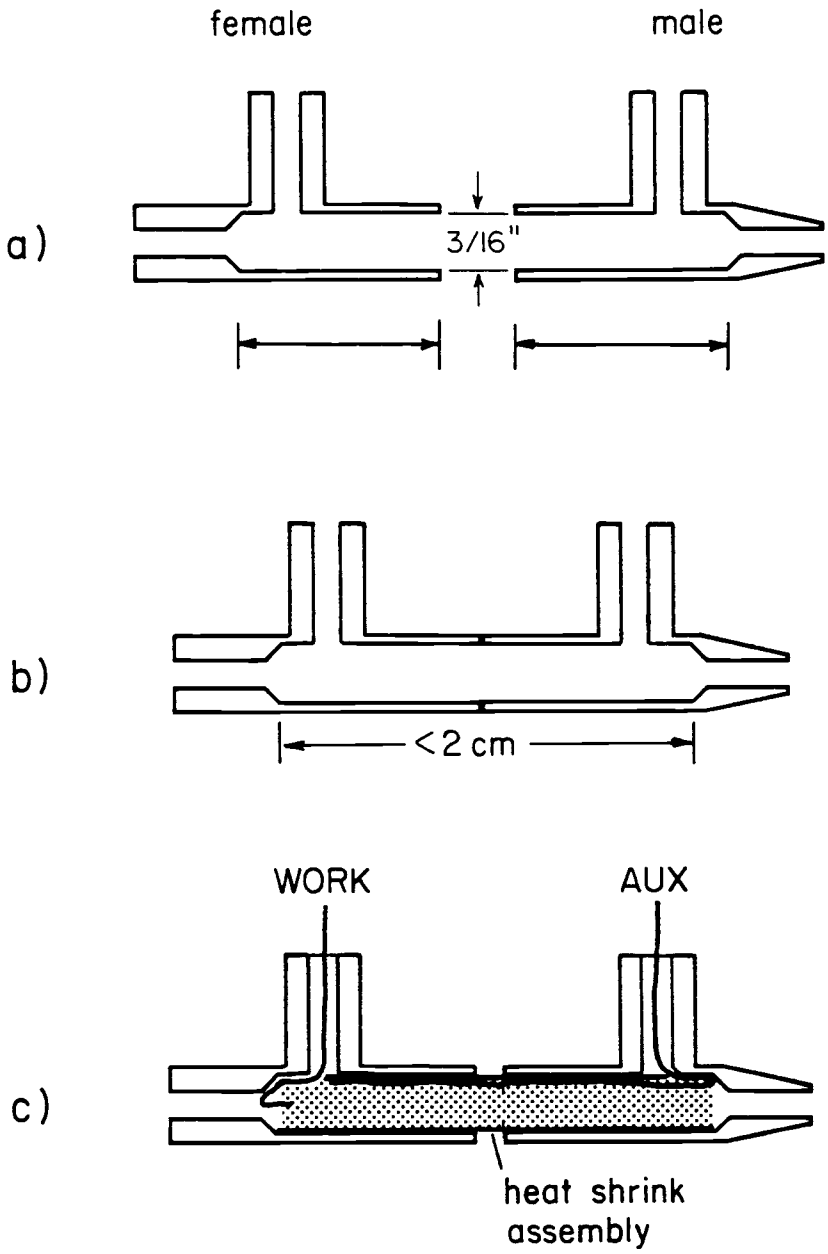

Figure 33. Final Assembly Details. (a) Female and male tees, arrows show length of 3/16" boring, (b) shortened to less than 2 cm, and (c) final assembly orientation showing routing of Pt leads.

liquid cement (Ambroid, Taunton, MA 02780). When the cement is dry, the platinum wire is wound like a helix around the RVC about four times, leaving about four centimeters for lead–out. The polypropylene fabric is wrapped around the RVC and platinum, and the platinum gauze is rolled around the fabric, loosely holding the assembly together. Now the auxiliary lead (6 centimeter) is held over the 2 centimeter cylinder such that the cylinder has a four centimeter lead extending from each end, and this assembly is slipped into the precut 2.6 centimeter piece of heat shrink teflon tube. Next the assembled parts are heated for 15 seconds on a plate of aluminum which remains inside a lab oven which is maintained at 150 degrees Celsius. After removing and cooling the cell, the resistance between the working and auxiliary lead should be greater than 10 megaohms, while the resistance between the working lead and the RVC probed with a small wire at the opposite end of the assembly should be about 15 ± 5 ohms. Historically, when the assembled cell was left in the oven too long, the working – auxiliary lead resistance was about 30 ohms because the separator material (non–woven fabric) softened and spread out around the ridge formed by the working electrode helix, allowing contact with the gauze auxiliary electrode.

The leads are then fed through the tees and the Teflon assembly is inserted to the shoulder of each tee. To obtain mechanical strength and durability of the leads, the platinum is soldered with resin core solder to short pieces of copper hook–up wire. To stabilize the hook–up wire and ensure a seal of the lead port of the tee, the cavities are filled with an epoxy resin which sets up in about 20

minutes (Tra–Bond 2129 from Tra–Con, Inc., 55 North Street, Medford, Mass. 02155). The same epoxy resin was used to ensure mechanical stability and to form a seal between the bored and shortened ends of the tees and the heat shrink tube; one blob of resin united the three pieces. The resistance measurements made above were repeated as a final check of each cell.

2.4.2. The Flow System. The module constructed above is a small but critical part in a system which includes sample deaeration, sample reservoirs, flow regulators, solution selection, a reference electrode and effluent collection. In general, all plumbing fittings were of the Luer lock type obtained from Value Plastics (see *Luer lock tees* above), and long distance connections were made with 0.045 inch inside diameter laboratory tubing (catalog number 116–0536–1000, Elkay Products, Inc., 800 Boston Turnpike, Shrewsbury, MA 01545). Figure 34 is a diagram of the integrated system. The subsections which follow describe further some of the modules in that figure.

2.4.2.1. Flow Control. Control of the flow rate of solution through the cell was by nitrogen head pressure in the solution reservoirs. In addition to a standard two stage regulator on the nitrogen tank, a Matheson 3701–70B nitrogen regulator was used to control the pressure accurately from 2 to 30 inches water column. The regulator comes equipped with a gauge, but resolution was not adequate so pressure was monitored with a water filled manometer constructed around a millimeter–graduated meter stick.

2.4.2.2. Solution Reservoirs. The reservoirs were 250 milliliter Nalgene

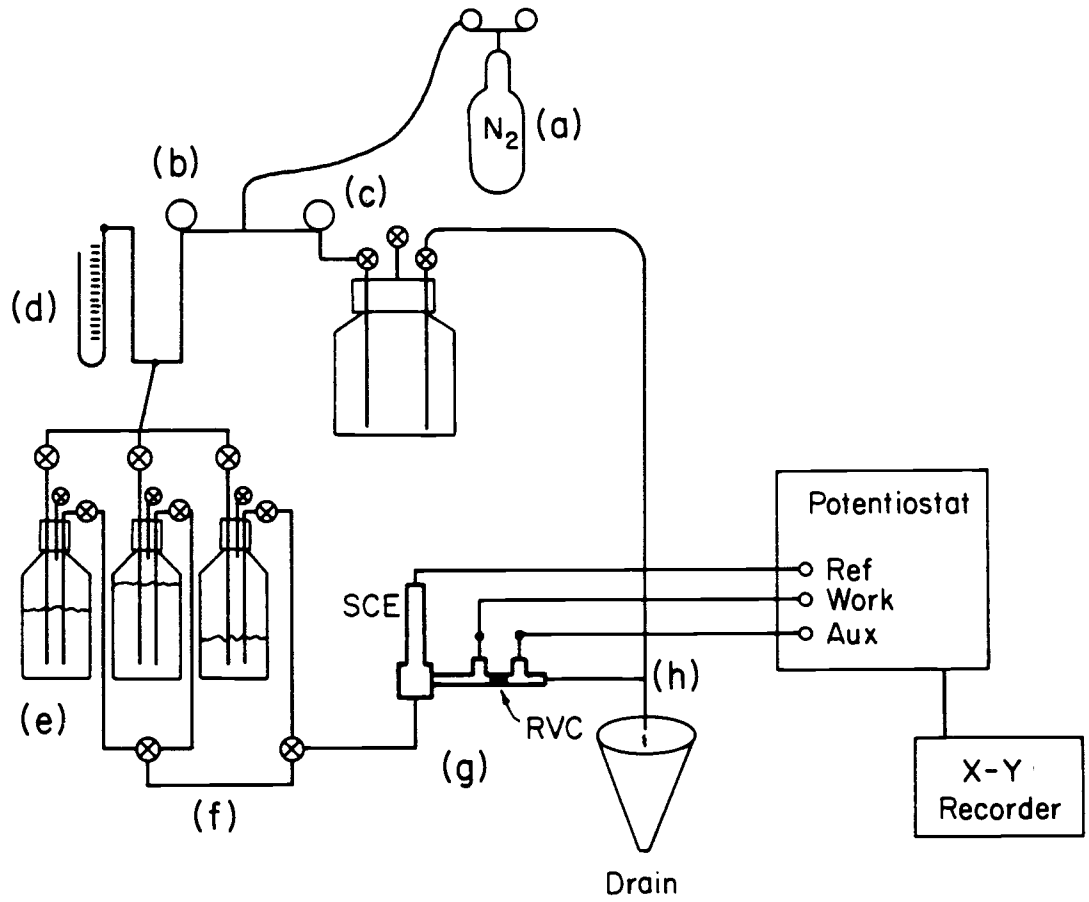

Figure 34. Flow–Cell Environment. (a) High pressure nitrogen and regulator, (b) analyte pressure regulator, (c) soap regulator, (d) water manometer, (e) analyte reservoirs with pressure in, vent and liquid out stopcocks, (f) three way valves (g) flow–cell and (h) analyte/soap mixing tee.

screw–top jars. Several jar lids were mounted with hose clamps to a support stand and attached to a nitrogen manifold so that several solutions of interest could be pressurized at the same time. Each attached jar lid had three Luer lock two–way valves; one for nitrogen inlet, one for liquid outlet and the third for venting to the atmosphere. If the head pressure were supplied to the top of the bottle, the pressure of the exiting solution would decrease as the liquid head in the jar decreased. This problem is overcome by extending the head pressure inlet to the bottom of the jar. This solution also made it convenient to deoxygenate the solution by closing the liquid–out valve and opening the other two. Luer lock valves in two, three and four–way configurations are manufactured by Medex Inc., Hilliard, Ohio 43026 and are distributed through Clinical Connections, Inc., P. O. Box 238, Orrville, Ohio 44667.

2.4.2.3. The Reference Electrode Holder The construction details of the reference electrode holder are shown in Figure 35. The holder was made from two pieces of 1–inch Teflon rod stock which are pulled together by four machine screws fitting through a ring collar on the top and threaded into a ring collar on the bottom. The two Teflon parts are joined with an O–ring seal, and the reference electrode seals in the top part with a second O–ring. The reference electrode was Orion's single junction model 900100 operated with their filling solution. Its potential is approximately that of a saturated calomel electrode. The inlet to the electrode holder was always on the bottom. The electrode was set in the holder by pushing it in until it bottomed out, then retracting it just enough to allow the reference electrode to be

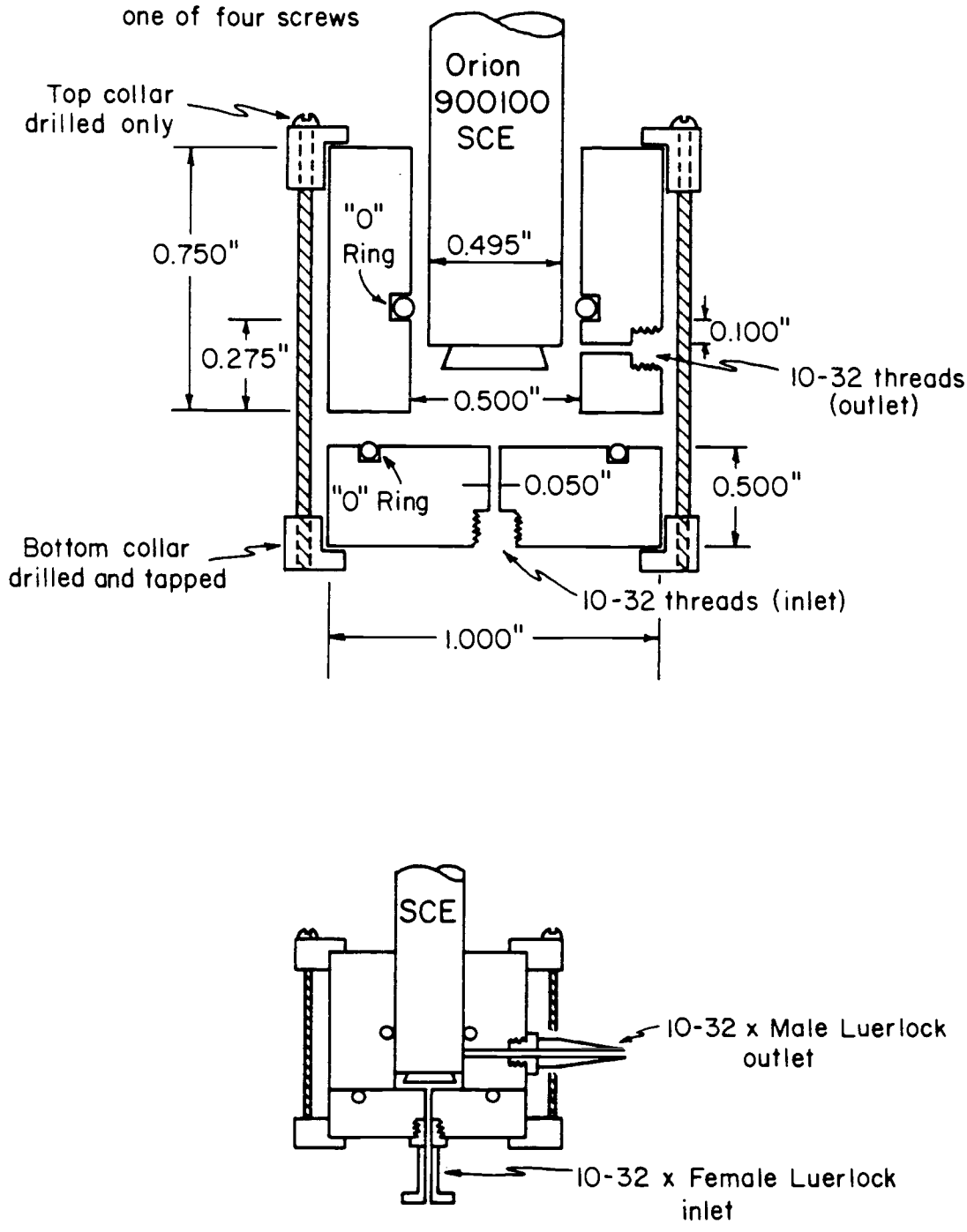

Figure 35. Reference Electrode Holder. The top figure shows detailed information for machining the holder, while the bottom shows the assembled holder.

manually bled, thus ensuring both low void volume in the holder and proper junction operation. The remainder of the flow–cell was always positioned below the level of the filling solution in the reference electrode to help ensure that the reference junction was leaking in the proper direction. The majority of the hydrostatic back–pressure in the system is caused by the small bore tubing (1.14 mm id) and hose barbs (0.635 mm id), which are upstream from the reference electrode and the flow–cell. The flow–cell, which was down stream from the reference electrode, has a very low resistance to solution flow.

2.4.2.4. Solution Effluent Tee. Consistent, periodic, and measurable fluctuations in cell current were correlated with the drip rate of the solution exiting the tube at the end of the system. The final solution to this problem was to mix the effluent with a surfactant at a small bore tee which was inserted into the 0.045 inch id tubing, and allow the surfactant–effluent to mix in about three centimeters of tube before exiting the tube in a continuous stream flowing down the side of funnel which ultimately drained into the sink. Lemon Fresh Joy (Proctor and Gamble, Cincinnati, OH) at a concentration of 50 mil–liliters per gallon of water was a satisfactory surfactant. Surfactant was injected into the tee from a pressurized gallon jar reservoir. The pressure applied to this reservoir was the minimum pressure which would give a continuous stream of surfactant down the side of the funnel when there was no flow through the cell.

2.5. PRELIMINARY EVALUATION OF THE CELL

The cell will be evaluated against four criteria: stability, sensitivity,

conversion efficiency and noise induced from unsteady flow.

2.5.1. Stability. The analyte used for the demonstration of cell stability is mercury because the reduction of mercury is not usually complicated by hydrogen interference and because we are interested in the benefits of mercury coating the RVC electrode. The electrolyte used is 1 M potassium nitrate rather than any chloride containing electrolyte, because stripping mercury in the presence of chloride tends to form a calomel layer on the mercury surface.

Stability of the cell is demonstrated by a series of 127 consecutive CV sweeps of 0.01 mM Hg^{2+} made continuously over a period of 1 hour and 16 minutes. The first seven scans are shown in Figure 36a; scans 76–80 in (36b); scans 88–95 in (36c); and scans 125–127 in (36d). Scan 88 (36c) was deliberately perturbed by stopping the sweep at an applied potential of −0.2 V for 10 seconds, which provided the largest stripping peak of that set. Subsequently smaller stripping peaks are attributed to replating the excess mercury remaining in the flow–cell from the previous strip, until ultimate return to steady state mercury content in the cell.

2.5.2. Sensitivity. We differentiate between sensitivity at bare RVC and sensitivity at mercury coated RVC. The benefits of mercury coating the working electrode have been discussed in Part 1. First we will describe here some of the problems encountered in plating the electrode with mercury, then we will discuss the performance of bare and mercury coated electrodes in the determination of cadmium and copper.

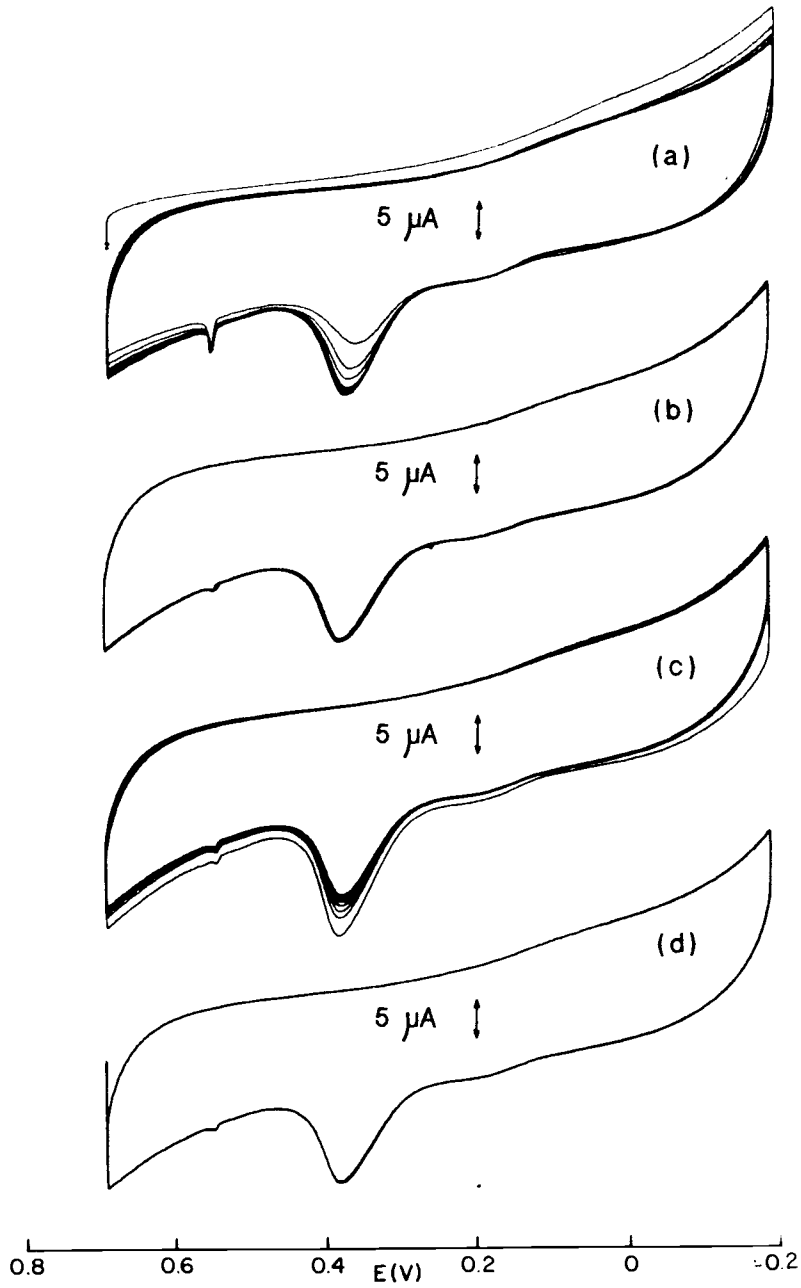

Figure 36. Long Term Electrode Stability. Electrolyte: in 0.01 mM Hg^{2+} in 1 M KNO_3. First 127 consecutive CVs, 50 mV/s, 1 ml/min. (a) first 7 scans, (b) scans 76–80, (c) scans 88–95, (d) scans 125–127. Scan 40 (in (c)) was deliberately perturbed by "holding" potential at −0.2 V for 10 seconds.

SCABE is not a satisfactory medium for plating and stripping of mercury because of the high chloride concentration. Stripping mercury in the presence of high chloride tends to form a calomel layer on the mercury surface, which precludes further stripping. Nitrate is not ideal because of the negative potential limit imposed by its depolarizing tendency. A sodium acetate – acetic acid buffer with about 1 molar total acetate at pH 4 was found to be satisfactory for mercury plating. A basic acetate buffer was found to be unsatisfactory because of formation and precipitation of red HgO.

Table 6 shows a comparison of absolute sensitivities obtained here with those reported in selected literature articles. The absolute sensitivity is defined here to be the stripping peak height in microamps divided by the product of the molarity of the analyte times the plating time, and has units of $\mu A/M \cdot s$. Several different electrode types are included from literature reports to give a feel for the broad applicability of this sensitivity calculation. Results for both ASV and CV experiments in this work are reported. The plate time for CV experiments is defined as the estimated time required to sweep the potential from the start of reduction to the start of stripping. The sensitivities of our cells compare favorably with the work of Blaedel and Wang (1979–b).

The CV sensitivity to cadmium on bare RVC is 250,000 and on mercury coated RVC the cadmium sensitivity is 1,100,000, Table 6. The cadmium sensitivity on mercury coated RVC is higher for CV (1,100,000) than for ASV (820,000) according to Table 6, but we believe these values do not give a fair indication of the utility of ASV. The

Reference (a)	Method (b)	Electrode (c)	Cu Sensitivity (d)	Cd Sensitivity (e)	Plate Time, s (f)
B&F	ASV	HMDE	1190	1270	1800
B&F	ASV	Graphite	5240	5240	300
B&F	ASV	GC,unp	11900	6670	300
B&F	ASV	GC,pol	11900	9250	300
W&D	ASV	Hg–Wall	19,000	22,000	120
B&W	ASV	Hg–RVC	740,000	1,100,000	120
Fig. 39	CV	Hg–RVC	220,000	–	8
Fig. 39	ASV	Hg–RVC	490,000	–	28
Fig. 37	CV	RVC	–	250,000	40
Fig. 41	ASV	RVC	–	310,000	130
Fig. 38a	CV	Hg–RVC	–	1,100,000	40
Fig. 38c	ASV	Hg–RVC	–	820,000	130

Table 6. Comparison of Absolute Sensitivities. (a) References: Bard and Faulkner (1980), Figure 10.8.7; Wang and Dewald (1983), Figures 3 and 7; Blaedel and Wang (1979–b), Figure 1; Remainder are figures in this work. (b) Methods: Anodic Stripping Voltammetry or Cyclic Voltammetry. (c) Electrode: HMDE = Hanging Mercury Drop; GC = Glassy Carbon, unpolished or polished; Hg–Wall = Mercury coated Glassy Carbon wall jet; RVC flow–cell or mercury coated RVC flow–cell. (d, e) Sensitivity: To Cu and Cd, $\mu A/M \cdot sec$. Sensitivity = stripping peak height, μA, divided by product of concentration, M, times plate time, s. (f) Plate time in seconds for ASV, or for CV the estimated time to sweep potential from start of reduction to start of strip.

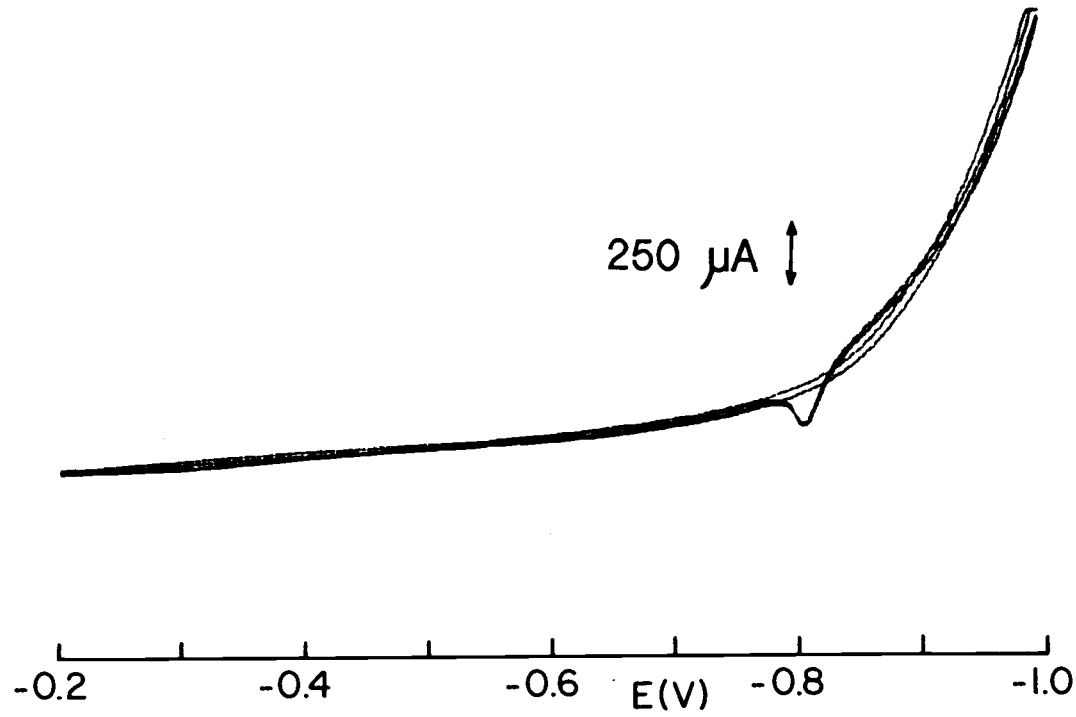

Figure 37. Flow-Cell Response with Bare RVC. CV of 0.01 mM Cd^{2+} in 33% SCABE, 10 mV/s, 1 ml/min.

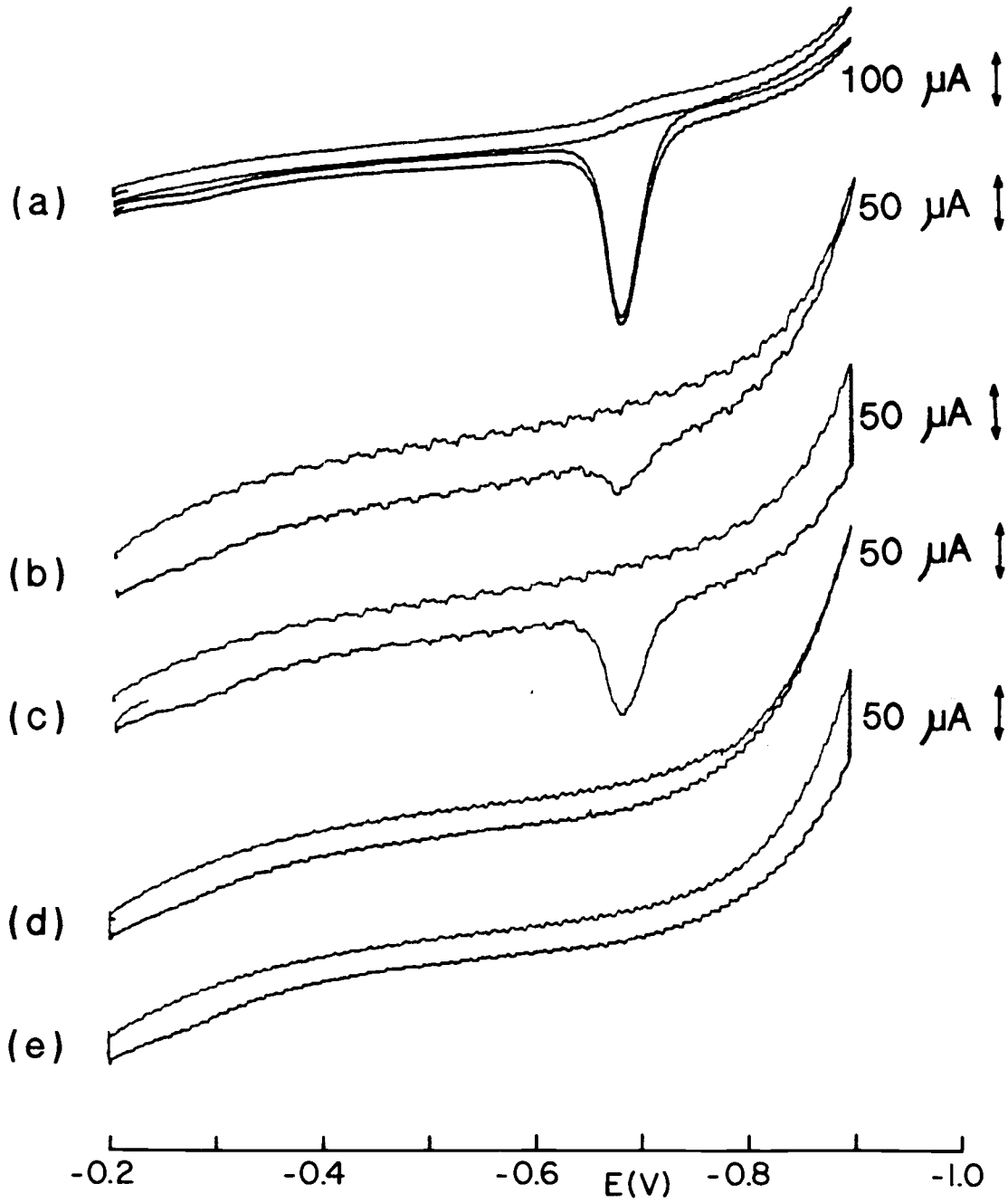

Figure 38. Flow-Cell Response to Cd on Mercury Plated RVC. All scans are 33% SCABE, 1 ml/min, 10 mV/s. (a) 0.01 mM Cd^{2+} CV. (b) 0.001 mM Cd^{2+} CV. (c) 0.001 mM Cd^{2+} ASV, 90 second hold. (d) blank CV. (e) blank ASV, 90 second hold.

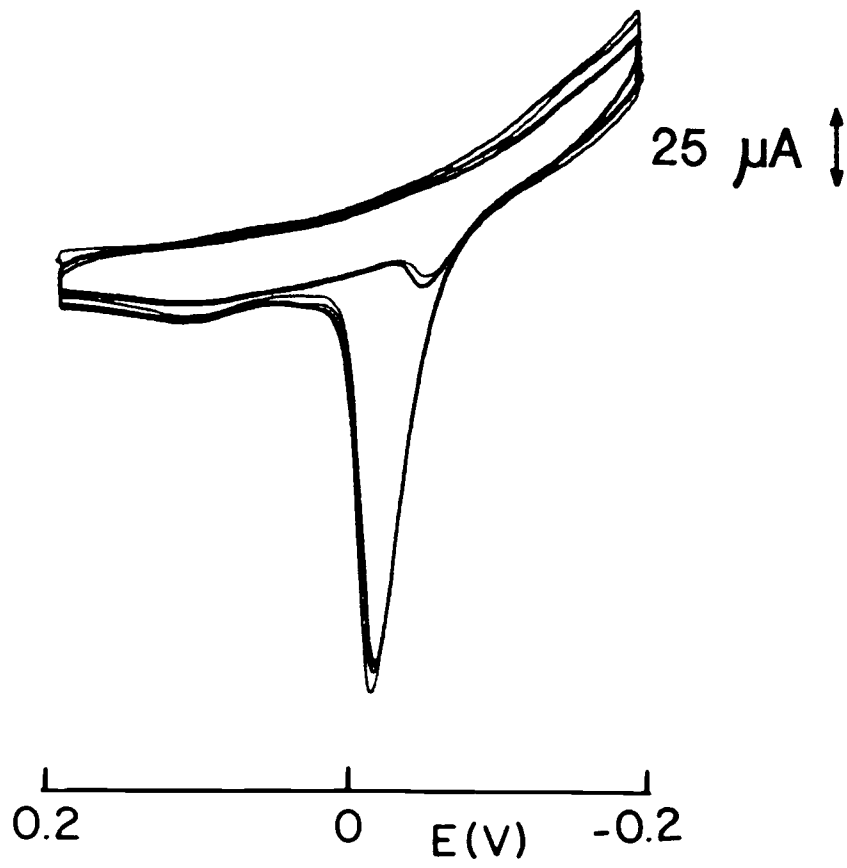

Figure 39. Flow–Cell Response to Cu on Mercury Plated RVC. CV and superimposed ASV with 20 second hold. 0.01 mM Cu^{2+} in 1 M KNO_3, 50 mV/s, 0.68 ml/min.

concentration of cadmium for the ASV trace, Figure 38c, is one–tenth the concentration of the CV trace, Figure 38a. A straight forward comparison in sensitivity between ASV and CV is shown in Figure 39, in which both traces were made with the same copper analyte concentration. The sensitivity values for copper are 220,000 for CV and 490,000 for ASV.

Two short comments on signal to noise ratio are appropriate before we leave the figures used for sensitivity data. First, the improvement in signal to noise ratios between CV and ASV is demonstrated by the traces shown in Figure 39 for a copper analyte and in Figure 38b and Figure 38c for a mercury analyte. Second, for the purposes of electrochemical preconcentration, a very low signal to noise ratio may be perfectly acceptable if electrochemical detection is not intended.

There were several ways we could have computed a number to represent sensitivity of these electrodes. We chose to normalize the data to account for the plating time because the plating time varies by a factor of more than 100. This normalization presumes that the techniques are linear with time, which is certainly not true beyond plating times of more than a few hours, or at short times where the effects of nucleation are predominant. The sensitivity is also dependent on the conversion efficiency of the cell (which we will see is dependent on the flow rate). Since these cells were operated at an estimated 50% efficiency, we suggest that the sensitivity could be increased by as much as a factor of two by decreasing the flow rate to achieve 100% conversion efficiency. A variation in conversion efficiency may also explain some of the variation in the sensitivities.

Finally, the large sensitivity values for the RVC cells are a reflection of the large surface area of these working electrodes. Their large area explains their ability to plate and strip large quantities of analyte. The surface area of our RVC cylinder is 10.6 cm^2, and Blaedel and Wang's (1979–b) electrode was 3.8 cm^2. For comparison, the surface area of a 2 mm diameter mercury drop is 0.13 cm^2, and the surface area of a 1 cm diameter glassy carbon electrode is 0.79 cm^2.

2.5.3. Conversion Efficiency. The conversion efficiency R is defined by

$$R = N_i / N_f \tag{13}$$

where N_i is is the number of moles electrolyzed and N_f is the number of moles entering the flow–cell.

The value of N_i if found by integrating the current

$$N_i = \frac{\int |i|\, dt}{nF} \tag{14}$$

where the n and F have their usual meaning, i is either the cathodic or anodic current, and t is the time the current is flowing. The integral of i with respect to time is simply the area of a "peak" in a voltamogram (with axis units of seconds and amps), and can be obtained, for example, by "counting squares", weighing graph paper, using a coulometer or integrator, etc.

The value of N_f is found from

$$N_f = vtC \quad (15)$$

where v is the volumetric flow rate, t is time and C is concentration.

The conversion efficiency for the cadmium CV shown in Figure 38a, when calculated with the anodic current integral, is 80%. The anodic conversion efficiency for the ASV shown in Figure 39 is 18%. We conclude that the cell operates with a reasonable degree of efficiency. We will present more data and examine conversion efficiency in greater detail in the next part of this report.

2.5.4. Smoothing the Flow. As illustrated in Figure 34 and discussed in section 2.4.2.4, the final design includes a surfactant to smooth the flow. Before that feature was developed, several interesting examples of noise induced irregularities in flow were observed. Figure 40 shows several time versus current traces which were made while plating the RVC working electrode with 1 mM Hg^{2+} in 1 M KNO_3, 1 ml/min. Figure 40a shows a variation in cell current on the order of +/− 10% with a possible period of about 20−30 seconds. Figure 40b illustrates the result of restricting the effluent port of the flow−cell. This restriction forced a smaller drop at higher frequency, thus causing much smaller variations in flow rate, and consequently cell current. A visual correlation was made in the lab between the transients shown in Figure 40c and gas generation/bubble movement within the flow−cell.

Figure 41a shows the results of inserting a small wire in the outlet orifice to break the drops. More satisfactory results are seen in Figures 41b and 41c where smooth flow was achieved by mixing the cell effluent with surfactant and letting the resulting continuous stream

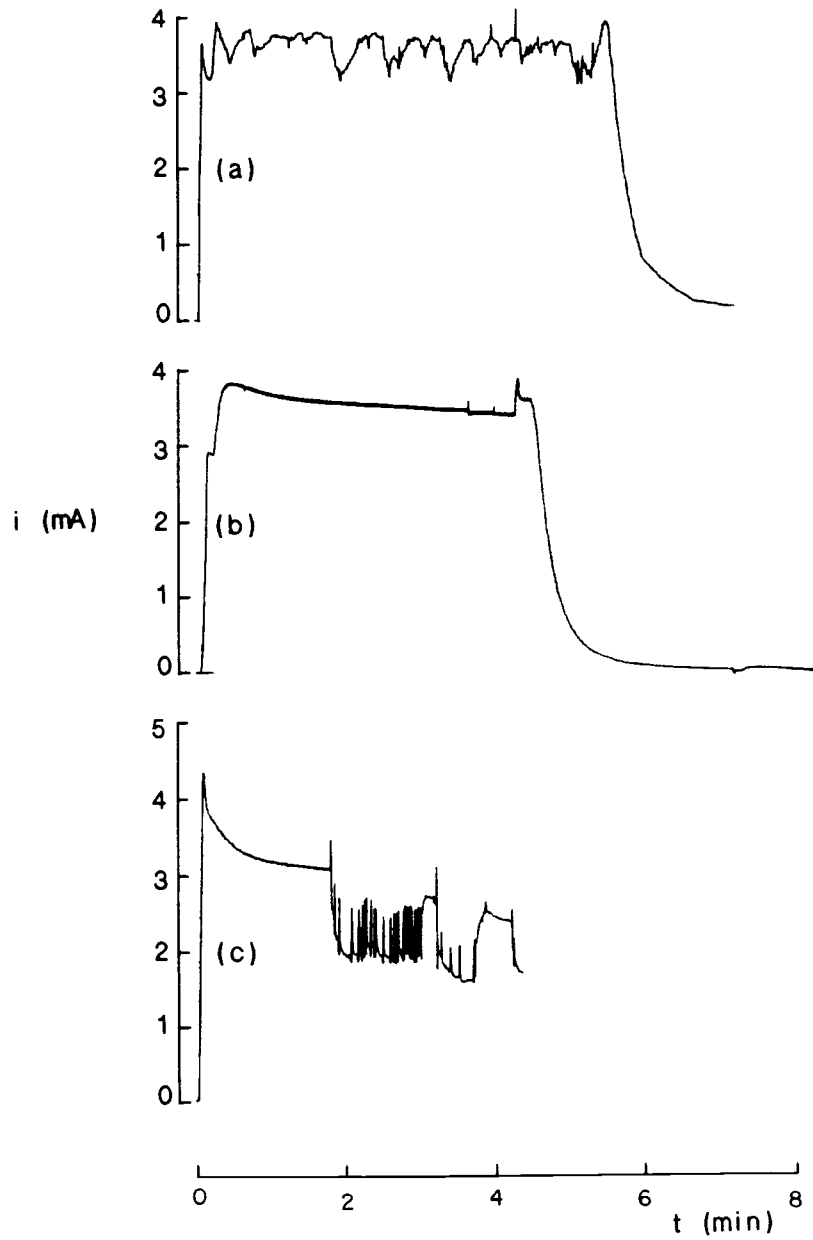

Figure 40. Smoothing the Flow I. All scans are time vs current traces of 1 mM Hg^{2+} in 0.1 M KNO_3, 1 ml/min. (a) Periodic fluctuation caused by effluent drops. (b) Restricted effluent port increases drop frequency, decreases magnitude of flow and current fluctuation. (c) Transients correlated with gas generation and bubble movement within the electrode.

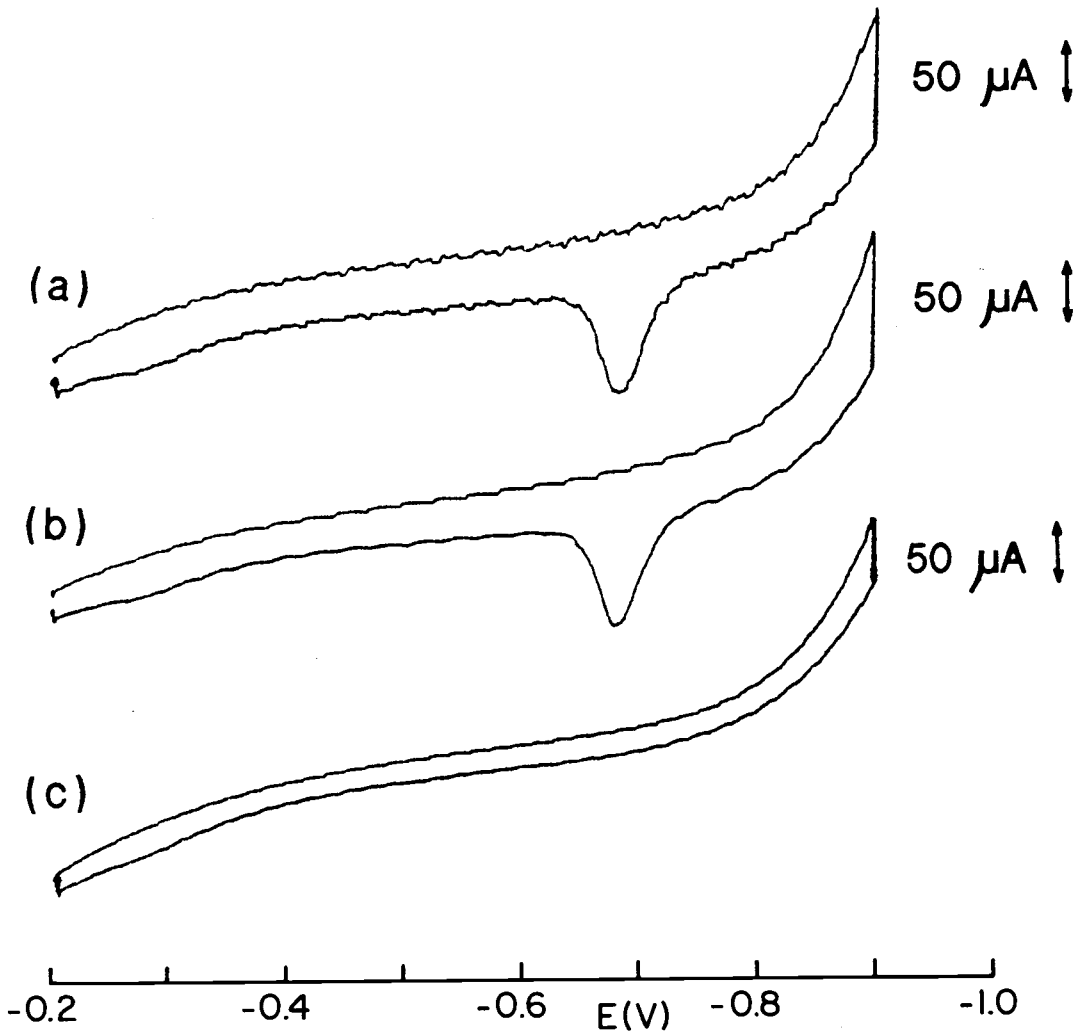

Figure 41. Smoothing the Flow II. All scans are combination CV and ASV with 90 second hold, 1 ml/min, 10 mV/s . (a and b) are 0.001 mM Cd^{2+} in 33% SCABE, (c) is Cd blank. (a) Attempt to smooth flow using wire in exhaust port to break drops. (b and c) Exhaust mixed with surfactant before exiting drain tube in smooth stream.

flow down the side of a funnel and subsequently to a drain.

2.5.5. Summary. This preliminary evaluation of the cylindrically symmetric flow–cells has shown that they are capable of stable, continuous operation for at least an hour when they are operated as described for Figure 36. The cells previous designs were worthless.

The sensitivity of these cells compares favorably to that of Blaedel and Wang (1979–b), as shown in Table 6. Sensitivity as defined here is related to stripping peak height, which is the second half of the preconcentration process; the first half of the preconcentration process is plating the analyte on the electrode.The conversion efficiency of these cells at a flow rate of 1 ml/min is about 50%.

Smooth flow of electrolyte through the cell is desirable because current output from the cell is dependent on, among other things, flow rate. Erratic flow rates make a noisy cell current baseline. Smooth current flow can be achieved by attention to detail at the inlet and outlet ends of the complete flow system.

PART 3: FLOW ELECTRODE EVALUATION

3.1. INTRODUCTION

In Part 1 of this investigation, we studied the suitability of RVC for preconcentration of cadmium from an aqueous hydrofluoric acid–zirconium solution. The results of that study were encouraging, but they were not conclusive because concentration limits, flowing systems and the advantages of mercury coating had not been rigorously investigated.

In Part 2 of this investigation, several cell designs were evaluated before the conclusion was reached that the electrolyte iR drop was the most important consideration in the design of a flow–cell. A cylindrically symmetric flow–cell was designed and fabricated after a careful review of the possible sources of iR drop. Preliminary evaluation of that cell against the criteria of stability, sensitivity, and efficiency gave positive results. Flow–induced noise was also identified as a major factor in cell performance, and modifications to the inlet and outlet of the cylindrically symmetric flow–cell made significant reductions in that noise.

In Part 3 of this investigation, we will compare the actual performance of this cell with the theoretical predictions of conversion efficiency and cell current as a function of flow rate. A favorable comparison will be further indication that the cylindrically symmetric flow–cell is potentially useful for electrochemical preconcentration and is worthy of continued development.

3.2. THEORY

This theoretical development is for a flow–through porous electrode which is operated at electrode potentials which produce mass transfer limited current from the analyte in the influent solution. We do not consider longitudinal or radial gradients in potential, radial inhomogeneities in current density, current attributed to interfering reactions like hydrogen generation, or other complications encountered in the operation of flow–cells. This theory can help in predicting the effect of changing dimensions and flow rate on total current and conversion efficiency of the cell. The theory can also help to predict and establish desirable operating parameters for routine use of a characterized cell.

3.2.1. Conversion Efficiency of a Flow-Cell. For complete conversion of the species of interest in a flow–cell, the current i is

$$i(100\%) = nFCv \tag{16}$$

where C is the concentration of the species of interest, mol cm^{-3}, v is the volumetric flow rate of the electrolyte, cm^3/s, and n and F have the usual meaning. Under conditions of less than complete conversion, the steady steady state current is found by multiplying both sides of Equation 16 by the conversion efficiency R

$$i = nFCvR \tag{17}$$

We now wish to derive an expression for R in terms of the

measurable characteristics of the flow–cell. Our approach is to express *R* as a function of the inlet and outlet concentrations

$$R = \frac{C(in) - C(out)}{C(in)} \tag{18}$$

and to derive an expression for C(out) in terms of C(in).

First we consider the parallel case of bulk electrolysis as is carried out in controlled potential coulometry with electrode potentials appropriate for limiting current conditions ($C^{*} >> C^{x=0}$). The concentration decays exponentially as a function of time:

$$C(t) = C(t=0)\exp(-mst) \tag{19}$$

where

C(t)	is concentration, mol cm^{-3}, as a function of time
m	is the mass transfer coefficient, cm/s
s	is the ratio of electrode surface area to the volume of solution, ($cm^2/cm^3 = cm^{-1}$)
t	is time, s

For a flow–cell, the time in Equation 19 can be found from the linear flow velocity and the length of the working electrode. The *linear* flow velocity for the electrolyte is

$$v = v/a \tag{20}$$

where v is the *linear* flow velocity, cm/s, and a is the cross sectional area of the working electrode, cm^2. The time t for a volume of electrolyte to pass through the cell is simply the cell length L divided by the linear flow velocity v,

$$t = L/v \tag{21}$$

Equation 19 can be transformed from a function of time to a function of distance through the porous working electrode by substitution of Equation 21 into 19

$$C(L) = C(L=0)\ \exp(-msL/v) \tag{22}$$

Equation 22 would be valid if the mass transfer coefficient were in reality independent of the flow velocity. Unfortunately it is not, but it can be related to the flow velocity by the empirical equation

$$m = bv^{\alpha} \tag{23}$$

where b is a constant, formally cm/s, and α is a valid exponent when v is expressed as cm/s. Substituting Equation 23 into 22 yields

$$C(L) = C(L=0)\ \exp(-bsLv^{\alpha-1}) \tag{24}$$

Recognizing that C(in) = C(L=0) and C(out) = C(L), we can substitute Equation 24 into 18 to obtain an expression for the conversion ef-

ficiency R as a function of a) the characteristics of the flow-cell, s and L, b) the operating characteristic $\overline{\nu}$, and c) the empirical parameters b and $\propto$.

$$R = 1 - \exp(-bsL\overline{\nu}^{\propto-1}) \tag{25}$$

Equation 25 is identical in form to one derived by Sioda (1970), who was among the first to develop the mathematical treatment of porous working electrodes, as noted by Bard and Faulkner (1980, reference 37, chapter 10).

3.2.2. Current at a Flow-Cell. We can combine Equations 17 and 25 to give an expression for the steady state current flowing through the cell as a function of cell characteristics and operating parameters

$$i = nFCv(1 - e^{-bsL\overline{\nu}^{\propto-1}}) \tag{26}$$

All of the terms except b and $\propto$ in Equation 26 are easily obtained (s is 66 cm^2/cm^3, a specification provided by the manufacturer of RVC). To determine the value of b and $\propto$, we rearrange Equation 26 obtaining

$$\exp[bsL(\overline{\nu})^{\propto-1}] = \frac{nFC(0)v}{nFC(0)v - i} \tag{27}$$

We can remove the exponential and the power of ($\propto$-1) term on the left

side of Equation 27 by taking the natural logarithm twice and converting to base 10 logarithms

$$(\alpha-1)\log(v) + \log bsL - \log(2.303) = \text{loglog}\ \frac{nFC(0)v}{nFC(0)v - i} \qquad (28)$$

If we plot the logarithmic quotient on the right against the log of the linear flow velocity v, the slope of the line will be $(\alpha-1)$ and the proportionality constant b can be found from the intercept.

3.3. ACTUAL vs THEORETICAL PERFORMANCE.

The actual performance of these cells will be compared to the predictions of the theory we have just developed. First we will compare conversion efficiency versus flow rate. Then, after we determine b and α from the slope and intercept suggested by Equation 28, we will compare the steady state current versus flow rate.

3.3.1. Flow Calibration. Evaluation of a flow-cell requires accurate measurement of analyte flow and current response. A convenient and precise method for integrating analyte flow is to switch (with a three-way valve) the cell's input stream from blank to analyte and back to blank. Since we know the concentration, flow rate and the time interval for the analyte stream, we can calculate the product nFC(0)v. Switching solutions is preferred to switching potential from oxidizing to reducing and back to oxidizing because it eliminates the high capacitive current surges and associated high iR drop encountered when the potential is switched.

The simplest method of obtaining data of sufficient accuracy

to calibrate flow rate versus head pressure was to collect the effluent from each cell on a digital top–loading balance (Mettler PE3600) while monitoring head pressure with a millimeter–resolution water filled manometer. The calibration procedure had to be repeated for each cell because of their individual, hand made nature. A typical calibration equation for flow F in ml/min as a function of pressure P in mm w.c. is

$$F = -9.109 + 0.0359P - 3.347\text{x}10^{-6}P^2 - 3.525\text{x}10^{-9}P^3 \qquad (29)$$

3.3.2. Flow and Current Measurements. Data were obtained from two different cells. The first cell, which we will call cell "j", was operated with a mercury analyte. Electrode "j" became completely inactive shortly after we completed data collection for the mercury analyte. The second cell, called "k", was operated successfully with a copper analyte. Electrode "k" was, however, completely inactive at the end of data collection with the mercury analyte.

A step input in concentration entering the flow–cell was provided by switching the input stream between 0.2 M NaAc, pH 4.0 electrolyte blank and the same electrolyte with 0.1 mM Hg[II] or Cu[II], both electroactive species. Mercury and copper were chosen as the analytes rather than cadmium because they do not require as negative an electrode potential for reduction. The reduction of copper and mercury is much less prone to interference from hydrogen than is the reduction of cadmium. We are also interested in coating the RVC electrode with mercury.

The duration of the step input was 90 seconds, after which the

blank was switched into the flow system and the response followed until baseline current was restored, Figure 42. The plated analyte was then stripped from the electrode. The stripping scan always started within 30 seconds of termination of the plating scan. There was never an interruption or change in electrode potential from the start of electrode plating until start of electrode stripping.

Photo-copies were made of the recorder traces, and the integrals were cut and weighed. Knowing analyte plug time, analyte concentration, flow rate, and the values for the plating and stripping integrals, we can compare the cell response to the theory we have developed.

3.3.3. Conversion Efficiency. Figure 43 shows the conversion efficiency, as calculated with reduction current integrals and the amount of analyte in the plug which flowed through the cell, Equations 13 – 15 (developed in Part 2, section 2.5.3). The shape of the curves shows the general form of exponential decay as indicated by Equation 25, and these curve shapes agree with Blaedel and Wang (1979). Similar results are obtained if the oxidation current integral is used.

We would expect the ratio of the oxidation current integral to the reduction current integral for these experiments to be 1.00. Figure 44 demonstrates that the stripping current to plating current ratio is *always less than 1.* The data supporting this statement represents 30 pairs of stripping and plating current integrals, obtained from two cells and two analytes. The fact that the ratio is consistently less than 1 is unexplained. Some comfort can be taken in the fact that the reduction current integral to oxidation current integral ratio of Schiffrin's ex-

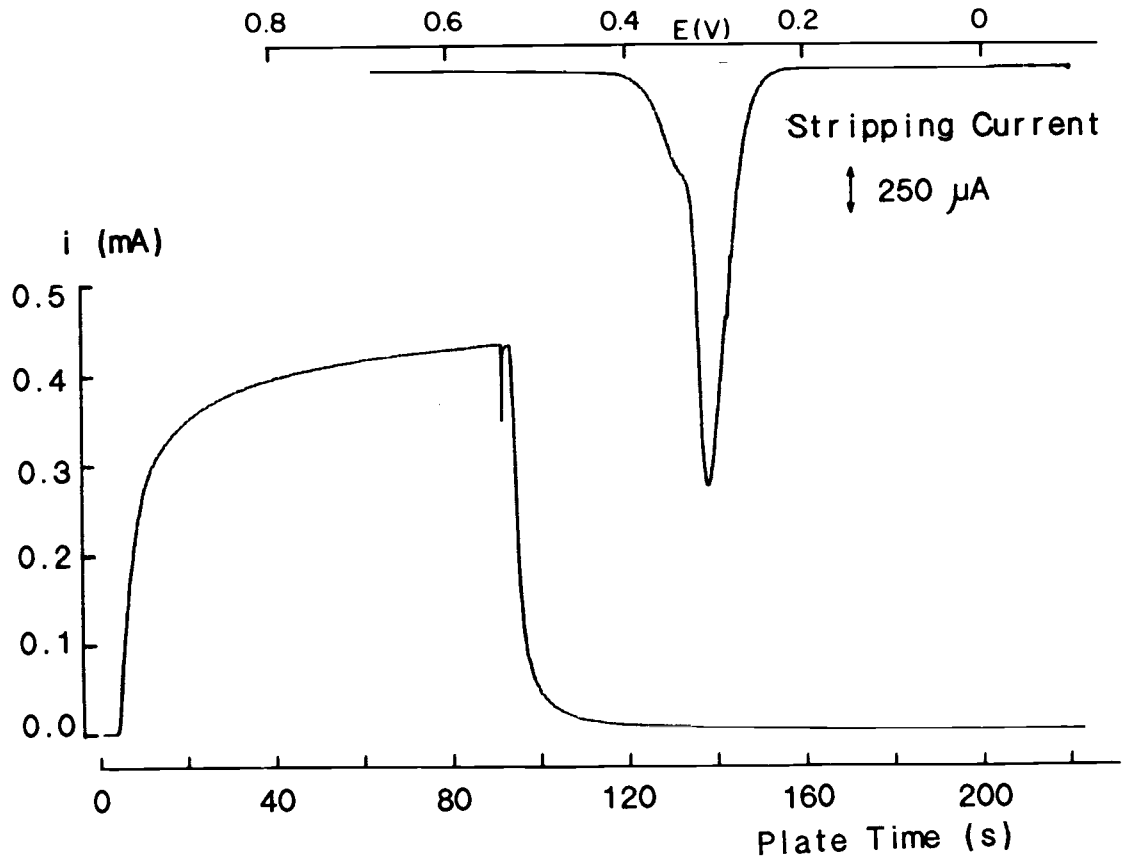

Figure 42. System Response to Plug Inputs. Plug (input at t=0) is 90 seconds of 0.1 mM Hg^{2+} in 0.2 M sodium acetate at pH 4.0, flowing at 7.36 ml/min. Plate potential and strip start potential is −0.1 V. (a) Stripping current at 5 mV/s, (b) Plating current.

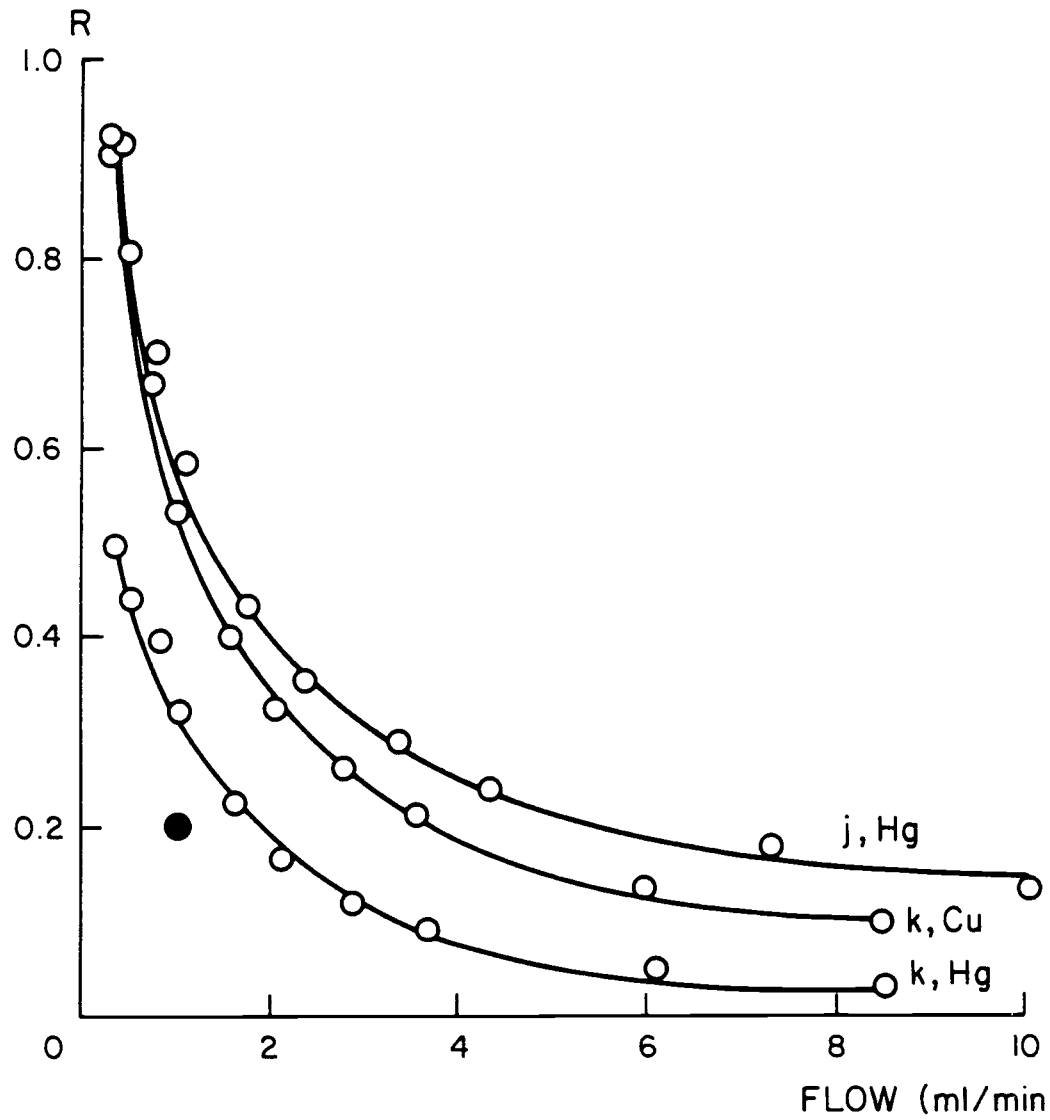

Figure 43. Conversion Efficiency *R* vs Flow Rate. Cell "j" with Hg analyte, and cell "k" with Cu and Hg analytes.

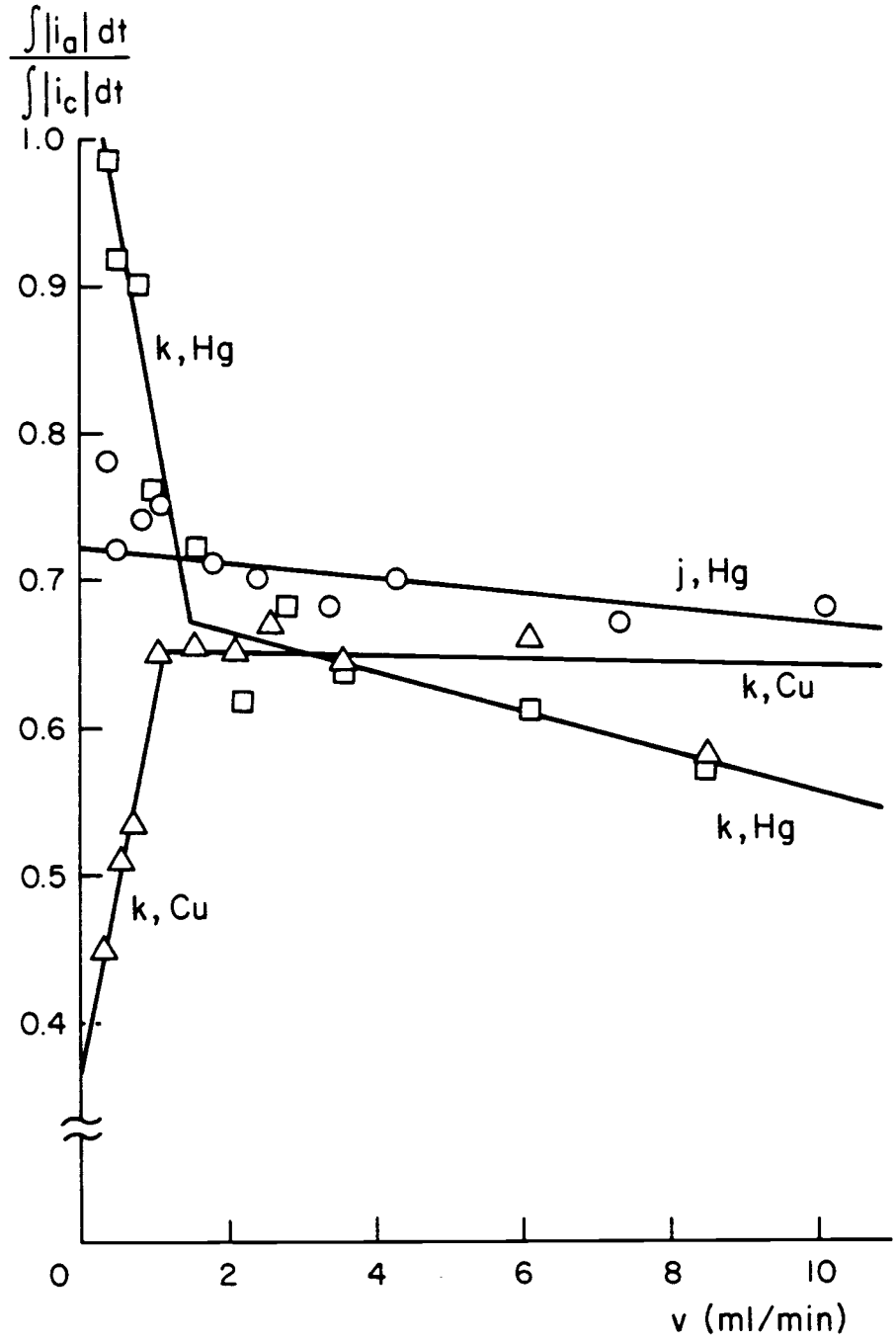

Figure 44. Stripping Current to Plating Current Ratio vs Flow Rate. Cell "j" with Hg analyte, and cell "k" with Cu and Hg analytes.

ample CV is 0.37 (see Figure 2 in Section 1.2.1.2.). These observations indicate a serious problem in the theory of cell operation; the subject is identified as one which requires further study.

3.3.4. Determining the Value of "b" and Alpha. The empirical factors *b* and α are determined from the plots of Equation 28 shown in Figure 45. According to Equation 28, the slope of each of the lines in this figure is equal to (α–1). When cell "j" was operated with a 0.1 mM mercury analyte, the value of alpha was 0.11. When cell "k" was operated with a 0.1 mM copper analyte, the value of alpha was 0.0066. Electrode "k" was subsequently operated with a 0.01 mercury analyte for which the value of alpha was 0.041. It is noteworthy that α is approximately equal to zero, or the mass transfer coefficient is approximately independent of flow rate (Equation 23).

The intercepts of the lines in Figure 45 are related to the constant *b* in Equation 28. For cell "j", b = 0.00196 cm/s for the mercury analyte. Electrode "k" gave values for *b* of 0.00135 cm/s for copper and 0.00055 cm/s for mercury. As noted in the previous paragraph, the value of α is almost zero, which means that the value of *b* is very close to the mass transfer coefficient *m*, Equation 23. For purposes of comparison, the value of *m* can be calculated as shown by Bard and Faulkner (1980, Equation 8.3.24 and Problem 1.2) in their treatment of forced convection as characterized by a rotating disk electrode. The calculated mass transfer coefficient for Fe^{3+} in an aqueous solution with a disk electrode rotating at 10 revolutions per second is 0.0032 cm/sec, which is about twice the value we have noted.

The values of *b* and alpha determined here will be used in the

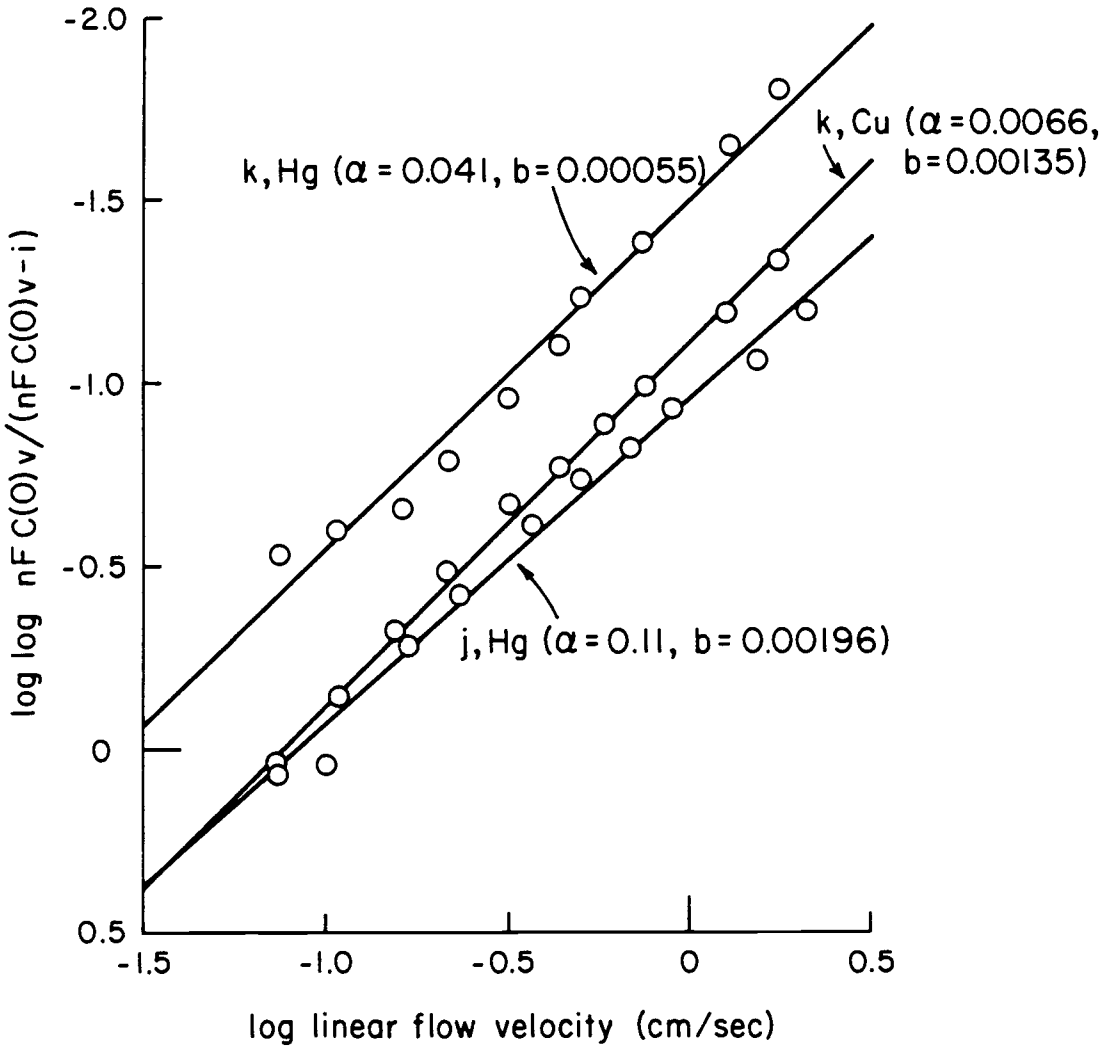

Figure 45. Determining the Value of ***b*** and Alpha. Cell "j" with Hg analyte, and cell "k" with Cu and Hg analytes. See the derivation of Equation 28 for explanation of the axes.

next section to generate a prediction of the steady state current of the flow–cells as a function of electrolyte flow rate.

3.3.5. Total Current. The continuous lines of Figure 46 represent the cell reduction current – flow rate response predicted by Equation 26 with values of α and b determined from Figure 45. The data points shown in Figure 46 were obtained for each flow rate and analyte by dividing the reduction current integral (current X time) by the time the analyte plug was switched into the flow–cell. That quotient is the average reduction current flowing in the cell.

The similarity of the experimental data and the predictions of Equation 26 shown in Figure 46 is encouraging because it tends to verify the model we have developed for the flow–cell. We should be able to predict the effects of changes in electrode cross sectional area, electrode length and analyte flow rate using this model

As mentioned in the Section 3.3.2 *Flow and Current Measurements*, cell "k" became inactive during the collection of data with the mercury analyte. The solid point in Figure 46 is the last datum collected for that cell; previous data had been taken in order of increasing flow rate. Whatever the mechanism of failure for this cell, it obviously had an effect on the data taken with the mercury analyte.

Sioda (1970) and Blaedel and Wang (1979) report current – flow response of their cells, but their results are best described as two straight lines intersecting in the region of low flow rates. The low–flow–rate line has the larger slope of the two lines. The *implication* in those reports is that the value of alpha changes at the flow rate corresponding to the point of intersection of the two lines. This change in

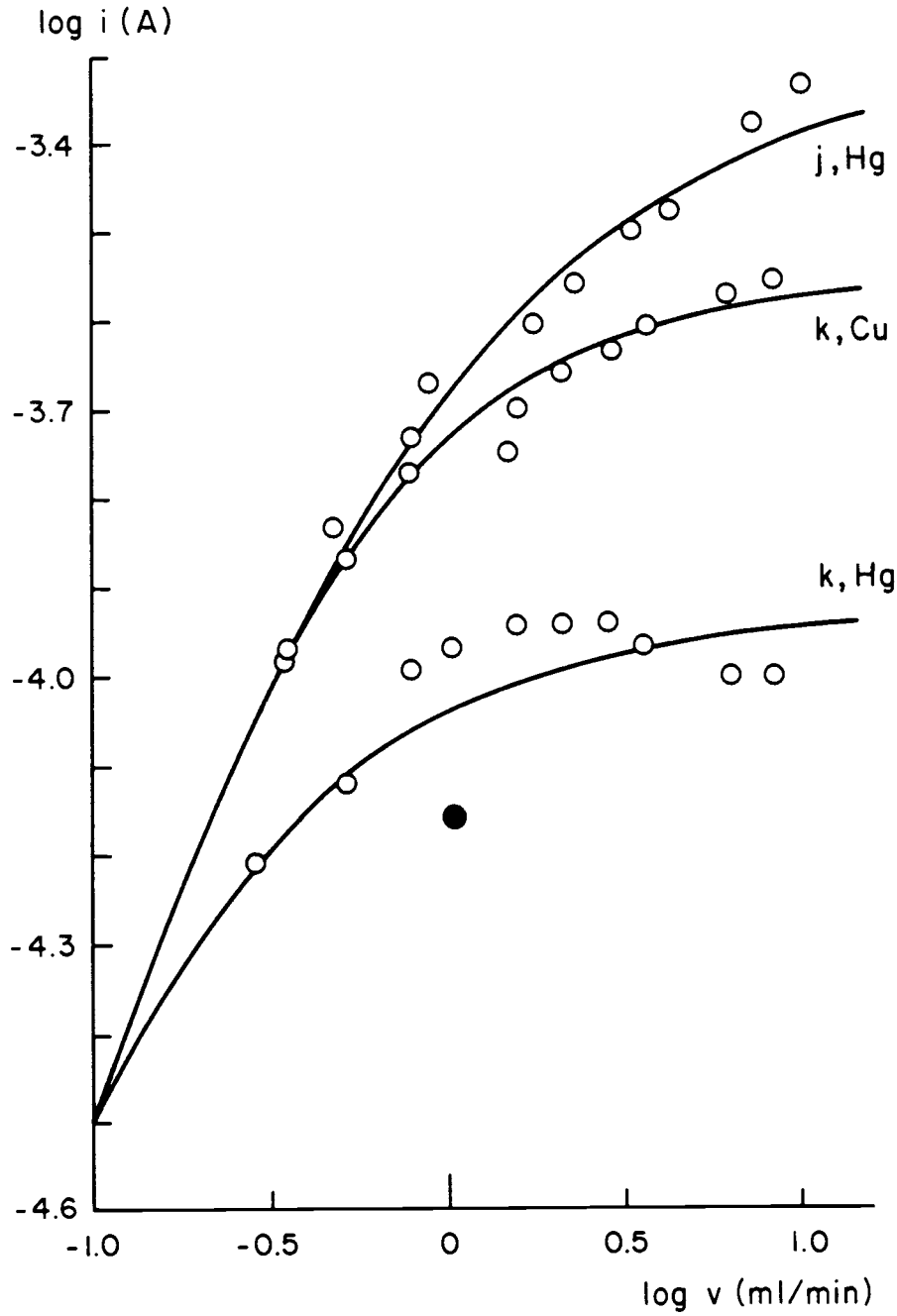

Figure 46. Steady State Limiting Current vs Flow Rate. Cell "j" with Hg analyte, and cell "k" with Cu and Hg analytes. Smooth curves are plots of Equation 26, with *b* and alpha as noted in Figure 45. The experimental data are also plotted.

alpha reflects a change from laminar to turbulent flow with increasing flow rate. We maintain that the the current – flow rate response of our cells is continuous and that the value of alpha remains constant throughout the range of flow rates (ca 0.3 – 10 ml/min) used in this work. The flow rate ranges were 0.5 – 10 ml/min for Blaedel and Wang's RVC cell and 0.3 – 200 ml/min for Sioda's platinum grid electrode.

3.4. CONCLUDING DISCUSSION

The cylindrically symmetric flow–cell designed in Part 2 of this inves–tigation appears to perform according to the theoretical predictions of conversion efficiency and total cell current. The determination of the flow characteristic constant alpha and the proportionality constant b by the methods suggested by Equation 28 is straightforward. The ability to evaluate these to parameters will facilitate the design and operation of future cells.

The cylindrically symmetric cell has a sensitivity to copper and cadmium which is better than or comparable to other electrodes and techniques (Table 6). Our cells are also capable of stable, long term (over 1 hour) operation (Figure 36).

The most serious limitation in the use of these cylindrically symmetric cells is their unpredictable useful lifetime and the lack of understanding of how cells become inactive. Often one cell fails to generate a Faradaic current, i.e. it becomes totally inactive, and there is no indication of why the cell has failed. Another cell may last through hundreds of cycles and many different electrolytes with no apparent reason for its longevity.

The only obvious difference in the cells is the simple fact that they are all hand made and assembled, and the coordination of all the pieces fitting into a small space is something that can be done much better by machine. It appears to this investigator that a reasonable next step in continuing this work would be to improve the precision of construction of these cells by building tools to improve the reproducibility of parts fabrication and jigs to improve the assembly phase. With a supply of consistent cells, the process of identifying the best and the worst parameters for operation would be simplified. Without consistency in cells, the task is perhaps impossible.

Much of the work done with these cells involved the use of high chloride concentrations in the electrolyte. Positive electrode potentials (+1.0 V vs SCE) is reported to cause degeneration of RVC in a chloride (sea water) medium (Blaedel and Wang (1979–b)). McLaren et al (1977) and Florence (1984) report that all forms of carbon are rapidly attacked by free chlorine. It is possible that the extensive work done here with 0.33 M chloride (33% SCABE) may have contributed to cell failure; further investigation is indicated.

If it could be determined that the electrolyte in use degrades the RVC electrode material, then obviously the best solution is to change electrolytes, but this may not be possible because of the analyte and/or sample matrix. In the latter case, valves could be arranged so that the adverse sample contacts the RVC for a minimum time; the remaining time the RVC could be bathed in some innocuous electrolyte.

The background current in the cell during the *stripping* phase of the analysis – preconcentration cycle could perhaps be reduced by

stopping the flow of electrolyte. Another method of reducing the stripping background current would be to change from the sample electrolyte to some ideal, low background electrolyte for the *stripping* phase, using the valve switching concept noted above. There may be a further reduction in stripping background current by implementing both stopped flow and ideal electrolyte.

Wang et al (1987), Sottery et al (1987) and Stulikova (1973) report that mercury plated on carbon substrates forms as *droplets*. Hoyer et al (1987) claim that the mercury *droplets* on glassy carbon are susceptible to dislodging and coalescing, and report on a method of stabilization by polymer coating. It appears that the mechanical stability of mercury plated on carbon surfaces is a concern, and further work is necessary to determine if there is a problem with removal of mercury by the shear effect of the flowing stream, or indeed if all reduced mercury adheres to the RVC surface.

The original target of this investigation was to develop a flow-cell for the electrochemical preconcentration of cadmium in an electrolyte of zirconium dissolved in hydrofluoric acid. The advantage of preconcentration with a flow-cell is the possibility of straightforward integration of this technique with the currently automated sample changing and analysis by spectrochemical equipment. Unfortunately, neither the method of cell manufacture used in this study or the level of understanding of cell failure is adequate. We have, however, made considerable progress in determining the important attributes of flow electrode design, construction and operation.

Now is a good time to look for alternative approaches which

would allow more tolerance in cell operating parameters. For example, perhaps zirconium can be complexed at a higher pH by something besides fluoride ion. Another alternative is automation of flow control and solution switching. Automation would reduce the frequency of operator–caused cell current excursions, which have caused a significant number of cell failures.

This investigation comes to an end because the cost of continued research is beyond the original scope of this work. The most logical next steps involve cell production technology and automation of flow–cell operation, both of which are large tasks. In light of these potential costs without guarantee of success, it is time now to review other potential methods of preconcentration and/or detection of cadmium.

In summary, this investigation concludes that the electrochemical preconcentration of cadmium in an electrolyte of zirconium dissolved in hydrofluoric acid is not practical with the current level of understanding of electrochemistry and flow–cell design; there still exist several significant paths for research which may make the goal practical. Some of those subjects have been identified in this section. The other subjects were discussed in Section 1.4.3 *Electrode Pretreatment*, Section 1.4.6.2 *The Nature of the Mercury Coating* and Section 3.3.3 *Conversion Efficiency*.

4. BIBLIOGRAPHY

Alkire, R. and Gould, R., "Analysis of Multiple Reaction Sequences in Flow–Through Porous Electrodes", J. Electrochemical Soc., 1976, 123(12), 1842–1849.

Astley, D. J., Harrison, J. A., and Thirsk, H. R., Trans. Faraday Soc., 1968, 64, 192.

Ateya, B. G. and Austin, L. G., "Steady–State Polarization at Porous, Flow–Through Electrodes with Small Pore Diameter", J. Electrochemical Soc., 1977, 124(1), 83–89.

Bard, A. J. and Faulkner, L. R., Electrochemical Methods. Fundamentals and Applications, John Wiley and Sons, New York, 1980.

Blaedel, W. J. and Wang, J., "Flow Electrolysis on a Reticulated Vitreous Carbon Electrode", Analytical Chemistry, 1979, 51(7) 799–802.

Blaedel, W. J. and Wang, J., "Anodic Stripping Voltammetry at a Reticulated Mercury Vitreous Carbon Electrode", Analytical Chemistry, 1979, 51(11) 1724–8.

Connic, R. E. and McVey, W. H., Journal of the American Chemical Society, 1949, 71, 3182–3191.

Florence, T. M., Journal of Electroanal. Chem., 1984, 168, 207–218.

Goldstein, Gerald, Analytical Chemistry, 1964, 36(1), 243–244.

Harrar, J. E. and Shain, I., "Electrode Potential Gradients and Cell Design in Controlled Potential Electrolysis Experiments", Analytical Chemistry, 1966, 38(9), 1148–1158.

Hills, G. J., Schiffrin, D. J. and Thompson, J., "Electrochemical Nucleation From Molten Salts I. Diffusion Controlled Electrodeposition of Silver from Alkali Molten Nitrates", Electrochimica Acta, 1974, 19(11), 657–70.

Hills, G. J., Schiffrin, D. J. and Thompson, J., "Electrochemical Nucleation From Molten Salts II. Time Dependent Phenomena in Electrochemical Nucleation", Electrochemica Acta, 1974, 19(11), 671–80.

Hoyer, B., Florence, T. M., and Batley, G. E., Analytical Chemistry, 1987, 59(3), 1608–1614.

Hoogvliet, J. C., Van Den Beld, C. M. B., and Van Der Poel, C. J., J. Electroanal. Chem., 1986, 201, 11–21.

Iacovangelo and Will, J. Electrochem. Soc., 1985, 132(4), 851.

Kolb, D. M., Przнsnyski, M. and Gerischer, H., "Underpotetial Deposition of Metals and Work Function Differences", J. Electroanal. Chem., 1974, 54, 25–39.

Kissinger, P. T. and Heineman, W. R., editors, Laboratory Techniques in Electroanalytical Chemistry, Marcel Dekker, Inc., New York, 1984.

Kazee, Beth, Weisshaar, Duane E., and Kuwana, Theodore, Analytical Chemistry, 1985, 57(13), 2736–2739.

Ladda, Brian, ERG Inc., Oakland, CA, personal communication.

Long, S. E. and Snook, R. D., "Electrochemical Preconcentration Technique for use with Inductively Coupled Plasma Atomic – Emission Spectrometry. Part I.", Analyst (London), 1983, 108(1292), 1331–8.

McLaren, K. G., Batley, G. E., J. Electroanal. Chem., 1977, 79, 169.

Nicholson, R. S., and Shain, I., Analytical Chemistry, 1964, 36, 706.

Ogaram, D. A. and Snook, R. D., "Electrochemical Preconcentration Technique for use with Inductively Coupled Plasma Atomic – Emission Spectroscopy. Part II.", Analyst (London), 1984, 109(12), 1597–601.

Randles, J. E. B., Trans. Faraday Soc., 1948, 44, 327.

Schiffrin, D. J., "Theory of Cyclic Voltammetry for Reversible Electrodeposition of Insoluble Products", Journal of Electroanalytical Chemistry, 1986, 201, 199–203.

Sevcik A., Collect. Czech. Chem. Commun., 1948, 13, 349.

Sioda, R. E., "Electrolysis With Flowing Solution on Porous and Wire Electrodes", Electrochemica Acta, 1970, 15, 783–793.

Sioda, R. E., "Distribution of Potential in a Porous Electrode Under Conditions of Flow Electrolysis", Electrochemica Acta, 1971, 16, 1569–1576.

Sioda, R. E., "Flow Electrolysis on a Porous Electrode Composed of Parallel Grids", Electroanalytical Chemistry, 1972, 34, 411–418.

Sioda, R. E., "Limiting Current in Flow Electrolysis on Porous Electrode", Electrochemica Acta, 1972, 17, 1939–1941.

Sottery, J. P., Anderson, C. W., Analytical Chemistry, 1987, 59(1), 140–144.

Sleszynski, Neal and Osteryoung, Janet, "Arrays of Very Small Voltametric Electrodes Based on Reticulated Vitreous Carbon", Analytical Chemistry, 1984, 56, 130–135.

Takana, Nobuyuki, "Electrodeposition" in Treatise on Analytical Chemistry, Part I Vol. 4, Chapter 48, I. M. Kolthoff and Philip J. Elving, eds, Interscience (John Wiley), New York, 1963.

Trainham, J. A. and Newman, J., "A Flow–Through Porous Electrode Model: Application to Metal Ion Removal From Dilute Streams", J. Electrochemical Soc., 1977, 124(10), 1528–1540.

Wang, Joseph, Electrochemica Acta, 1981, 26(12), 1721–1726.

Wang, Joseph and Dewald, Howard D., "A Porous–Jet Flow–Through Electrode", Talanta, 1982, 29, 453–456.

Wang, J., Tuzhi, P., and Zadeii, J., Analytical Chemistry, 1987, 59(17), 2119–2122.

APPENDIX

5. APPENDIX

5.1. SOLUTION RESISTANCE

The ionic conductivity *k* of a solution is a function of the ionic mobility of the species in solution, Bard and Faulkner (1980, Section 2.3.3), and is calculated by

$$k = F\Sigma|z_i|u_iC_i \qquad \text{(A1-1)}$$

where

k	is the ionic conductivity, S cm^{-1}
F	is the Faraday, coul mol^{-1}
z	is the charge on ion i
C_i	is the concentration of the ion, mol cm^{-1}
u	is the ionic mobility, $cm^2 sec^{-1} V^{-1}$

The restivity *rho* (units Ω-cm) is the reciprocal of the conductivity (op. cit., Equation 4.2.8)

$$rho = 1/k \qquad \text{(A1-2)}$$

The conductance *G* of a solution is directly proportional to the cross sectional area of the solution (perpendicular to the electric field) and inversely proportional to the length of the current path. The proportionality constant between conductance and this ratio (A/l) is the ionic conductivity *k*:

$$G = k(A/l) \qquad \text{(A1-3)}$$

The resistance of a given solution element is the reciprocal of the conductance G.

$$R = 1/kA \qquad \text{(A1-4)}$$

IONIC CONDUCTANCE OF 33% *SCABE*

$$k = F(u(Na^+)[Na^+] + u(Cl^-)[Cl^-] + u(OAc^-)[OAc^-])$$

$$= 96485((5.193\text{x}10^{-4})(6.6\text{x}10^{-4}) + (7.912\text{x}10^{-4})(3.3\text{x}10^{-4}) + (4.24\text{x}10^{-4})(3.3\text{x}10^{-4}))$$

$$= 7.18\text{x}10^{-2} \text{ s cm}^{-1}$$

$$\text{rho} = 1/k = 13.9 \ \Omega\text{-cm}$$

RESISTANCE OF VARIOUS 33% *SCABE* VOLUMES

1) Cylinder: 0.32 cm dia x 2 cm long.

$$R = 2/(7.18\text{x}10^{-2})(0.32/2)^2\pi = 350 \ \Omega$$

2) Cylinder: 0.114 cm dia x 8 cm long (0.045 inch tubing).

$$R = 8/(7.18\text{x}10^{-2})(0.114/2)^2\pi = 10900 \ \Omega$$

3) Hose barb: 0.0635 cm dia x 1 cm long.

$$R = 1/(7.18\text{x}10^{-2})(0.0635/2)^2\pi = 4400 \ \Omega$$

4) Nipple, 10-32 threads: 0.2 cm dia x 1 cm long.

$$R = 1/(7.18\text{x}10^{-2})(0.2/2)^2\pi = 440 \ \Omega$$

5.2. BASIC PROGRAMS

5.2.1. BOX1.BAS

```
5 REM
6 REM box1.bas computes iR drop across box electrode with only one
7 REM            auxiliary lead at a corner edge of the box
8 REM
10 R=1
20 D=2*R
30 SUMIR=0
40 PATH=0
50 VOL=2*R*R
200 INPUT "n=";N
210 DEL=D/N
250 PRINT "path          area      current     resis       ir
300 FOR I=1 TO N
305 REM PRINT "path=",PATH;"r=";R
310 PATH = PATH + DEL
320 IF (PATH > R) GOTO 1000
500 REM
510 REM path < radius
511 REM
520 AREA = PATH + PATH
530 CURRENT = VOL-(PATH*PATH)
531 PRINT "<";
540 GOTO 2000
1000 REM
1010 REM path length > radius
1020 REM
1021 REM IF I < 8 THEN GOTO 1030
1022 REM PRINT "d=",D;
1023 REM PRINT "path=",PATH
1024 PRINT ">";
1030 AREA = 2*(D-PATH)
1040 CURRENT = (D-PATH)*(D-PATH)
2000 IF AREA<.0001 THEN AREA=.001
2005 RES = DEL/AREA
2010 IR=RES*CURRENT
2020 SUMIR=SUMIR+IR
3000 PRINT USING "###.##     ";PATH;
3010 PRINT USING "###.##     ";AREA;
3020 PRINT USING "###.##     ";CURRENT;
3030 PRINT USING "###.###    ";RES;
3040 PRINT USING "###.###    ";IR;
3050 PRINT USING "###.###    ";SUMIR
4000 NEXT
```

5.2.2. BOX2.BAS

```
5 REM
6 REM box2.bas computes iR drop across box electrode with two
7 REM           auxiliary leads, one each at opposite corner edges
8 REM
10 R=1
20 D=R
30 SUMIR=0
40 PATH=0
50 VOL=R*R
200 INPUT "2-wire box n=",N
210 DEL=D/N
250 PRINT "path          area     current      resis        ir
300 FOR I=1 TO N
305 REM PRINT "path=",PATH;"r=";R
310 PATH = PATH + DEL
500 REM
510 REM path < radius
511 REM
520 AREA = PATH + PATH
530 CURRENT = VOL-(PATH*PATH)
531 PRINT "<";
540 GOTO 2000
2000 IF AREA<.0001 THEN AREA=.001
2005 RES = DEL/AREA
2010 IR=RES*CURRENT
2020 SUMIR=SUMIR+IR
3000 PRINT USING "###.##     ";PATH;
3010 PRINT USING "###.##     ";AREA;
3020 PRINT USING "###.##     ";CURRENT;
3030 PRINT USING "###.###    ";RES;
3040 PRINT USING "###.###    ";IR;
3050 PRINT USING "###.###    ";SUMIR
4000 NEXT
```

5.2.3. BOX4.BAS

```
5 REM
6 REM box4.bas computes iR drop across box electrode with four
7 REM           auxiliary leads, one at each corner edge of box
8 REM
10 R=.5
20 D=2*R
30 SUMIR=0
40 PATH=0
50 VOL=2*R*R
200 INPUT "4-wire box; n=";N
210 DEL=D/N
250 PRINT "path          area     current      resis        ir
300 FOR I=1 TO N
305 REM PRINT "path=",PATH;"r=";R
310 PATH = PATH + DEL
320 IF (PATH > R) GOTO 1000
500 REM
510 REM path < radius
511 REM
520 AREA = PATH + PATH
530 CURRENT = VOL-(PATH*PATH)
531 PRINT "<";
540 GOTO 2000
1000 REM
1010 REM path length > radius
1020 REM
1021 REM IF I < 8 THEN GOTO 1030
1022 REM PRINT "d=",D;
1023 REM PRINT "path=",PATH
1024 PRINT ">";
1030 AREA = 2*(D-PATH)
1040 CURRENT = (D-PATH)*(D-PATH)
2000 IF AREA<.0001 THEN AREA=.001
2005 RES = DEL/AREA
2010 IR=RES*CURRENT
2020 SUMIR=SUMIR+IR
3000 PRINT USING "###.##     ";PATH;
3010 PRINT USING "###.##     ";AREA;
3020 PRINT USING "###.##     ";CURRENT;
3030 PRINT USING "###.###    ";RES;
3040 PRINT USING "###.###    ";IR;
3050 PRINT USING "###.###    ";SUMIR
4000 NEXT
```